ISSN: 2687 - 4539

CHAOS

THEORY AND APPLICATIONS

IN APPLIED SCIENCES AND ENGINEERING

VOLUME 5, ISSUE 1, MARCH 2023

AN INTERDISCIPLINARY JOURNAL OF NONLINEAR SCIENCE

ISSN: 2687 - 4539

CHAOS

THEORY AND APPLICATIONS

IN APPLIED SCIENCES AND ENGINEERING

Chaos Theory and Applications (CHTA)
Volume: 5– Issue No: 1 (March 2023)
https://dergipark.org.tr/en/pub/chaos/issue/75756

Editorial Advisory Board Members

Language Editors

Technical Coordinator

ISSN: 2687 - 4539

CHAOS

THEORY AND APPLICATIONS

IN APPLIED SCIENCES AND ENGINEERING

Chaos Theory and Applications (CHTA)
Volume: 5– Issue No: 1(March 2023)
https://dergipark.org.tr/en/pub/chaos/issue/75756

Contents

CHAOS
Theory and Applications
in Applied Sciences and Engineering

e-ISSN: 2687-4539
EDITORIAL
Volume:5 Number:1 Pages:1-2

Dynamic Equations, Control Problems on Time Scales, and Chaotic Systems

Martin Bohner *,[1]
*Department of Mathematics and Statistics, Missouri University of Science and Technology, Rolla, Missouri 65409-0020, USA.

ABSTRACT The unification of integral and differential calculus with the calculus of finite differences has been rendered possible by providing a formal structure to study hybrid discrete-continuous dynamical systems besides offering applications in diverse fields that require simultaneous modeling of discrete and continuous data concerning dynamic equations on time scales. Therefore, the theory of time scales provides a unification between the calculus of the theory of difference equations with the theory of differential equations. In addition, it has become possible to examine diverse application problems more precisely by the use of dynamical systems on time scales whose calculus is made up of unification and extension as the two main features. In the meantime, chaos theory comes to the foreground as a concept that a small change can result in a significant change subsequently, and thus, it is suggested that nonlinear dynamical systems which are apparently random are actually deterministic from simpler equations. Consequently, diverse techniques have been devised for chaos control in physical systems that change across time-dependent spatial domains. Accordingly, this Editorial provides an overview of dynamic equations, time-variations of the system, difference and control problems which are bound by chaos theory that is capable of providing a new way of thinking based on measurements and time scales. Furthermore, providing models that can be employed for chaotic behaviors in chaotic systems is also attainable by considering the arising developments and advances in measurement techniques, which show that chaos can offer a renewed perspective to proceed with observational data by acting as a bridge between different domains.

KEYWORDS
Dynamic equations on time scales
Chaotic systems
Nonlinearity and chaos
Unification and extension
Control problems
Time-variations of systems

The theory of time scales, conceptualized and introduced by Stefan Hilger in 1988, makes a unification between the calculus of the theory of difference equations with the theory of differential equations. In other words, the unification of integral and differential calculus with the calculus of finite differences became possible by providing a formal structure to study hybrid discrete-continuous dynamical systems and offering applications in diverse fields which require simultaneous modeling of discrete and continuous data with regard to dynamic equations on time scales. It is also possible to investigate many application problems in a more precise way through the use of dynamical systems on time scales.

Manuscript received: 31 January 2023,
Accepted: 1 February 2023.

[1] bohner@mst.edu (**Corresponding Author**)

Unification and extension make up the two main features of time scales calculus, with subject matters such as existence and uniqueness of solutions, periodicity, stability, Floquet theory, Cantor sets as well as boundedness, among many others, regarding solutions can be investigated in a more precise way and by and large by utilizing dynamical systems and differential (dynamic) equations on time scales. The study of dynamic equations on time scales enables one to avoid proving the related results twice: one time for differential equations and another time for difference equations (Bohner and Peterson 2001), (Bohner and Georgiev 2016).

The core concept is the proving of a result for a dynamic equation in which the unknown function's domain is a so-called time scale, which is, in fact, an arbitrary closed subset of the reals. As the time scale is chosen to be the set of real numbers, the general result generates a result pertaining to an ordinary differential equation as examined in a first course in differential equations. The same general result yields a result for difference equations by choosing

the time scale to be the set of integers (Hilger 1990). A time scale, as a special case of a measure chain, refers to an arbitrary nonempty closed subset of real numbers such as, for example, $\mathbb{R}$, $\mathbb{Z}$, $\mathbb{N}$, $\mathbb{N}_0$, $[0,1] \cup [2,3]$, $[0,1] \cup \mathbb{N}$, and the Cantor set, whereas $\mathbb{Q}$, $\mathbb{R} \setminus \mathbb{Q}$, $\mathbb{C}$, $(0,1)$ are not time scales (Agarwal *et al.* 2002).

As chaotic systems can be characterized by a certain degree of spontaneous self-order, examining the interplay of nonlinearity and chaos can ensure a deep understanding of such systems, while the theory of calculus on time scales enables a sort of unification of the theories with respect to differential equations and difference equations, delay differential equations as well as population dynamics (Bohner *et al.* 2022b), outspreading the theories toward other types of dynamic equations. As a type of differential equation, delay differential equations, or time-delay systems, in mathematics hold that the derivative of the unknown function at a particular time is provided in terms of the function's values at previous times.

Delay differential equations often emerge as simple infinite-dimensional models in the highly complex scope of partial differential equations. Systems such as hereditary ones, equations that have deviating argument or differential-difference equations belong to the class of systems having functional state. Delay differential equations (Durga and Muthukumar 2019), (Bohner *et al.* 2022a) have aftereffect or dead-time, which is an applied problem since there is the emerging need of having models that behave more like the real process when the increasing expectations of dynamic performances arise. Many processes include aftereffect phenomena in their inherent dynamics besides the sensors, actuators and communication networks being involved in feedback control loops introducing the delays. Therefore, delay differential equations maintain their applicability in the areas of science, particularly in engineering fields related to control as voluntary introduction of delays can prove to be beneficial for the control system (Richard 2003), (Lavaei *et al.* 2010).

Time scales in different models that employ optimal control theory, with the extension of the calculus of variations as a mathematical optimization method, have significant applications to deal with finding a control for a particular dynamical system across a period of time so that an objective function affecting the dynamics can be optimized (Zacchia Lun *et al.* 2019). Dynamics being essentially nonautonomous (Wu *et al.* 2023) makes it compelling to verify the ingredients of chaos for unspecified time scales.

The paradigm of information processing by dynamical systems at the range of phase-space scales reflects the chaotic systems which show an opposite inclination, which is the phase-space expansion as a result of exponentially diverging trajectories. On the other hand, the forecasting of the final state necessitates more precise measurements related to the initial state as the separation of them over time goes up. At this point, chaos theory, as a mathematical field of study, seems as it is a concept which suggests that a small change can bring about a significant change afterwards.

Accordingly, it posits that nonlinear dynamical systems which are apparently random are actually deterministic from simpler equations (Devaney 2022). Control of chaos refers to the stabilization through as small system of perturbations and the result is to make an otherwise chaotic motion more predictable and also stable. Many techniques have been devised for chaos control for physical systems that change on time-dependent spatial domains. In these regards, small perturbations can change a system's behavior with the sensitivity serving to be beneficial for control purposes in chaos as has been implied.

Taken together, dynamic equations, time-variations of the system, difference and control problems are bound by chaos theory which can provide a novel way of thinking based on an innovative concept of measurements and time scales, enabling models to be used for chaotic behaviors. Based on the processing and comprehension of huge amounts of experimental data which can be analyzed by emerging developments and advances in measurement techniques, exploits that motivate mathematical developments can be modeled. As a matter of fact, chaos can offer a renewed perspective to proceed with observational data which may be erratic in natural phenomena by providing a bridge between different domains.

Conflicts of interest

The author declares that there is no conflict of interest regarding the publication of this paper.

Availability of data and material

Not applicable.

LITERATURE CITED

Agarwal, R., M. Bohner, D. O'Regan, and A. Peterson, 2002 Dynamic equations on time scales: a survey. J. Comput. Appl. Math. **141**: 1–26.

Bohner, M., T. Cuchta, and S. Streipert, 2022a Delay dynamic equations on isolated time scales and the relevance of one-periodic coefficients. Math. Methods Appl. Sci. **45**: 5821–5838.

Bohner, M. and S. G. Georgiev, 2016 *Multivariable dynamic calculus on time scales*. Springer, Cham.

Bohner, M., J. Mesquita, and S. Streipert, 2022b The Beverton–Holt model on isolated time scales. Math. Biosci. Eng. **19**: 11693–11716.

Bohner, M. and A. Peterson, 2001 *Dynamic equations on time scales*. Birkhäuser Boston, Inc., Boston, MA, An introduction with applications.

Devaney, R. L., 2022 *An introduction to chaotic dynamical systems*. CRC Press, Boca Raton, FL, third edition.

Durga, N. and P. Muthukumar, 2019 Optimal control of fractional neutral stochastic differential equations with deviated argument governed by Poisson jumps and infinite delay. Optimal Control Appl. Methods **40**: 880–899.

Hilger, S., 1990 Analysis on measure chains—a unified approach to continuous and discrete calculus. Results Math. **18**: 18–56.

Lavaei, J., S. Sojoudi, and R. M. Murray, 2010 Simple delay-based implementation of continuous-time controllers. In *Proceedings of the 2010 American Control Conference*, pp. 5781–5788.

Richard, J.-P., 2003 Time-delay systems: an overview of some recent advances and open problems. Automatica J. IFAC **39**: 1667–1694.

Wu, Y., Z. Huang, M. Bohner, and J. Cao, 2023 Impulsive boundedness for nonautonomous dynamic complex networks with constraint nonlinearity. Appl. Math. Model. **115**: 853–867.

Zacchia Lun, Y., A. D'Innocenzo, F. Smarra, I. Malavolta, and M. D. Di Benedetto, 2019 State of the art of cyber-physical systems security: An automatic control perspective. J. Syst. Softw. **149**: 174–216.

How to cite this article: Bohner, M. Dynamic Equations, Control Problems on Time Scales, and Chaotic Systems. *Chaos Theory and Applications*, 5(1), 1-2, 2023.

CHAOS
Theory and Applications
in Applied Sciences and Engineering

e-ISSN: 2687-4539
RESEARCH ARTICLE
Vol.5 / No.1 / 2023 / pp.3-10
https://doi.org/10.51537/chaos.1162383

Alpha-Stable Autoregressive Modeling of Chua's Circuit in the Presence of Heavy-Tailed Noise

Serpil Yılmaz [*,1] **and Deniz Kutluay** [β,2]
[*]Department of Computer Engineering, İzmir Katip Çelebi University, İzmir, Türkiye, [β]R&D Department, Vestel Electronics Corporation, Manisa, Türkiye.

ABSTRACT This study presents alpha-stable autoregressive (AR) modeling of the dynamics of Chua's circuit in the presence of heavy-tailed noise. The parameters of the AR time series are estimated using the covariation-based Yule-Walker method, and the parameters of alpha-stable distributed residuals are calculated using the regression type method. Visual depictions of the calculated parameters of the AR model and alpha-stable distributions of residuals are presented. The medians of the estimated parameters of the AR model and alpha-stable distributions parameters of residuals are presented for heavy-tailed noise with various stability index parameters. Thus, the impulsive behavior of Chua's circuit can be modeled as alpha-stable AR time series, and the model can provide an alternative approach to describe the chaotic systems driven by heavy-tailed noise.

KEYWORDS
Alpha-stable distribution
Chua's circuit
Autoregressive model
Yule-Walker equations

INTRODUCTION

There has been an increasing interest in stochastic processes based on heavy-tailed distributions for real-world data modeling. It is well known that stochastic fluctuations are inevitable due to various uncertainties or unpredictable factors in the real-world systems. Understanding the effect of fluctuations on the chaotic dynamics is also of fundamental interest. The importance of additive noise in chaotic attractors is considered in (Argyris *et al.* 1998). The effect of stochastic excitations which have asymmetric distributions on chaotic dynamics is analyzed in (Yilmaz *et al.* 2018) by considering the generalized Chua's circuit driven by skew-Gaussian distributed noise. However, Gaussian distribution cannot be applied for modeling data across multiple application areas for which real-world data exhibit significant peaks.

Some examples that might have heavy-tailed behavior include tracking highly maneuvering objects (Gan and Godsill 2020; Gan *et al.* 2021), interference in IoT networks (Clavier *et al.* 2021), financial data (McCulloch 1996; Maleki *et al.* 2020; Janczura *et al.* 2011; Wesselhöfft 2021), chaotic systems (Savaci and Yilmaz 2015; Contreras-Reyes 2021), frequency fluctuations in the power grid (Schäfer *et al.* 2018; Anvari *et al.* 2020), the dose distributions for proton breast treatment (Van den Heuvel *et al.* 2015), proton pencil beams for cancer therapy (Van den Heuvel *et al.* 2018), climate dynamics (Ditlevsen 1999; Broszkiewicz-Suwaj and Wyłomańska 2021). Therefore, alpha-stable (α-stable) distributions are more suitable for modeling such impulsive behavior (Nolan 2003). Alpha-stable distributions require four parameters: skewness parameter (β), scale parameter (σ), location parameter (μ), and stability index (α), which is responsible for the heavy-tailedness of the distribution.

To model the real-world data based on heavy-tailed time series, the α-stable autoregressive (AR) model is proposed in (Gallagher 2001), and generalized Yule-Walker equations are used to estimate the parameters of the α-stable AR process. The use of α-stable distributions in multivariate processes is presented in (Pai and Ravishanker 2010) and the approach is illustrated on time series of daily average temperatures.

The α-stable distribution with $\alpha = 2$ corresponds to the Gaussian distribution. Since stable distributions have an infinite variance for $\alpha < 2$, autocorrelation is not defined for heavy-tailed random sequences. Therefore, other measures of dependence, such as autocovariation are needed for consideration in an infinite variance system. A new autocovariation estimator for α-stable AR processes is introduced in (Gallagher 2001), in which the real-world data set is considered as the time series of sea surface temperatures.

Manuscript received: 16 August 2022,
Revised: 15 December 2022,
Accepted: 16 December 2022.

[1] serpil.yilmaz@ikcu.edu.tr (**Corresponding Author**)
[2] kutluaydenizz@gmail.com

A modified method of Yule-Walker is presented in (Kruczek *et al.* 2017) to estimate the parameters of the stable periodic autoregressive (PAR) model. This method obtains the PAR model for electricity market data describing the hourly volume of up-regulating bid prices in Norway. The classical one-dimensional α-stable AR model is generalized to the multidimensional case in (Grzesiek *et al.* 2021). The method is applied to a real data set which contains daily prices of KGHM and copper.

This paper considers a stochastic nonlinear electronic circuit, specifically the Chua's circuit with α-stable noise. Chua's circuit is a nonlinear chaotic circuit, and the presence of heavy-tailed noise makes the circuit more unpredictable and complex. Our study focuses on applying the α-stable autoregressive (AR) model to characterize the impulsive behavior of the Chua's circuit, and thus aims to provide a better-linearized way to analyze the dynamics of the states of stochastic Chua's circuit.

The paper is structured as follows. In the first part, Chua's circuit in the presence of heavy-tailed noise is presented, and its α-stable AR model is proposed. The next part gives the modified Yule-Walker equations for α-stable AR models based on the autocovariation estimator. In the last part, the dynamical behaviors of the system are obtained by using the Euler-Maruyama method, and the estimation method presented is applied to the simulated data.

CHUA'S CIRCUIT IN THE PRESENCE OF ALPHA-STABLE NOISE

The set of differential equations representing the dynamics of dimensionless Chua's circuit in the presence of heavy-tailed noise is given as follows (Suykens and Huang 1997):

$$\begin{aligned} dx &= a[y - h(x)]dt + dL_\alpha(t) \\ dy &= (x - y + z)dt \\ dz &= -bydt. \end{aligned} \tag{1}$$

with the bifurcation parameters a, b and the piecewise-linear function $h(x)$:

$$h(x) = m_1 x + 0.5(m_0 - m_1)(|x+1| - |x-1|) \tag{2}$$

and $dL_\alpha(t)$ is α-stable random variable $\sim S_\alpha(\beta, \sigma, \mu)$ with the stability index $\alpha \in (0, 2]$, the skewness parameter $\beta \in [-1, 1]$, the scale parameter $\sigma \in \mathbb{R}_+$ and the location parameter $\mu \in \mathbb{R}$ (Samorodnitsky and Taqqu 1994; Nikias and Shao 1995).

The characteristic function of an α-stable random variable is given as (Samorodnitsky and Taqqu 1994; Nikias and Shao 1995)

$$\varphi(w) = \begin{cases} exp\left\{-|\gamma w|^\alpha [1 - i\beta sign(w) \tan(\frac{\pi\alpha}{2})] + i\mu w\right\} & \text{for} \quad \alpha \neq 1 \\ exp\left\{-|\gamma w|[1 + i\beta sign(w)\frac{2}{\pi} log(|w|)] + i\mu w\right\} & \text{for} \quad \alpha = 1 \end{cases} \tag{3}$$

where *sign(w)* is signum function.

Due to the lack of analytical expression for α-stable density functions, the numerical approximation of the corresponding density function $f(y; \alpha, \beta, \sigma, \mu)$ of an α-stable random variable can be evaluated by the inverse Fourier transform of the characteristic function given in (3) as:

$$f(y; \alpha, \beta, \sigma, \mu) = \frac{1}{2\pi} \int_{-\infty}^{\infty} e^{-jwy} \varphi(w) dw. \tag{4}$$

When $\beta = 0$, the distribution is symmetric around μ. The impulsiveness of the distribution increases with the decreasing stability index α, which makes the tails of the corresponding distributions heavier. Gaussian distribution ($\alpha = 2$ and $\beta = 0$), Cauchy distribution ($\alpha = 1$ and $\beta = 0$), and Lévy distribution ($\alpha = 0.5$ and $\beta = 1$) are the exceptional cases of the α-stable distributions.

In this paper, steady states of the dynamical behaviors of the system (1) are proposed to model as an α-stable third-order AR process given as

$$\begin{aligned} x(t) &= \sum_{i=1}^{3} \phi_{1,i} x(t-i) + \xi_1(t) \\ y(t) &= \sum_{i=1}^{3} \phi_{2,i} y(t-i) + \xi_2(t) \\ z(t) &= \sum_{i=1}^{3} \phi_{3,i} z(t-i) + \xi_3(t) \end{aligned} \tag{5}$$

where $\phi_{j,i}$ is the AR parameter and $\xi_i(t)$ is the sequence of i.i.d. symmetric alpha-stable (SαS) random variables for $i, j = 1, 2, 3$.

ESTIMATION METHOD FOR ALPHA-STABLE AR MODELS

The autoregressive model parameters are commonly estimated using the Yule-Walker method based on the autocorrelation function (ACF) (Brockwell and Davis 2002). Since ACF is not defined for α-stable random variables, the modified Yule-Walker method is introduced based on the autocovariation function in (Gallagher 2001), and the parameters of α-stable AR models are found using the modified Yule-Walker method. The procedure of the method is described in the following part:

Let X_t be an autoregressive process of order p which satisfies the following equation:

$$X_t - \phi_1 X_{t-1} - \phi_2 X_{t-2} - \cdots \phi_p X_{t-p} = \xi_t \tag{6}$$

where the sequence $\{\xi_t\}$ is an i.i.d. SαS random variables with $\alpha > 1$.

Multiplying (6) by vector $\mathbf{S} = [S_{t-1}, S_{t-2}, \ldots, S_{t-p}]'$ where $S_t = sign(X_t)$ and taking the expectation, the system consisting of p number of equations is obtained as follows:

$$\begin{aligned} \mathbb{E}X_t S_{t-1} &- \sum_{i=1}^{p} \phi_i \mathbb{E}X_{t-i} S_{t-1} = \mathbb{E}\xi_t \\ \mathbb{E}X_t S_{t-2} &- \sum_{i=1}^{p} \phi_i \mathbb{E}X_{t-i} S_{t-2} = \mathbb{E}\xi_t \\ &\vdots \\ \mathbb{E}X_t S_{t-p} &- \sum_{i=1}^{p} \phi_i \mathbb{E}X_{t-i} S_{t-p} = \mathbb{E}\xi_t \end{aligned} \tag{7}$$

Then dividing the equations respectively by $\mathbb{E}|X_{t-1}|, \mathbb{E}|X_{t-2}|, \ldots, \mathbb{E}|X_{t-p}|$ the following system is obtained:

$$\begin{aligned} \frac{\mathbb{E}X_t S_{t-1}}{\mathbb{E}|X_{t-1}|} &- \sum_{i=1}^{p} \phi_i \frac{\mathbb{E}X_{t-i} S_{t-1}}{\mathbb{E}|X_{t-1}|} = 0 \\ \frac{\mathbb{E}X_t S_{t-2}}{\mathbb{E}|X_{t-2}|} &- \sum_{i=1}^{p} \phi_i \frac{\mathbb{E}X_{t-i} S_{t-2}}{\mathbb{E}|X_{t-2}|} = 0 \\ &\vdots \\ \frac{\mathbb{E}X_t S_{t-p}}{\mathbb{E}|X_{t-p}|} &- \sum_{i=1}^{p} \phi_i \frac{\mathbb{E}X_{t-i} S_{t-p}}{\mathbb{E}|X_{t-p}|} = 0 \end{aligned} \tag{8}$$

in which $\mathbb{E}\xi_t = 0$ since ξ_t has SαS distribution with $\alpha > 1$.

By using the normalized autocovariation (NCV) for stationary SαS process $\{X_t\}$ for lag k proposed in (Gallagher 2001), the matrix form of (8) can be written as follows:

$$\lambda = \Lambda\Phi \tag{9}$$

where λ and ϕ are vectors with the length of p, and they are defined as

$$\begin{aligned} \lambda &= \left[NCV(X_t, X_{t-1}), \ldots, NCV(X_t, X_{t-p})\right]' \\ \Phi &= \left[\phi_1, \ldots, \phi_p\right]' \end{aligned} \tag{10}$$

in which

$$NCV(X_t, X_{t-k}) = \frac{\mathbb{E}X_t sign(X_{t-k})}{\mathbb{E}|X_{t-k}|} \tag{11}$$

The Λ is the $p \times p$ matrix, and its elements are described by:

$$\Lambda(i,j) = NCV(X_t, X_{t-i+j}) \quad \text{for i, j=1, \ldots,p.} \tag{12}$$

The values of the model parameters Φ can be estimated using the sample autocovariation estimator $\widehat{NCV}$ based on p-th moment. The sample estimator of the normalized autocovariation $\widehat{NCV}$ for $\{X(t)\}$ proposed in (Gallagher 2001) is given by:

$$\widehat{NCV}(X_t, X_{t-k}) = \frac{\sum_{t=l}^{r} x_t sign(x_{t-k})}{\sum_{t=1}^{N} |x_t|} \tag{13}$$

where $x_1, x_2, \ldots, x_N$ is a vector set denotes the realization of the random variable $X(t)$, N is the trajectory size, $l = \max(1, 1+k)$, and $r = \min(N, N+k)$.

If the matrix Λ is nonsingular, then the estimators for AR parameters $\hat{\Phi}$ can be written as:

$$\hat{\Phi} = \hat{\Lambda}^{-1}\hat{\lambda} \tag{14}$$

Since the residuals of the model are thought to be a sample of i.i.d. SαS random variables, having estimated the parameters of the AR(p) model, the distribution of the residuals is analyzed using the Kolmogorov-Smirnov (KS) test.

SIMULATION RESULTS

The bifurcation parameters of (1) are fixed as $a = 9$, $b = 14.28$, and the parameters of the piecewise-linear function (2) are chosen as $m_0 = -1/7, m_1 = 2/7$. Using the Euler-Maruyama method given in (Janicki and Weron 1993; Platen 1999) with the step size $\tau = 0.01$, the system of (1) is solved numerically as

$$\mathbf{X}(t_i) = \mathbf{X}(t_{i-1}) + \mathbf{F}(\mathbf{X}(t_{i-1}))\tau + \Delta L^{\tau}_{\alpha,i} \tag{15}$$

where $\tau = t_i - t_{i-1}$. An increment of the α-stable Lévy process is an α-stable random variable generated in (Janicki and Weron 1993) and is defined by

$$L^{\tau}_{\alpha,i} = L_{\alpha}([t_{i-1}, t_i]) \sim S_{\alpha}(\beta, \sigma, \mu). \tag{16}$$

In the first case, Chua's circuit is regarded in the presence of α-stable noise with $\alpha = 1.6$, $\beta = 0$, $\sigma = 4.217 \times 10^{-5}$ and $\mu = 0$ and a time series consisting of 10^5 data is obtained for each state variable.

The parameters $\phi_{j,i}$ of the AR(3) model in (5) are estimated using the sample autocovariation estimator based on the p-th moment proposed in (Gallagher 2001). Afterward, it is assumed that

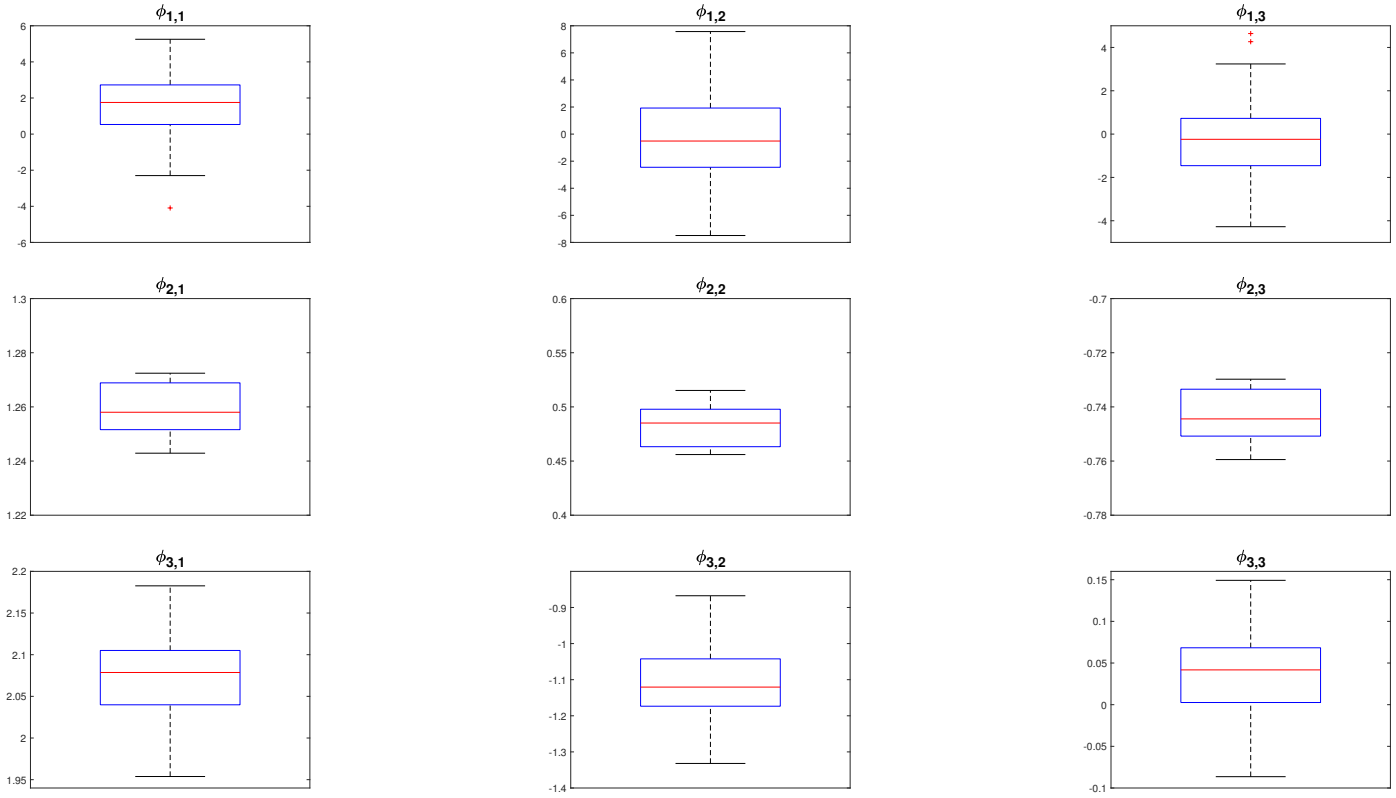

Figure 1 Visual depictions of the calculated parameters of AR(3) model (5) for the system (1) in the presence of α-stable noise with $\alpha = 1.6$, $\beta = 0$, $\sigma = 4.217 \times 10^{-5}$, $\mu = 0$ and $N = 10^5$. Simulations were carried out 100 times using the Monte Carlo method.

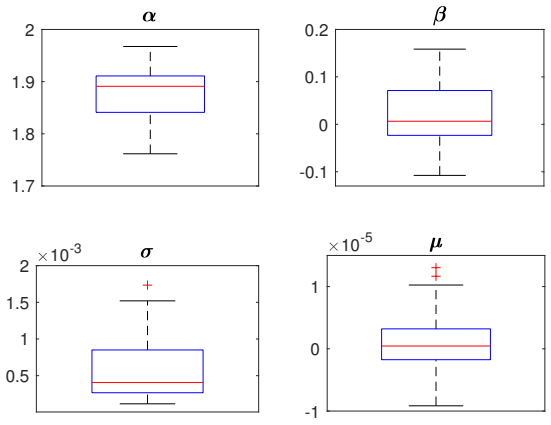

(a) Visual depictions of the calculated parameters of α-stable distribution residuals $\xi_1(t)$.

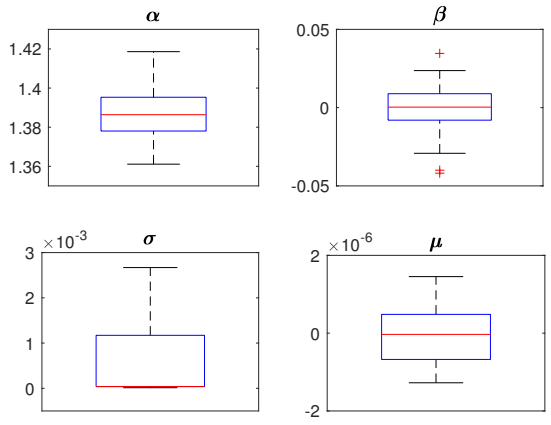

(b) Visual depictions of the calculated parameters of α-stable distribution residuals $\xi_2(t)$.

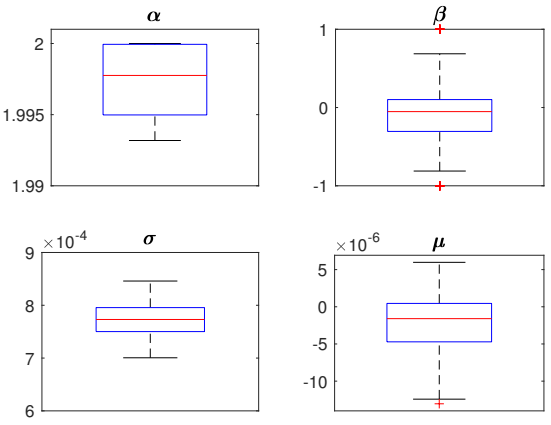

(c) Visual depictions of the calculated parameters of α-stable distribution residuals $\xi_3(t)$.

Figure 2 Each box visually represents the estimated parameter value of the α-stable AR(3) model in (5). Simulations were performed 100 times using the Monte Carlo method.

the noise series ξ_1, ξ_2 and ξ_3 for each state are the representatives of independent α-stable distributed random variables. These residuals are analyzed using the KS test to confirm that they are drawn from the α-stable distribution. By utilizing the KS test, it is obtained that the hypothesis of α-stable distribution for univariate samples and $\xi_1(t)$, $\xi_2(t)$, and $\xi_3(t)$ cannot be rejected at the significance level of 0.05. Then, the α-stable distribution is fitted to the residual time series of each state, and the parameters of the corresponding α-stable distribution for ξ_1, ξ_2 and ξ_3 are estimated using the regression type method. This procedure is performed 100 times using the Monte Carlo simulations, and the boxplots of the estimated parameters are created.

Visual depictions of the calculated parameters of AR(3) model and residuals distributions are presented in Figure 1 and Figure 2, respectively. Each box visually represents the estimated parameter value of the α-stable AR model. The red line indicates the sample median on each box, and the bottom and top edges of the box denoted by blue lines indicate the first and third quartiles, respectively. The black lines represent the most extreme data points, and an outlier is plotted using the red '+' marker symbol. For the presence of α-stable noise with the parameters $\alpha = 1.6$, $\beta = 0$, $\sigma = 4.217 \times 10^{-5}$ and $\mu = 0$, the medians of parameters of the α-stable AR model (5) which corresponds to the red line on each box shown in Figure 1 are obtained as:

$$\begin{aligned} \phi_{1,1} &= 1.7599, \quad \phi_{1,2} = -0.5207, \quad \phi_{1,3} = -0.2393, \\ \phi_{2,1} &= 1.2615, \quad \phi_{2,2} = \ 0.4779, \quad \phi_{2,3} = -0.7408, \\ \phi_{3,1} &= 2.1048, \quad \phi_{3,2} = -1.1734, \quad \phi_{3,3} = 0.0688 \end{aligned} \tag{17}$$

The medians of α-stable distribution parameters $(\hat{\alpha}, \hat{\beta}, \hat{\sigma}, \hat{\mu})$ for residual series ξ_1, ξ_2 and ξ_3 are estimated $(1.8882, -0.004, 0.3666 \times 10^{-3}, 0.105 \times 10^{-6})$, $(1.3865, 0.0019, 0.4 \times 10^{-4}, 0.0898 \times 10^{-6})$ and $(1.9983, -0.0074, 0.7492 \times 10^{-3}, -0.1028 \times 10^{-5})$, respectively, as shown in Figure 2.

In the second case, Chua's circuit is considered in the presence of α-stable noise with different impulsive behaviors. The stability index α ranges from 1.1 to 1.9, and the estimation method is applied for each α value. The medians of the estimated parameters of the AR(3) model are obtained as shown in Table 1. After the analysis of residuals, the medians of the parameters of α-stable distribution for the residual series $\xi_1(t)$, $\xi_2(t)$ and $\xi_3(t)$ are obtained as given in Table 2, 3, and 4, respectively.

As seen in Table 2, the estimated stability index $\hat{\alpha}$ for the series ξ_1 is in the range of 1.898 to 1.932, and the estimated value of the scale parameter $\hat{\sigma}$ decreases as the Chua's circuit is driven by noise with heavier tails. It is also seen in Table 3 that the estimated stability index $\hat{\alpha}$ for the residual series ξ_2 is around 1.38, which implies the residual series ξ_2 is impulsive. On the other hand, the estimated stability index $\hat{\alpha}$ for the residual series ξ_3 is around 1.998, as seen in Table 4, which implies that the corresponding distribution is the Gaussian. The phase portrait of the system (5) with the parameters in (17) is obtained as shown in Figure 3. Figure 3 shows that the attractors reconstructed from the time series (5) characterize the double scroll observed in Chua's circuit.

Moreover, the largest Lyapunov exponents of both systems (1) and (5) are determined numerically. Largest Lyapunov exponents from the time series are estimated using the algorithm presented in (Wolf *et al.* 1985). Figure 4 presents the time evolution of the largest Lyapunov exponents. The blue line shows the value of the Lyapunov exponent obtained from the system of (1) (blue line) and the red line shows the Lyapunov exponents obtained from the simulated data of the proposed system of (5).

Table 1 The medians of the estimated parameters of AR(3) in (5).

α	$\phi_{1,1}$	$\phi_{1,2}$	$\phi_{1,3}$	$\phi_{2,1}$	$\phi_{2,2}$	$\phi_{2,3}$	$\phi_{3,1}$	$\phi_{3,2}$	$\phi_{3,3}$
1.1	2.9705	-2.9362	0.9657	1.2614	0.4781	-0.7409	2.0907	-1.1461	0.0554
1.2	2.8887	-2.7765	0.8877	1.2656	0.4696	-0.7366	2.0754	-1.1158	0.0402
1.3	2.6506	-2.3026	0.6520	1.2603	0.4803	-0.7420	2.0944	-1.1528	0.0583
1.4	2.2825	-1.5650	0.2824	1.2647	0.4714	-0.7375	2.0925	-1.1492	0.0566
1.5	1.8815	-0.7660	-0.1155	1.2627	0.4755	-0.7395	2.0948	-1.1529	0.0580
1.6	1.7599	-0.5207	-0.2393	1.2615	0.4779	-0.7408	2.1048	-1.1734	0.0688
1.7	1.5509	-0.1055	-0.4454	1.2594	0.4821	-0.7408	2.1190	-1.2024	0.0829
1.8	1.4834	0.0029	-0.4863	1.2631	0.4747	-0.7391	2.1361	-1.2375	0.1013
1.9	1.6056	-0.2196	-0.3861	1.2621	0.4767	-0.7401	2.1397	-1.2451	0.1053

Table 2 The medians of the estimated parameters of α-stable distribution for the residual series $\xi_1(t)$ in (5).

α	$\hat{\alpha}$	$\hat{\beta}$	$\hat{\sigma}$ $(\times 10^{-3})$	$\hat{\mu}$ $(\times 10^{-6})$
1.1	1.8987	-0.0019	0.0858	-0.1476
1.2	1.8985	-0.0123	0.1203	-0.1750
1.3	1.8839	-0.0049	0.1678	-02307
1.4	1.9004	0.0076	0.2892	-0.2303
1.5	1.8924	0.0054	0.3360	0.3027
1.6	1.8882	-0.0040	0.3666	0.1050
1.7	1.8967	0.0009	0.4142	0.5840
1.8	1.9037	-0.0086	0.4641	0.3841
1.9	1.9320	0.0018	0.5109	0.1495

Table 3 The medians of the parameters of α-stable distribution for the residual series $\xi_2(t)$ in (5).

α	$\hat{\alpha}$	$\hat{\beta}$	$\hat{\sigma}$ $(\times 10^{-4})$	$\hat{\mu}$ $(\times 10^{-6})$
1.1	1.3850	-0.0023	0.3954	-0.0955
1.2	1.3834	0.036	0.4048	0.3872
1.3	1.3836	-0.0005	0.4015	0.0148
1.4	1.3863	-0.0002	0.3985	0.2201
1.5	1.3854	-0.0012	0.4042	0.0455
1.6	1.3865	0.0019	0.4000	0.0898
1.7	1.3898	-0.0044	0.3989	-0.2566
1.8	1.3879	0.0016	0.3963	0.0507
1.9	1.3996	-0.0034	0.4137	-0.1121

Table 4 The medians of the parameters of α-stable distribution for the residual series $\xi_3(t)$ in (5).

α	$\hat{\alpha}$	$\hat{\beta}$	$\hat{\sigma}$ $(\times 10^{-3})$	$\hat{\mu}$ $(\times 10^{-5})$
1.1	1.9976	-0.0091	0.7518	0.0349
1.2	1.9984	0.0093	0.7561	-0.0897
1.3	1.9981	-0.0028	0.7493	-0.0293
1.4	1.9987	0.0112	0.7514	-0.0735
1.5	1.9986	0.0342	0.7560	-0.1394
1.6	1.9983	-0.0074	0.7492	-0.1028
1.7	1.9994	-0.0169	0.7436	-0.0556
1.8	1.9982	-0.0534	0.7329	-0.0061
1.9	1.9984	-0.0184	0.7257	-0.0408

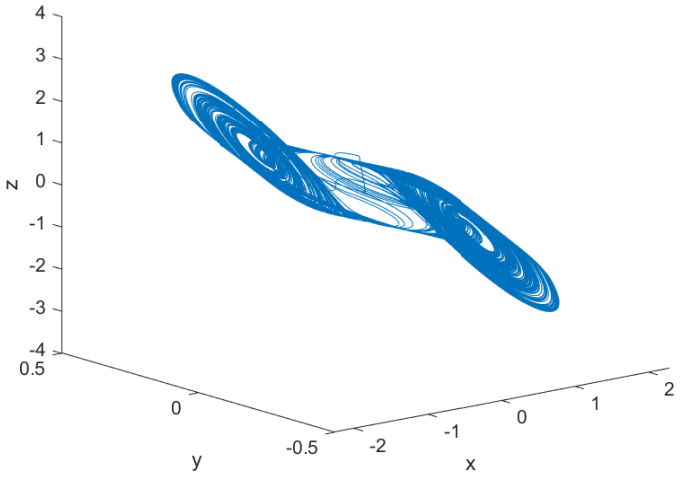

Figure 3 3D phase portrait of system (5) in the presence of α-stable noise with $\alpha = 1.6$, $\beta = 0$, $\sigma = 4.217 \times 10^{-5}$ and $\mu = 0$. The corresponding estimated parameters of (5) are given in Table 1-4.

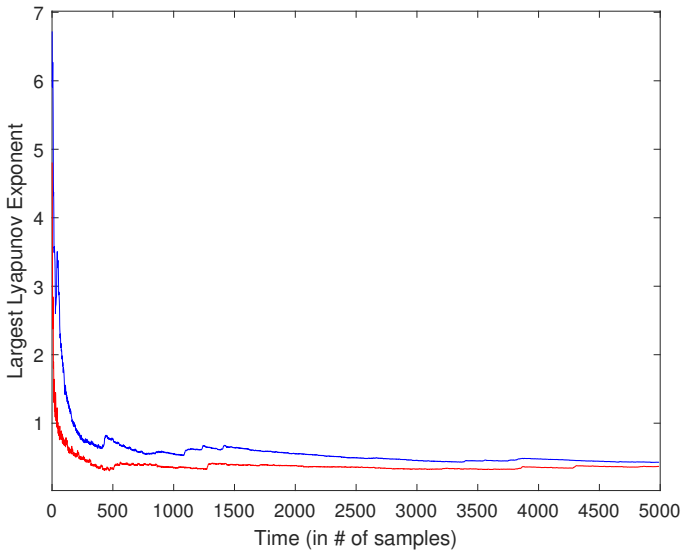

Figure 4 The largest Lyapunov exponents obtained from the system of (1) (blue line) and the system of (5) (red line).

CONCLUSION

In this study, the states of Chua's circuit in the presence of α-stable noise have been modeled as α-stable autoregressive processes. The AR model parameters have been estimated by using the modified Yule-Walker equations and calculating the autocovariation function based on the p-th moment. By estimating the model parameters, the α-stable distribution is fitted to the residual time series of each state, and the parameters of the α-stable distribution have been obtained using the regression type method.

The structure of the double scroll has been observed using the estimated parameters and it has been shown that the model fits very well on simulated data. Chua's circuit has also been considered in the presence of α-stable noise with various stability index α, and the corresponding α-stable AR models have been obtained. Such models will provide new insights into studying nonlinear dynamics in chaotic systems involving stochastic noises. However, further researchs could be considered by using more complex models such as the trivariate vector autoregressive fractional integrated moving average (VARFIMA) model (Contreras-Reyes 2022) instead of simple univariate AR processes. VARFIMA models are considered adaptive estimation methods and also defined for α-stable distributions (Pai and Ravishanker 2010).

Conflicts of interest

The authors declare that there is no conflict of interest regarding the publication of this paper.

Availability of data and material

Not applicable.

LITERATURE CITED

Anvari, M., L. R. Gorjão, M. Timme, D. Witthaut, B. Schäfer, *et al.*, 2020 Stochastic properties of the frequency dynamics in real and synthetic power grids. Physical review research **2**: 013339.

Argyris, J., I. Andreadis, G. Pavlos, and M. Athanasiou, 1998 The influence of noise on the correlation dimension of chaotic attractors. Chaos, Solitons & Fractals **9**: 343–361.

Brockwell, P. J. and R. A. Davis, 2002 *Introduction to time series and forecasting*. Springer.

Broszkiewicz-Suwaj, E. and A. Wyłomańska, 2021 Application of non-gaussian multidimensional autoregressive model for climate data prediction. International Journal of Advances in Engineering Sciences and Applied Mathematics **13**: 236–247.

Clavier, L., T. Pedersen, I. R. Larrad, and M. Egan, 2021 Alpha-stable model for interference in iot networks. In *2021 IEEE Conference on Antenna Measurements & Applications (CAMA)*, pp. 575–578, IEEE.

Contreras-Reyes, J. E., 2021 Chaotic systems with asymmetric heavy-tailed noise: Application to 3d attractors. Chaos, Solitons & Fractals **145**: 110820.

Contreras-Reyes, J. E., 2022 Rényi entropy and divergence for varfima processes based on characteristic and impulse response functions. Chaos, Solitons & Fractals **160**: 112268.

Ditlevsen, P. D., 1999 Observation of α-stable noise induced millennial climate changes from an ice-core record. Geophysical Research Letters **26**: 1441–1444.

Gallagher, C. M., 2001 A method for fitting stable autoregressive models using the autocovariation function. Statistics & probability letters **53**: 381–390.

Gan, R., B. I. Ahmad, and S. J. Godsill, 2021 Lévy state-space models for tracking and intent prediction of highly maneuverable objects. IEEE Transactions on Aerospace and Electronic Systems **57**.

Gan, R. and S. Godsill, 2020 α-stable lévy state-space models for manoeuvring object tracking. In *2020 IEEE 23rd International Conference on Information Fusion (FUSION)*, pp. 1–7, IEEE.

Grzesiek, A., M. Mrozińska, P. Giri, S. Sundar, and A. Wyłomańska,

2021 The covariation-based yule–walker method for multidimensional autoregressive time series with α-stable distributed noise. International Journal of Advances in Engineering Sciences and Applied Mathematics **13**: 394–414.

Janczura, J., S. Orzeł, and A. Wyłomańska, 2011 Subordinated α-stable ornstein–uhlenbeck process as a tool for financial data description. Physica A: Statistical Mechanics and its Applications **390**: 4379–4387.

Janicki, A. and A. Weron, 1993 *Simulation and chaotic behavior of alpha-stable stochastic processes*. CRC Press.

Kruczek, P., A. Wyłomańska, M. Teuerle, and J. Gajda, 2017 The modified yule-walker method for α-stable time series models. Physica A: Statistical Mechanics and its Applications **469**: 588–603.

Maleki, M., D. Wraith, M. R. Mahmoudi, and J. E. Contreras-Reyes, 2020 Asymmetric heavy-tailed vector auto-regressive processes with application to financial data. Journal of Statistical Computation and Simulation **90**: 324–340.

McCulloch, J. H., 1996 13 financial applications of stable distributions. Handbook of statistics **14**: 393–425.

Nikias, C. L. and M. Shao, 1995 *Signal processing with alpha-stable distributions and applications*. Wiley-Interscience.

Nolan, J., 2003 *Stable distributions: models for heavy-tailed data*. Birkhauser New York.

Pai, J. S. and N. Ravishanker, 2010 Fast bayesian estimation for varfima processes with stable errors. Journal of Statistical Theory and Practice **4**: 663–677.

Platen, E., 1999 An introduction to numerical methods for stochastic differential equations. Acta numerica **8**: 197–246.

Samorodnitsky, G. and M. S. Taqqu, 1994 *Stable Non-Gaussian Random Processes*. Chapman & Hall.

Savaci, F. A. and S. Yilmaz, 2015 Bayesian stable mixture model of state densities of generalized chua's circuit. International Journal of Bifurcation and Chaos **25**: 1550038.

Schäfer, B., C. Beck, K. Aihara, D. Witthaut, and M. Timme, 2018 Non-gaussian power grid frequency fluctuations characterized by lévy-stable laws and superstatistics. Nature Energy **3**: 119–126.

Suykens, J. A. and A. Huang, 1997 A family of n-scroll attractors from a generalized chua's circuit. Archiv fur Elektronik und Ubertragungstechnik **51**: 131–137.

Van den Heuvel, F., B. George, N. Schreuder, and F. Fiorini, 2018 Using stable distributions to characterize proton pencil beams. Medical physics **45**: 2278–2288.

Van den Heuvel, F., S. Hackett, F. Fiorini, C. Taylor, S. Darby, *et al.*, 2015 Su-f-brd-04: Robustness analysis of proton breast treatments using an alpha-stable distribution parameterization. Medical Physics **42**: 3526–3526.

Wesselhöfft, N., 2021 Utilizing self-similar stochastic processes to model rare events in finance .

Wolf, A., J. B. Swift, H. L. Swinney, and J. A. Vastano, 1985 Determining lyapunov exponents from a time series. Physica D: nonlinear phenomena **16**: 285–317.

Yilmaz, S., M. E. Cek, and F. A. Savaci, 2018 Stochastic bifurcation in generalized chua's circuit driven by skew-normal distributed noise. Fluctuation and Noise Letters **17**: 1830002.

How to cite this article: Yılmaz, S., and Kutluay, D. Alpha-Stable Autoregressive Modeling of Chua's Circuit in the Presence of Heavy-Tailed Noise. *Chaos Theory and Applications*, 5(1), 3-10, 2023.

CHAOS
Theory and Applications
in Applied Sciences and Engineering

e-ISSN: 2687-4539
RESEARCH ARTICLE
Vol.5 / No.1 / 2023 / pp.11-19
https://doi.org/10.51537/chaos.1204481

Chaos in a Pendulum Adaptive Frequency Oscillator Circuit Experiment

XiaoFu Li[⋆,1], **Aubrey N. Beal**[β,2], **Robert N. Dean**[α,3] **and Edmon Perkins**[⋆,4]

[⋆]LAB2701, Atwood, OK 74827, USA, [β]Dept. of Electrical & Computer Engineering, University of Alabama in Huntsville, Huntsville, AL 35899, USA, [α]Dept. of Electrical & Computer Engineering, Auburn University, Auburn, AL 36849, USA.

ABSTRACT Adaptive oscillators can learn and encode information in dynamic, plastic states. The pendulum has recently been proposed as the base oscillator of an adaptive system. In a mechanical setup, the horizontally forced pendulum adaptive frequency oscillator seeks a resonance condition by modifying the length of the pendulum's rod. This system stores the external forcing frequency when the external amplitude is small, while it can store the resonance frequency, which is affected by the nonlinearity of the pendulum, when the external amplitude is large. Furthermore, for some frequency ranges, the pendulum adaptive frequency oscillator can exhibit chaotic motion when the amplitudes are large. This adaptive oscillator could be used as a smart vibratory energy harvester device, but this chaotic region could degrade its performance by using supplementary energy to modify the rod length. The pendulum adaptive frequency oscillator's equations of motions are discussed, and a field-programmable analog array is used as an experimental realization of this system as an electronic circuit. Bifurcation diagrams are shown for both the numerical simulations and experiments, while period-3 motion is shown for the numerical simulations. As little work has been done on the stability of adaptive oscillators, the authors believe that this work is the first demonstration of chaos in an adaptive oscillator.

KEYWORDS
Adaptive oscillator
Nonlinear dynamics
Bifurcation diagrams
Field-programmable analog array
Chaotic circuits

INTRODUCTION

Adaptive oscillators were inspired by the synchronization of networks of neurons (Kempter *et al.* 1999). Dynamic Hebbian learning has been employed to encode the frequency in a plastic state of adaptive oscillators (Righetti *et al.* 2006). These plastic states are dynamic states, and the DC offset values of these plastic states correspond to information learned from an external signal. For instance, an adaptive frequency oscillator is composed of a base oscillator and a plastic frequency state, which can learn and store an external forcing frequency. Adaptive oscillators have been proposed as analog frequency analyzers (Buchli *et al.* 2008; Corron 2022) and controllers for robotic gait (Righetti *et al.* 2009). There are relatively few experimental results for adaptive oscillators, but a 4-state adaptive Hopf oscillator was implemented as an analog circuit (Li *et al.* 2021a) and a 3-state adaptive oscillator was implemented as a digital circuit (Maleki *et al.* 2015). The effects of noise on adaptive oscillators was studied with the full Fokker-Planck equation with comparisons to a physical experiment (Li *et al.* 2021b) and with a simplified Fokker-Planck equation (Buchli *et al.* 2008).

The learning tasks for adaptive oscillators are embedded in the plastic dynamic states of the system. However, oscillators are capable of other types of computation as well, even without adaptive states. For instance, the classical, non-adaptive Hopf oscillator can be realized as a powerful, reconfigurable reservoir computer (Shougat *et al.* 2021b, 2022). In this reservoir computing architecture, the physics of the oscillator are utilized as a computational resource through machine learning. Interestingly, reservoir computers can exhibit chaotic behavior as well, such as topological mixing that was observed in the Duffing array reservoir computer (Shougat *et al.* 2021a).

Manuscript received: 23 November 2022,
Revised: 16 January 2023,
Accepted: 25 January 2023.

[1] xfxyyh0812@gmail.com
[2] aubrey.beal@uah.edu
[3] deanron@auburn.edu
[4] edmon@lab2701.com (**Corresponding Author**)

Adaptive frequency oscillators are similar to Kuramoto phase oscillators (Acebrón *et al.* 2005; Xu and Jin 2012; Makarov *et al.* 2016; Dénes *et al.* 2021, 2019) and phase-locked loops (PLLs) (Métivier *et al.* 2020; Dürig *et al.* 1997; Kuznetsov *et al.* 2017) since they are capable of learning an external forcing frequency. However, in the literature, adaptive oscillators are usually constructed from a nonlinear oscillator by including the addition of dynamic, plastic states. Although chaos has been exhibited by Kuramoto arrays (Bick *et al.* 2018) and PLLs (Olson *et al.* 2011; Banerjee *et al.* 2014; Paul and Banerjee 2019; Chakraborty *et al.* 2016; Zhao *et al.* 2009; Harb and Harb 2004; Piqueira 2017) chaos has not been explored in adaptive oscillators to the authors' knowledge.

The forced single pendulum (d'Humieres *et al.* 1982; Xu *et al.* 2005; Bishop *et al.* 2005) and the unforced double pendulum were two of the prototypical systems that can exhibit chaos (Shinbrot *et al.* 1992; Levien and Tan 1993; Stachowiak and Okada 2006). Chaos synchronization between a controlled pendulum and Duffing oscillator was studied analytically (Luo and Min 2011). The energy localization phenomenon and stability for an array of coupled pendulums was investigated under different forcing conditions (Jallouli *et al.* 2017). Similar to the present work, the complete bifurcation characteristics of a rotating pendulum under nonlinear perturbation was found (Han and Cao 2016). A numerical investigation of an inverted pendulum on varying the base forcing amplitude displays the transition to chaos via an infinite sequence of period-doubling bifurcations (Kim and Hu 1998).

The extensible pendulum, where the pendulum's rod is modeled as an extensible spring, can also exhibit chaos (Nunez-Yepez *et al.* 1990). The bifurcation diagram was found for a mechanical, forced pendulum experiment (de Paula *et al.* 2006) and a forced torsional pendulum (Miao *et al.* 2014). An array of coupled nonlinear pendulum oscillators was studied to determine the effect of damping, the size of the ensemble, and the local coupling strength on its chaotic response (Munyaev *et al.* 2021). Since the pendulum is a relatively simple system that exhibits chaos, it has been used to test chaotic controllers (Pereira-Pinto *et al.* 2004; Wang and Jing 2004).

Of relevance to the current paper, the authors proposed a mechanical pendulum adaptive frequency oscillator, whose rod length is a dynamic state (Li *et al.* 2022). Instead of the adaptive frequency state learning the external forcing frequency, it was found that this type of adaptive oscillator instead learns a *resonance condition*, which maximizes the displacement of the amplitude of the pendulum. This resonance-tracking quality could make it an excellent candidate as a vibratory energy harvester. Importantly, it was observed that the pendulum adaptive frequency oscillator can exhibit chaotic motion, but the mechanical system could not explore the range of values causing this behavior. In this current paper, the pendulum adaptive frequency oscillator was implemented on a field-programmable analog array circuit, which is capable of operating at a range of parameters that exhibit chaos.

Circuit implementations of chaotic systems are widely used, such as realizations of a three-state chaotic flow (Pham *et al.* 2019), a jerk oscillator (Harrison *et al.* 2022; Rhea *et al.* 2020; Nana *et al.* 2009), a nonlinear feedback control input-introduced memristor chaotic oscillator (Lai *et al.* 2020), a novel autonomous four-dimensional hyperjerk system with hyperbolic sine nonlinearity (Leutcho *et al.* 2018), a fractional-order-based chaos system (Ouannas *et al.* 2017), a three-state chaotic system with applications to robotic navigation (Nwachioma and Pérez-Cruz 2021), and a snap system with adjustable symmetry and nonlinearity (Leutcho and Kengne 2018).

Although most papers report either simulated or experimental bifurcation diagrams, some work has compared simulated bifurcation diagrams with experimental bifurcation diagrams directly, such as a circuit implementation of the Rössler system (Ricco *et al.* 2016), an analog system realization of a time-delay chaotic oscillator (Biswas and Banerjee 2016), a Chua's circuit (Viana Jr *et al.* 2010), and a physical circuit realization of a four-dimensional chaotic system (Jahanshahi *et al.* 2021). In the current paper, both the bifurcation diagrams from numerical simulations and from the experiments are compared. For the experimental work, the pendulum adaptive frequency oscillator equations are implemented as an electronic circuit by utilizing a field-programmable analog array. The authors believe that this is the first time that chaos has been demonstrated in an adaptive oscillator and that this is the first circuit implementation of this pendulum adaptive frequency oscillator.

EQUATION OF MOTION OF HORIZONTALLY FORCED PENDULUM ADAPTIVE FREQUENCY OSCILLATOR

Table 1 List of parameters and states.

Symbol	Description
a	Forcing amplitude
k_ω	Coupling in ω state
c	Damping
l	Pendulum length
m	Mass
g	Acceleration due to gravity
Ω	External sinusoidal forcing frequency
θ	Angular position of pendulum
$\dot{\theta}$	Angular velocity of pendulum
$x(t)$	Angular position in state space
$y(t)$	Angular velocity in state space
$\omega(t)$	Adaptive frequency

In Fig. 1, the horizontally forced pendulum is depicted. In this pendulum, it is assumed that the rod is inelastic, and the horizontal forcing kinematically moves the pivot point. For reference, the constants and states are listed in Table 1. By using Lagrange's equations and assuming a Rayleigh dissipation of the form $\frac{1}{2}cml^2\dot{\theta}^2$, the governing equation can be written as follows:

$$ml^2\ddot{\theta} + cml^2\dot{\theta} + mgl\sin(\theta) = l\cos(\theta)f(t) \tag{1}$$

After dividing both sides of the equation by ml^2, eq. (1) becomes:

$$\ddot{\theta} + c\dot{\theta} + \omega_n^2\sin(\theta) = \frac{1}{ml}\cos(\theta)f(t) \tag{2}$$

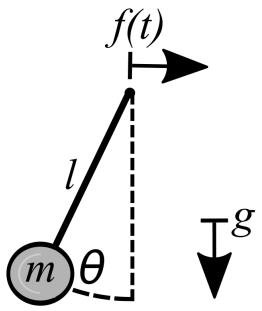

Figure 1 Pendulum with horizontal forcing, which kinematically moves the pivot point.

Converting eq. (2) into state space with $x = \theta$ and $y = \dot{\theta}$, the following set of ordinary differential equations may be written:

$$\begin{aligned} \dot{x}(t) &= y(t) \\ \dot{y}(t) &= -cy(t) - \omega_n^2 \sin\left(x(t)\right) + \frac{1}{ml}\cos\left(x(t)\right) f(t) \end{aligned} \tag{3}$$

Setting $f(t) = \hat{a}\sin\left(\Omega t\right)$ with $\hat{a} = aml$, eq. (3) can be written as:

$$\begin{aligned} \dot{x}(t) &= y(t) \\ \dot{y}(t) &= -cy(t) - \omega_n^2 \sin\left(x(t)\right) + a\cos\left(x(t)\right)\sin\left(\Omega t\right) \end{aligned} \tag{4}$$

Here, a is the amplitude of the sinusoidal forcing. Using these pendulum equations as a base oscillator, a pendulum adaptive frequency oscillator can be constructed by adding a plastic, dynamic state that can learn the external forcing frequency:

$$\begin{aligned} \dot{x}(t) &= y(t) \\ \dot{y}(t) &= -cy(t) - \omega^2(t)\sin\left(x(t)\right) + a\cos\left(x(t)\right)\sin\left(\Omega t\right) \\ \dot{\omega}(t) &= \frac{-k_\omega x(t) a \sin\left(\Omega t\right)}{\sqrt{x^2(t)+y^2(t)}} \end{aligned} \tag{5}$$

The $\dot{\omega}$ equation is responsible for learning and storing the external frequency in the ω state. The right-hand side of this equation is a mixture of two time-varying signals, $x(t)$ and $a\sin\left(\Omega t\right)$. When the system is not undergoing chaotic motion, $x(t)$ becomes entrained to the external sinusoid, which causes the ω state to converge to Ω. The right-hand side of this equation is also normalized by the amplitude of the cyclic motion of the pendulum, $\sqrt{x^2(t)+y^2(t)}$. k_ω is the coupling strength in this third state.

It should also be noted that the damped pendulum (eq. (4)) does not have an analytical solution (Gitterman 2010). By extension, it is very unlikely that the damped adaptive pendulum (eq. (5)) would have an analytical solution either. For this reason, numerical simulations and experiments are used to exhibit chaos in this adaptive oscillator.

When eq. (5) is in a regime in which it correctly learns the external forcing frequency, a local stability analysis can be constructed. For this analysis, the external sinusoid can be replaced with an additional oscillator to convert eq. (5) into an autonomous system (Perkins 2019). When this additional oscillator undergoes a supercritical Andronov-Hopf bifurcation, it resonates with a frequency of Ω Perkins and Fitzgerald (2018). The set of autonomous equations can be written as:

$$\begin{aligned} \dot{x}(t) &= y(t) \\ \dot{y}(t) &= -cy(t) - \omega^2(t)\sin\left(x(t)\right) + a\cos\left(x(t)\right)u \\ \dot{\omega}(t) &= \frac{-k_\omega x(t) a u}{\sqrt{x^2(t)+y^2(t)}} \\ \dot{u} &= u + \Omega v - u(u^2+v^2) \\ \dot{v} &= v - \Omega u - v(u^2+v^2) \end{aligned} \tag{6}$$

Here, the last two equations represent the additional oscillator. The Jacobian, J, for eq. (6) may be written as:

$$J = \begin{bmatrix} 0 & j_1 & 0 & 0 & 0 \\ j_2 & j_3 & j_4 & j_5 & 0 \\ j_6 & j_7 & 0 & j_8 & 0 \\ 0 & 0 & 0 & j_9 & j_{10} \\ 0 & 0 & 0 & j_{11} & j_{12} \end{bmatrix} \tag{7}$$

The elements for this Jacobian are: $j_1 = 1$, $j_2 = -\omega^2\cos\left(x\right) - au\sin\left(x\right)$, $j_3 = -c$, $j_4 = -2\omega\sin\left(x\right)$, $j_5 = a\cos\left(x\right)$, $j_6 = \frac{ak_\omega u x^2}{(x^2+y^2)^{\frac{3}{2}}} - \frac{ak_\omega u}{(x^2+y^2)^{\frac{1}{2}}}$, $j_7 = \frac{ak_\omega u x y}{(x^2+y^2)^{\frac{3}{2}}}$, $j_8 = \frac{-ak_\omega x}{(x^2+y^2)^{\frac{3}{2}}}$, $j_9 = 1 - 3u^2 - v^2$, $j_{10} = -2uv + \Omega$, $j_{11} = -2uv - \Omega$, and $j_{12} = 1 - u^2 - 3v^2$. For the fixed point $(x, y, u, v) = (2\pi, 0, 0, 0)$, the eigenvalues for the Jacobian are $1 \pm i\Omega$, $\frac{-c\pm\sqrt{c^2-4\omega^2}}{2}$, and 0. The first conjugate pair, $1 \pm i\Omega$, corresponds to the additional oscillator, which oscillates at a frequency of Ω.

The second conjugate pair is $\frac{-c\pm\sqrt{c^2-4\omega^2}}{2}$. Noting that eq. (4) is a pendulum with an effective mass equal to 1, we may rewrite this conjugate pair of eigenvalues as $-\zeta\omega_n \pm i\omega_n\sqrt{1-\zeta^2}$. Here, ζ is the damping factor and ω_n is the linear natural frequency of the pendulum. Thus, the second conjugate pair of eigenvalues corresponds to the damped pendulum, which oscillates at the damped natural frequency, $\omega_d = \omega_n\sqrt{1-\zeta^2}$. The last eigenvalue, 0, corresponds to the ω state. This state is neither stable nor unstable, which allows it to deform to the external forcing frequency.

SIMULATION RESULTS

For most values of the forcing frequency, Ω, the pendulum adaptive frequency oscillator behaves as expected: the frequency state converges to the forcing frequency. This behavior is depicted in Fig. 2. For this figure and for the subsequent bifurcation diagrams, a quasi-static frequency sweep was performed, for both the numerical simulations and the experiments. In Figs. 2 and 3, *ode45* in MATLAB was used to simulate eq. (5) for 400 periods of the forcing function, $\sin\left(\Omega t\right)$. Only the last 100 cycles were used to create Figs. 2 and 3, to avoid any transient behavior. Poincaré sections were taken of the pendulum's dynamics, using the external sinusoid as the clock with frequency Ω.

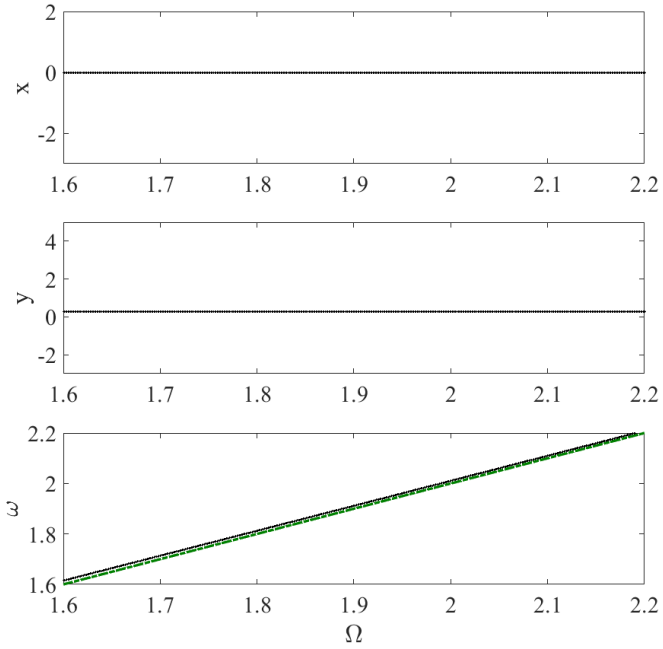

Figure 2 Poincaré sections of the states of the horizontally forced pendulum adaptive frequency oscillator for Ω ranging from 1.6 rad/s to 2.2 rad/s. Here, $a = 0.1$, $c = 0.35$, and $k_\omega = 0.707$. The green dashed line represents the line $\omega = \Omega$. For this combination of parameters, the pendulum adaptive frequency oscillator correctly learns the external forcing frequency. This figure can be compared with the chaotic bifurcation diagram that is shown in Fig. 3.

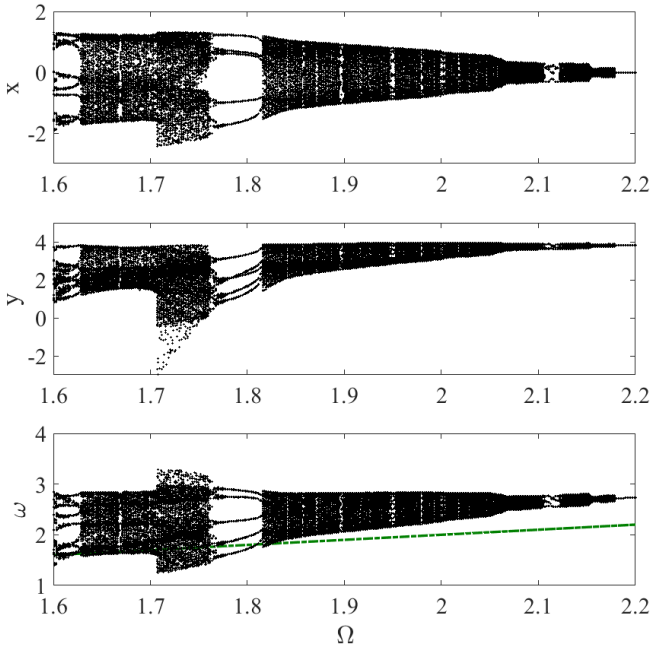

Figure 3 Bifurcation diagram using the Poincaré sections of the states of the horizontally forced pendulum adaptive frequency oscillator for Ω ranging from 1.6 rad/s to 2.2 rad/s. Here, $a = 1.8$, $c = 0.35$, and $k_\omega = 0.707$. The green dashed line represents the line $\omega = \Omega$. Instead of learning the external forcing frequency, the bifurcation diagram exhibits chaotic behavior. This figure can be compared with the non-chaotic bifurcation diagram that is shown in Fig. 2.

In Fig. 2, the pendulum adaptive frequency oscillator's Poincaré sections show that the ω state has properly learned the external forcing frequency, Ω. Since the x and y states are periodic with the same frequency as the external sinusoid, their Poincaré sections appear stationary with respect to this clock.

Repeating this same procedure that was used for Fig. 2, the bifurcation diagram is constructed, which is depicted in Fig. 3. For this set of parameters, the pendulum adaptive frequency oscillator does not properly learn the external forcing frequency. Instead, the system has a chaotic response.

Other combinations of parameters can also result in a chaotic response. Two other bifurcation diagrams are shown in Figs. 4 and 5. In these bifurcation diagrams, the k_ω (Fig. 4) and c (Fig. 5) parameters were varied to highlight that the pendulum adaptive frequency oscillator may also experience chaotic motion.

In general, these bifurcation diagrams provide some insights into a working range for the parameters of the pendulum adaptive frequency oscillator. The forcing amplitude, a, and the coupling term, k_ω, should be relatively small. A higher value of the damping, c, hinders the chaotic motion for the parameters considered here. Further, this adaptive oscillator works better when the forcing frequency, Ω, is relatively large. When the pendulum adaptive frequency oscillator is tasked with learning a low frequency response with a large amplitude, it can result in a chaotic response.

For some parameter combinations, period-3 motion may be observed, which shows that this system is indeed chaotic (Li and Yorke 2004). In Fig. 6, period-3 motion may be seen in the time history. The three dimensional trajectory of the system is shown for comparison.

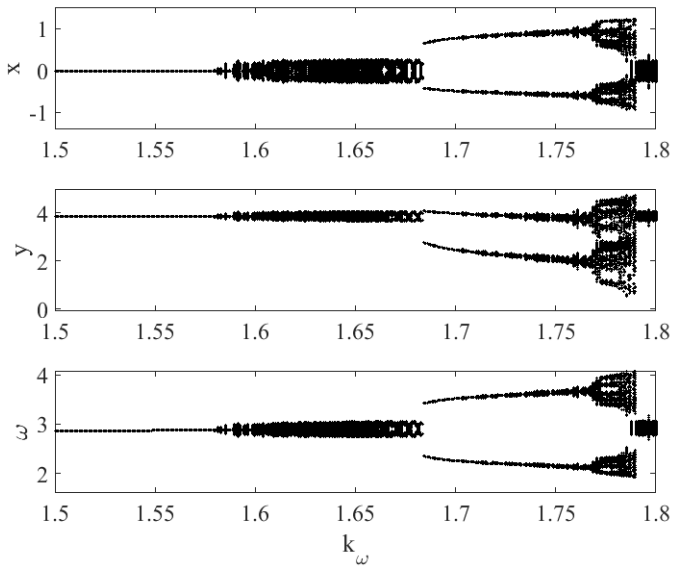

Figure 4 Bifurcation diagram using the Poincaré sections of the states of the horizontally forced pendulum adaptive frequency oscillator for k_ω ranging from 1.5 to 1.8. Here, $a = 1.8$, $c = 0.35$, and $\Omega = 2.2$ rad/s. Some of these values of k_ω can result in chaotic motion.

For other parameters, strange attractors may be observed. One of these strange attractors is depicted in Fig. 7.

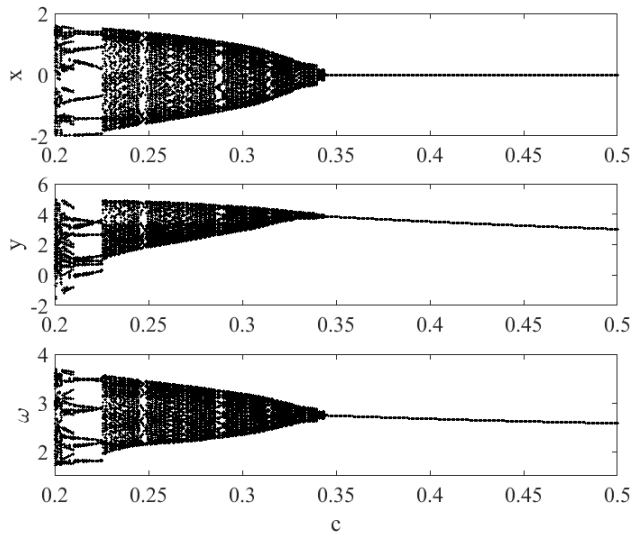

Figure 5 Bifurcation diagram using the Poincaré sections of the states of the horizontally forced pendulum adaptive frequency oscillator for c ranging from 0.2 to 0.5. Here, $a = 1.8$, $k_\omega = 0.707$, and $\Omega = 2.2$ rad/s. Some of these values of c can result in chaotic motion.

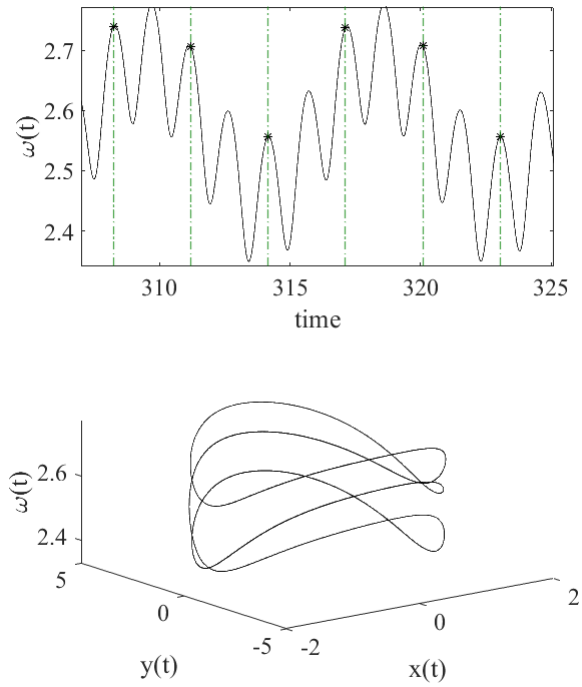

Figure 6 For $\Omega = 2.12$ rad/s, the response of the ω state has period-3 motion. Here, $a = 1.8$, $c = 0.35$, and $k_\omega = 0.707$. In the top plot, the Poincaré sections are shown for a portion of the time history. The vertical green dashed lines depict the clock's sampling rate for the stroboscope, and the * is the value of the ω state at these times. In the bottom plot, the three dimensional trajectory of the system is shown.

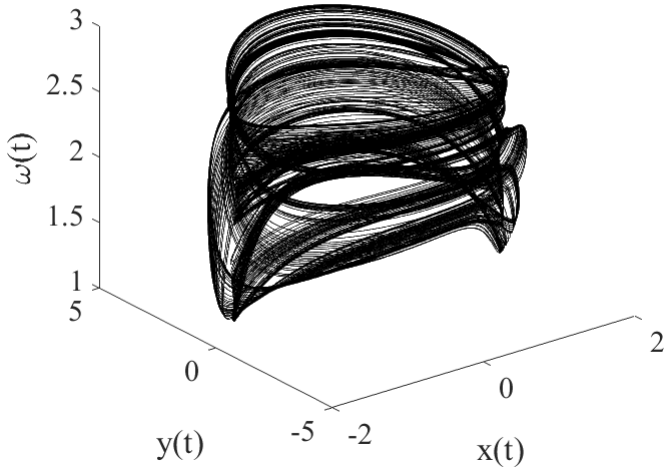

Figure 7 For $\Omega = 1.67$, a strange attractor is shown. For this simulation, $a = 1.8$, $c = 0.35$, and $k_\omega = 0.707$.

FIELD-PROGRAMMABLE ANALOG ARRAY CIRCUIT

The pendulum adaptive frequency oscillator was implemented as a field-programmable analog array circuit. Field-programmable analog arrays (FPAAs) are dynamically programmable analog signal processing devices that use switched-capacitor technology (Kutuk and Kang 1996). FPAAs contains configurable analog blocks (CABs), which create analog operations. Each math operation is further achieved by configurable analog modules (CAMs). By using FPAAs, the design of nonlinear systems are significantly reduced, as the technology is highly reconfigurable (Kilic and Dalkiran 2009).

Several FPAA implementations of nonlinear dynamical system have been widely studied, which include the implementation of the Lorenz system (Tlelo-Cuautle *et al.* 2020), a cellular network-based Lorenz-like system (Günay and Altun 2018), the Sprott N chaotic oscillator (Li *et al.* 2018; Çiçek 2019), the Nahrain chaotic map (Abdullah and Abdullah 2019), a fractional-order chaotic system (Silva-Juárez *et al.* 2020), a chaotic oscillator (Dalkiran and Sprott 2016), and the Hindmarsh–Rose Neuron model (Dahasert *et al.* 2012). As compared with printed circuit boards, FPAAs can accomplish faster prototyping, without using large amounts of operational amplifiers and analog multipliers. The nonlinear functions, such as the sinusoids and square root operation in eq. (5), can be approximated as a user-defined voltage transfer function with CAMs. Utilizing the modular design of FPAAs, this pendulum frequency adaptive oscillator is implemented as a physical experiment.

However, the FPAA's input and output must be in a range between ± 3 volts. This necessitates that the response amplitude must be rescaled. Based on the numerical time response results shown in Fig. 3, only the y state significantly exceeds the maximum voltage range of the FPAA. It should also be noted that the FPAA experiment runs at 1000 times faster than the numerical simulations, due to the RC time constant of the FPAA. Thus, new states are introduced such that $x = X$, $y = 2Y$, and $\omega = 1000W$. Using these relationships, eq. (5) is modified for use on the FPAA as follows:

$$
\begin{aligned}
\dot{X}(t) &= 2Y(t) \\
\dot{Y}(t) &= -cY(t) - \tfrac{1}{2}\left(W^2(t)\sin X(t) - a\cos\left(X(t)\right)\sin\left(\Omega t\right)\right) \\
\dot{W}(t) &= \frac{-k_\omega X(t) a \sin\left(\Omega t\right)}{1000\sqrt{X^2(t)+4Y^2(t)}}
\end{aligned}
\tag{8}
$$

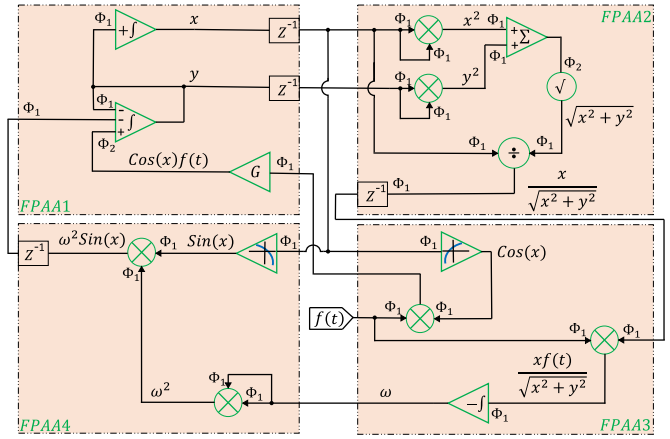

Figure 8 FPAA circuit schematic of pendulum adaptive frequency oscillator. An external forcing signal was sent to the FPAA via differential input IO3 of FPAA3.

An Anadigm Quad Apex v2.0 FPAA development board with 4 AN231E04 chips was used. The *AnadigmDesigner*2 simulator developed by Anadigm was used for FPAA hardware routing and design. All the external stimuli for the experimental results were generated in MATLAB, and they were then input to the FPAA through the differential IO cell using a National Instruments (NI) cDAQ-9174. Similarly, all the outputs of the FPAA are collected by the NI unit.

EXPERIMENTAL RESULTS

In this section, results from the FPAA pendulum adaptive frequency oscillator prototype are shown. For Figs. 9 and 10, the same procedure was used that was described for Figs. 2 and 3. A frequency sweep was performed on the FPAA analog circuit, and only the last 100 cycles were used for the Poincaré section plots in Figs. 9 and 10 to avoid any transient behavior.

In Fig. 9, the FPAA's Poincaré sections show that the ω state (where $1000 \times W = \omega$) closely learned the external forcing frequency, Ω. However, nonlinear features of the FPAA cause some errors that were not seen in the numerical simulations. Since the x and y states are periodic with the same frequency as the external sinusoid, their Poincaré sections appear stationary with respect to this clock.

Repeating this same procedure that was used for Fig. 9, the bifurcation diagram is also constructed for the FPAA, which is depicted in Fig. 10. For this set of parameters, the FPAA has a chaotic response.

In the experimental FPAA prototype, strange attractors are also present. One of these strange attractors is depicted in Fig. 11.

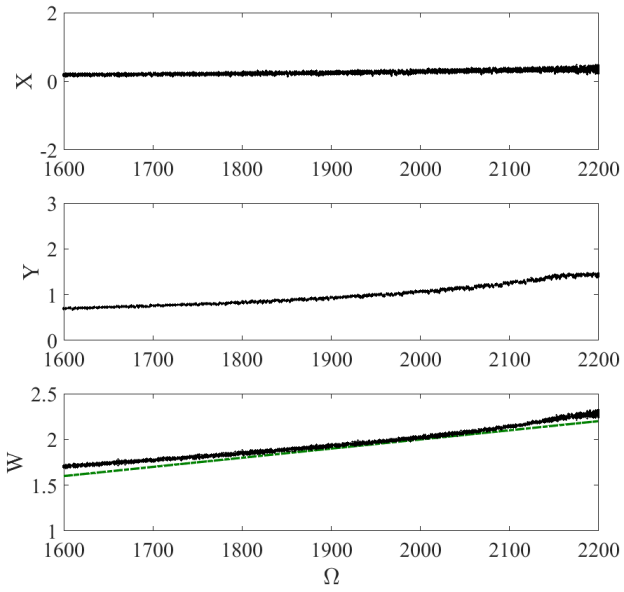

Figure 9 Poincaré sections of the states of the FPAA circuit for Ω ranging from 1600 rad/s to 2200 rad/s. Note that the FPAA runs at 1000 times faster than the simulations due to the RC time constant, so the W state should be multiplied by 1000 to calculate the learned frequency. Here, $a = 0.1$, $c = 0.35$, and $k_\omega = 0.707$. The green dashed line represents the line $\frac{\omega}{1000} = \Omega$. For this combination of parameters, the FPAA correctly learns the external forcing frequency.

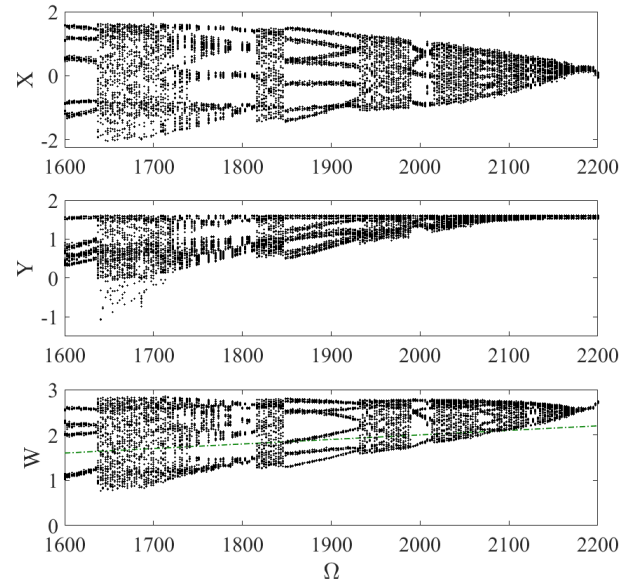

Figure 10 Bifurcation diagram using the Poincaré sections of the states of the FPAA for Ω ranging from 1600 rad/s to 2200 rad/s. Note that the FPAA runs at 1000 times faster than the simulations due to the RC time constant, so the W state should be multiplied by 1000 to calculate the learned frequency. Here, $a = 1.8$, $c = 0.35$, and $k_\omega = 0.707$. The green dashed line represents the line $\frac{\omega}{1000} = \Omega$. Instead of learning the external forcing frequency, the bifurcation diagram exhibits chaotic behavior.

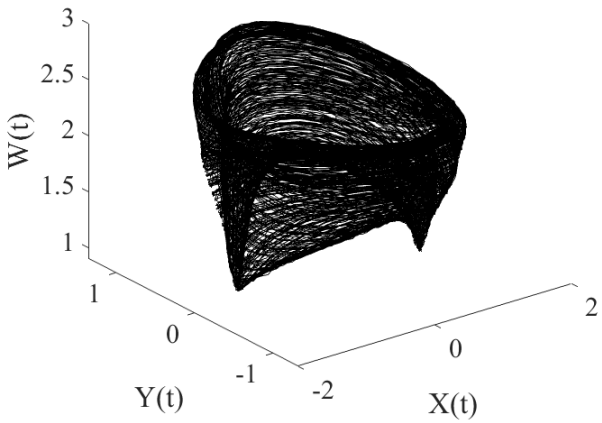

Figure 11 For $\Omega = 1640$, a strange attractor is shown. For this experiment, $a = 1.8$, $c = 0.35$, and $k_\omega = 0.707$.

Since the FPAA's frequency is scaled by 1000 from the simulations, the frequency for the strange attractor in Fig. 11 is comparable to the attractor shown in Fig. 7. Period-5 motion is depicted in Fig. 12 for the FPAA's response.

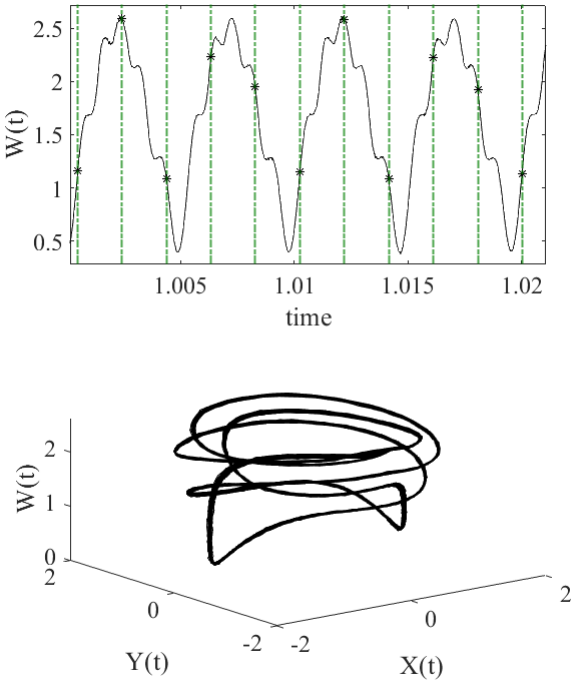

Figure 12 For $\Omega = 1880$ rad/s, the response of the W state has period-5 motion. Here, $a = 1.8$, $c = 0.35$, and $k_\omega = 0.707$. In the top plot, the Poincaré sections are shown for a portion of the time history. The vertical green dashed lines depict the clock's sampling rate for the stroboscope, and the * is the value of the W state at these times. In the bottom plot, the three dimensional trajectory of the system is shown.

CONCLUSIONS

Adaptive oscillators are a potentially useful subset of nonlinear oscillators. However, they have not been thoroughly explored. In this paper, the pendulum adaptive frequency oscillator was studied. To the authors' knowledge, this is the first circuit prototype of a pendulum adaptive frequency oscillator, and this is the first time that chaos has been observed for an adaptive oscillator. This pendulum adaptive frequency oscillator was studied through numerical simulations and a field-programmable analog array experiment. As there is interest in using a mechanical pendulum as the base oscillator (Li *et al.* 2022), this FPAA prototype provides a method of experimentally interrogating the dynamics of this system without building multiple costly mechanical prototypes.

It was found that for some parameter combinations, the pendulum adaptive frequency oscillator performed as expected in learning the external forcing frequency. At other parameter combinations, the pendulum adaptive frequency oscillator behaved chaotically. As the pendulum adaptive frequency oscillator has been proposed as a vibratory energy harvester, it is important to avoid this chaotic behavior, since the system would use energy to adapt the rod length of the pendulum.

Bifurcation diagrams were constructed for both the numerical simulations and the experiment. It should be noted that the bifurcation diagrams for the simulations and experiments were very similar, although they are not identical. Since this is a chaotic system, it is difficult to match the bifurcation diagrams of a model with an experiment, as chaotic systems have sensitive dependence on system parameters. In other words, it would be very difficult to tune the experiment's parameters to exactly match those used in the model. Strange attractors for both the simulations and experiment were also reported. Period-3 motion was found, which implies that the system is indeed chaotic.

Acknowledgments

Partial support for this project from DARPA's Young Faculty Award is greatly appreciated. Research was sponsored by the Army Research Office and was accomplished under Grant Number **W911NF-20-1-0336**. The views and conclusions contained in this document are those of the authors and should not be interpreted as representing the official policies, either expressed or implied, of the Army Research Office or the U.S. Government. The U.S. Government is authorized to reproduce and distribute reprints for Government purposes notwithstanding any copyright notation herein.

Conflicts of interest

The authors declare that there is no conflict of interest regarding the publication of this paper.

Availability of data and material

Not applicable.

LITERATURE CITED

Abdullah, H. A. and H. N. Abdullah, 2019 Design and fpaa implementation of novel chaotic system. Univ Politehnica Bucharest Scient Bull Ser C-Electrical Eng Comput Sci **81**: 153–164.

Acebrón, J. A., L. L. Bonilla, C. J. P. Vicente, F. Ritort, and R. Spigler, 2005 The kuramoto model: A simple paradigm for synchronization phenomena. Reviews of modern physics **77**: 137.

Banerjee, T., B. Paul, and B. Sarkar, 2014 Spatiotemporal dynamics of a digital phase-locked loop based coupled map lattice system.

Chaos: An Interdisciplinary Journal of Nonlinear Science **24**: 013116.

Bick, C., M. J. Panaggio, and E. A. Martens, 2018 Chaos in kuramoto oscillator networks. Chaos: An Interdisciplinary Journal of Nonlinear Science **28**: 071102.

Bishop, S., A. Sofroniou, and P. Shi, 2005 Symmetry-breaking in the response of the parametrically excited pendulum model. Chaos, Solitons & Fractals **25**: 257–264.

Biswas, D. and T. Banerjee, 2016 A simple chaotic and hyperchaotic time-delay system: design and electronic circuit implementation. Nonlinear Dynamics **83**: 2331–2347.

Buchli, J., L. Righetti, and A. J. Ijspeert, 2008 Frequency analysis with coupled nonlinear oscillators. Physica D: Nonlinear Phenomena **237**: 1705–1718.

Chakraborty, S., M. Dandapathak, and B. Sarkar, 2016 Oscillation quenching in third order phase locked loop coupled by mean field diffusive coupling. Chaos: An Interdisciplinary Journal of Nonlinear Science **26**: 113106.

Çiçek, S., 2019 Fpaa based desıgn and implementation of sprott n chaotic system. In *International Scientific and Vocational Studies Congress*, pp. 476–482, BILMES 2019 Ankara.

Corron, N. J., 2022 Complex waveform estimation using adaptive frequency oscillators. Chaos, Solitons & Fractals **158**: 111991.

Dahasert, N., İ. Öztürk, and R. Kiliç, 2012 Experimental realizations of the hr neuron model with programmable hardware and synchronization applications. Nonlinear Dynamics **70**: 2343–2358.

Dalkiran, F. Y. and J. C. Sprott, 2016 Simple chaotic hyperjerk system. International Journal of Bifurcation and Chaos **26**: 1650189.

de Paula, A. S., M. A. Savi, and F. H. I. Pereira-Pinto, 2006 Chaos and transient chaos in an experimental nonlinear pendulum. Journal of sound and vibration **294**: 585–595.

Dénes, K., B. Sándor, and Z. Néda, 2019 Pattern selection in a ring of kuramoto oscillators. Communications in Nonlinear Science and Numerical Simulation **78**: 104868.

Dénes, K., B. Sándor, and Z. Néda, 2021 Synchronization patterns in rings of time-delayed kuramoto oscillators. Communications in Nonlinear Science and Numerical Simulation **93**: 105505.

d'Humieres, D., M. Beasley, B. Huberman, and A. Libchaber, 1982 Chaotic states and routes to chaos in the forced pendulum. Physical Review A **26**: 3483.

Dürig, U., H. Steinauer, and N. Blanc, 1997 Dynamic force microscopy by means of the phase-controlled oscillator method. Journal of applied physics **82**: 3641–3651.

Gitterman, M., 2010 *The Chaotic Pendulum*. World Scientific.

Günay, E. and K. Altun, 2018 Lorenz-like system design using cellular neural networks. Turkish Journal of Electrical Engineering & Computer Sciences **26**: 1812–1819.

Han, N. and Q. Cao, 2016 Global bifurcations of a rotating pendulum with irrational nonlinearity. Communications in Nonlinear Science and Numerical Simulation **36**: 431–445.

Harb, B. A. and A. M. Harb, 2004 Chaos and bifurcation in a third-order phase locked loop. Chaos, Solitons & Fractals **19**: 667–672.

Harrison, R. C., A. OLDAG, E. PERKİNS, *et al.*, 2022 Experimental validation of a chaotic jerk circuit based true random number generator. Chaos Theory and Applications **4**: 64–70.

Jahanshahi, H., O. Orozco-López, J. M. Munoz-Pacheco, N. D. Alotaibi, C. Volos, *et al.*, 2021 Simulation and experimental validation of a non-equilibrium chaotic system. Chaos, Solitons & Fractals **143**: 110539.

Jallouli, A., N. Kacem, and N. Bouhaddi, 2017 Stabilization of solitons in coupled nonlinear pendulums with simultaneous external and parametric excitations. Communications in Nonlinear Science and Numerical Simulation **42**: 1–11.

Kempter, R., W. Gerstner, and J. L. Van Hemmen, 1999 Hebbian learning and spiking neurons. Physical Review E **59**: 4498.

Kilic, R. and F. Y. Dalkiran, 2009 Reconfigurable implementations of chua's circuit. International Journal of Bifurcation and Chaos **19**: 1339–1350.

Kim, S.-Y. and B. Hu, 1998 Bifurcations and transitions to chaos in an inverted pendulum. Physical Review E **58**: 3028.

Kutuk, H. and S.-M. Kang, 1996 A field-programmable analog array (fpaa) using switched-capacitor techniques. In *1996 IEEE International Symposium on Circuits and Systems. Circuits and Systems Connecting the World. ISCAS 96*, volume 4, pp. 41–44, IEEE.

Kuznetsov, N. V., G. A. Leonov, M. V. Yuldashev, and R. V. Yuldashev, 2017 Hidden attractors in dynamical models of phase-locked loop circuits: limitations of simulation in matlab and spice. Communications in Nonlinear Science and Numerical Simulation **51**: 39–49.

Lai, Q., Z. Wan, P. D. K. Kuate, and H. Fotsin, 2020 Coexisting attractors, circuit implementation and synchronization control of a new chaotic system evolved from the simplest memristor chaotic circuit. Communications in Nonlinear Science and Numerical Simulation **89**: 105341.

Leutcho, G., J. Kengne, and L. K. Kengne, 2018 Dynamical analysis of a novel autonomous 4-d hyperjerk circuit with hyperbolic sine nonlinearity: chaos, antimonotonicity and a plethora of coexisting attractors. Chaos, Solitons & Fractals **107**: 67–87.

Leutcho, G. D. and J. Kengne, 2018 A unique chaotic snap system with a smoothly adjustable symmetry and nonlinearity: Chaos, offset-boosting, antimonotonicity, and coexisting multiple attractors. Chaos, Solitons & Fractals **113**: 275–293.

Levien, R. and S. Tan, 1993 Double pendulum: An experiment in chaos. American Journal of Physics **61**: 1038–1044.

Li, C., W. J.-C. Thio, J. C. Sprott, H. H.-C. Iu, and Y. Xu, 2018 Constructing infinitely many attractors in a programmable chaotic circuit. IEEE Access **6**: 29003–29012.

Li, T.-Y. and J. A. Yorke, 2004 Period three implies chaos. In *The theory of chaotic attractors*, pp. 77–84, Springer.

Li, X., P. Kallepalli, T. Mollik, M. R. E. U. Shougat, S. Kennedy, *et al.*, 2022 The pendulum adaptive frequency oscillator. Mechanical Systems and Signal Processing **179**: 109361.

Li, X., M. R. E. U. Shougat, S. Kennedy, C. Fendley, R. N. Dean, *et al.*, 2021a A four-state adaptive hopf oscillator. Plos one **16**: e0249131.

Li, X., M. R. E. U. Shougat, T. Mollik, A. N. Beal, R. N. Dean, *et al.*, 2021b Stochastic effects on a hopf adaptive frequency oscillator. Journal of Applied Physics **129**: 224901.

Luo, A. C. and F. Min, 2011 The chaotic synchronization of a controlled pendulum with a periodically forced, damped duffing oscillator. Communications in Nonlinear Science and Numerical Simulation **16**: 4704–4717.

Makarov, V., A. Koronovskii, V. Maksimenko, A. Hramov, O. Moskalenko, *et al.*, 2016 Emergence of a multilayer structure in adaptive networks of phase oscillators. Chaos, Solitons & Fractals **84**: 23–30.

Maleki, M. A., A. Ahmadi, S. V. A.-D. Makki, H. Soleimani, and M. Bavandpour, 2015 Networked adaptive non-linear oscillators: a digital synthesis and application. Circuits, Systems, and Signal Processing **34**: 483–512.

Métivier, D., L. Wetzel, and S. Gupta, 2020 Onset of synchronization in networks of second-order kuramoto oscillators with delayed coupling: Exact results and application to phase-locked loops. Physical Review Research **2**: 023183.

Miao, C., W. Luo, Y. Ma, W. Liu, and J. Xiao, 2014 A simple method to improve a torsion pendulum for studying chaos. European Journal of Physics **35**: 055012.

Munyaev, V. O., D. S. Khorkin, M. I. Bolotov, L. A. Smirnov, and G. V. Osipov, 2021 Appearance of chaos and hyperchaos in evolving pendulum network. Chaos: An Interdisciplinary Journal of Nonlinear Science **31**: 063106.

Nana, B., P. Woafo, and S. Domngang, 2009 Chaotic synchronization with experimental application to secure communications. Communications in nonlinear science and Numerical Simulation **14**: 2266–2276.

Nunez-Yepez, H., A. Salas-Brito, C. Vargas, and L. Vicente, 1990 Onset of chaos in an extensible pendulum. Physics Letters A **145**: 101–105.

Nwachioma, C. and J. H. Pérez-Cruz, 2021 Analysis of a new chaotic system, electronic realization and use in navigation of differential drive mobile robot. Chaos, Solitons & Fractals **144**: 110684.

Olson, C., J. Nichols, J. Michalowicz, and F. Bucholtz, 2011 Signal design using nonlinear oscillators and evolutionary algorithms: Application to phase-locked loop disruption. Chaos: An Interdisciplinary Journal of Nonlinear Science **21**: 023136.

Ouannas, A., Z. Odibat, and T. Hayat, 2017 Fractional analysis of co-existence of some types of chaos synchronization. Chaos, Solitons & Fractals **105**: 215–223.

Paul, B. and T. Banerjee, 2019 Chimeras in digital phase-locked loops. Chaos: An Interdisciplinary Journal of Nonlinear Science **29**: 013102.

Pereira-Pinto, F. H. I., A. M. Ferreira, and M. A. Savi, 2004 Chaos control in a nonlinear pendulum using a semi-continuous method. Chaos, Solitons & Fractals **22**: 653–668.

Perkins, E., 2019 Restricted normal mode analysis and chaotic response of p-mode intrinsic localized mode. Nonlinear Dynamics **97**: 955–966.

Perkins, E. and T. Fitzgerald, 2018 Continuation method on cumulant neglect equations. Journal of Computational and Nonlinear Dynamics **13**.

Pham, V.-T., S. Jafari, C. Volos, and L. Fortuna, 2019 Simulation and experimental implementation of a line–equilibrium system without linear term. Chaos, Solitons & Fractals **120**: 213–221.

Piqueira, J. R. C., 2017 Hopf bifurcation and chaos in a third-order phase-locked loop. Communications in Nonlinear Science and Numerical Simulation **42**: 178–186.

Rhea, B. K., R. C. Harrison, F. T. Werner, E. Perkins, and R. N. Dean, 2020 Approximating an exactly solvable chaotic oscillator using a colpitts oscillator circuit. IEEE Transactions on Circuits and Systems II: Express Briefs **68**: 1028–1032.

Ricco, R. A., A. Verly, and G. F. V. Amaral, 2016 A circuit for automatic measurement of bifurcation diagram in nonlinear electronic oscillators. IEEE Latin America Transactions **14**: 3042–3047.

Righetti, L., J. Buchli, and A. J. Ijspeert, 2006 Dynamic hebbian learning in adaptive frequency oscillators. Physica D: Nonlinear Phenomena **216**: 269–281.

Righetti, L., J. Buchli, and A. J. Ijspeert, 2009 Adaptive frequency oscillators and applications. The Open Cybernetics & Systemics Journal **3**.

Shinbrot, T., C. Grebogi, J. Wisdom, and J. A. Yorke, 1992 Chaos in a double pendulum. American Journal of Physics **60**: 491–499.

Shougat, M., R. E. Ul, X. Li, T. Mollik, and E. Perkins, 2021a An information theoretic study of a duffing oscillator array reservoir computer. Journal of Computational and Nonlinear Dynamics **16**.

Shougat, M. R. E. U., X. Li, T. Mollik, and E. Perkins, 2021b A hopf physical reservoir computer. Scientific Reports **11**: 1–13.

Shougat, M. R. E. U., X. Li, and E. Perkins, 2022 Dynamic effects on reservoir computing with a hopf oscillator. Physical Review E **105**: 044212.

Silva-Juárez, A., E. Tlelo-Cuautle, L. G. de la Fraga, and R. Li, 2020 Fpaa-based implementation of fractional-order chaotic oscillators using first-order active filter blocks. Journal of advanced research .

Stachowiak, T. and T. Okada, 2006 A numerical analysis of chaos in the double pendulum. Chaos, Solitons & Fractals **29**: 417–422.

Tlelo-Cuautle, E., A. D. Pano-Azucena, O. Guillén-Fernández, and A. Silva-Juárez, 2020 *Analog/digital implementation of fractional order chaotic circuits and applications*. Springer.

Viana Jr, E. R., R. M. Rubinger, H. A. Albuquerque, A. G. de Oliveira, and G. M. Ribeiro, 2010 High-resolution parameter space of an experimental chaotic circuit. Chaos: An Interdisciplinary Journal of Nonlinear Science **20**: 023110.

Wang, R. and Z. Jing, 2004 Chaos control of chaotic pendulum system. Chaos, Solitons & Fractals **21**: 201–207.

Xu, J.-q. and G. Jin, 2012 Synchronization of parallel-connected spin-transfer oscillators via magnetic feedback.

Xu, X., M. Wiercigroch, and M. Cartmell, 2005 Rotating orbits of a parametrically-excited pendulum. Chaos, Solitons & Fractals **23**: 1537–1548.

Zhao, Y.-B., D.-Q. Wei, and X.-S. Luo, 2009 Study on chaos control of second-order non-autonomous phase-locked loop based on state observer. Chaos, Solitons & Fractals **39**: 1817–1822.

How to cite this article: Li, X., Beal, A. N., Dean, R. N., and Perkins, E. Chaos in a Pendulum Adaptive Frequency Oscillator Circuit Experiment. *Chaos Theory and Applications*, 5(1), 11-19, 2023.

CHAOS
Theory and Applications
in Applied Sciences and Engineering

e-ISSN: 2687-4539
RESEARCH ARTICLE
Vol.5 / No.1 / 2023 / pp.20-26
https://doi.org/10.51537/chaos.1183849

Respiratory Diseases Prediction from a Novel Chaotic System

Mohammed Mansour *,[1], **Turker Berk Donmez** *,[2], **Mustafa Kutlu** *,[3] **and Chris Freeman** β,[4]
*Mechatronics Engineering Department, Sakarya University of Applied Sciences, Türkiye, βElectronics and Computer Science, University of Southampton, UK.

ABSTRACT

Pandemics can have a significant impact on international health systems. Researchers have found that there is a correlation between weather conditions and respiratory diseases. This paper focuses on the non-linear analysis of respiratory diseases and their relationship to weather conditions. Chaos events may appear random, but they may actually have underlying patterns. Edward Lorenz referred to this phenomenon in the context of weather conditions as the butterfly effect. This inspired us to define a chaotic system that could capture the properties of respiratory diseases. The chaotic analysis was performed and was related to the difference in the daily number of cases received from real data. Stability analysis was conducted to determine the stability of the system and it was found that the new chaotic system was unstable. Lyapunov exponent analysis was performed and found that the new chaotic system had Lyapunov exponents of (+, 0, -, -). A dynamic neural architecture for input-output modeling of nonlinear dynamic systems was developed to analyze the findings from the chaotic system and real data. A NARX network with inputs (maximum temperature, pressure, and humidity) and one output was used to to overcome any delay effects and analyze derived variables and real data (patients number). Upon solving the system equations, it was found that the correlation between the daily predicted number of patients and the solution of the new chaotic equation was 90.16%. In the future, this equation could be implemented in a real-time warning system for use by national health services.

KEYWORDS
Chaos
Chaotic systems
Respiratory
Diseases
Weather

INTRODUCTION

Seasonal climatic conditions and respiratory diseases such as influenza are believed to be related to each other. In fact, certain meteorological factors, such as temperature and relative humidity, and the incidence of some respiratory viruses have been hypothesized to have opposite relationships or those found in temperate regions. This may be because the majority of virus transmission takes place indoors, in air-conditioned spaces, which are cooler and less humid environments that are more conducive to airborne virus survival and transmission. In order to better plan hospital services for admissions, it is still necessary to comprehend the relationship between respiratory disorders, respiratory virus occurrence, and meteorological conditions in various countries. This is especially important now because viruses have just started to appear.

While investigating a meteorological problem, Lorenz (1963) stumbled upon a phenomenon that would become known as the "Butterfly Effect" (Kuhfittig and Davis 1990). Lorenz, a mathematician and meteorologist, was studying the behavior of weather systems using a simplified model of atmospheric convection. As he varied the initial conditions of his model, he noticed that small changes could lead to dramatically different outcomes in the long-term behavior of the system. This idea, that seemingly minor perturbations can have large and potentially unpredictable conse-

Manuscript received: 4 October 2022,
Revised: 6 January 2023,
Accepted: 11 January 2023.

[1] mmansour755@gmail.com (**Corresponding Author**)
[2] turkerberkdonmez@yahoo.com
[3] mkutlu@sakarya.edu.tr
[4] cf@ecs.soton.ac.uk

quences, came to be known as the Butterfly Effect and has had a significant impact on the field of chaos theory (Gleick 1987; Holbrook 2003). The concept has been widely applied to a range of systems, including economics, biology, and even social networks, and has helped to shed light on the inherent unpredictability of certain types of complex systems.

In mathematics, chaos theory is a branch of study that investigates the behavior of dynamic systems that are highly sensitive to initial conditions. Non-linear systems that are chaotic or chaotic systems are sensitive to their initial conditions. The non-linearity systems have a specific case known as chaos. This line succinctly expresses the definition of chaos: chaos is the regularity of irregularity. Chaotic systems are complicated systems due to their nonlinear and deterministic nonlinear dynamical systems. Van der Pol and Van der Mark referred to the anarchy as noise. Dynamical systems that exhibit complicated behavior are considered chaotic systems (Van der Pol and Van Der Mark 1927; Kennedy 1995; Siegelmann and Fishman 1998; Akgül *et al.* 2022).

Chaotic systems exhibit the following characteristics: unpredictability in the time dimension, accuracy in the initial circumstances, an infinite number of distinct periodic oscillations, a broad power spectrum that resembles noise, and positive Lyapunov (Kia 2011; de la Fraga *et al.* 2012). Numerous chaotic systems, including Lorenz, Rikitake, Rossler, Sprott, Chen, Pehlivan and Akgul (Rikitake 1958; Rössler 1976; Sprott 1994; Chen and Ueta 1999; Akgul *et al.* 2016), have been introduced up until this point.

One way to study such systems is through the use of nonlinear differential equations, which are called "chaos equations." The solutions to these equations often exhibit complex and seemingly random behavior, giving rise to the term "chaos." However, despite their apparent randomness, the solutions of chaos equations are actually deterministic, meaning that they are completely determined by the initial conditions and the underlying equations. In other words, given the same initial conditions and equation, the system will always evolve in the same way. Following the development of the mathematical representation of chaos, it can be used in a wide range of fields, including engineering, computing, communications, biology and medicine, management and finance, consumer electronics (Ditto and Munakata 1995; Hilborn *et al.* 2000; Banerjee *et al.* 2012; Jun 2022; Yavari *et al.* 2022).

Respiratory diseases, such as asthma and chronic obstructive pulmonary disease (COPD), can be affected by weather conditions (Ayres *et al.* 2009; D'Amato *et al.* 2014, 2016; Mirsaeidi *et al.* 2016; Duan *et al.* 2020; Joshi *et al.* 2020). Cold air can cause the airways to narrow, leading to difficulty breathing and increased symptoms for those with respiratory conditions. Conversely, warm and humid air can also worsen respiratory symptoms, as it can make it more difficult for mucus to clear from the airways. Pollen and other allergens, which are more prevalent in certain weather conditions, can also trigger respiratory symptoms. It is important for individuals with respiratory conditions to pay attention to weather forecasts and take necessary precautions, such as carrying medications and wearing a mask, when conditions may worsen their symptoms. Cold air can cause the airways to narrow, leading to difficulty breathing and increased symptoms for those with respiratory conditions. Conversely, warm and humid air can also worsen respiratory symptoms, as it can make it more difficult for mucus to clear from the airways. Pollen and other allergens, which are more prevalent in certain weather conditions, can also trigger respiratory symptoms.

In this paper, we aim to investigate the feasibility of using the Lorenz equation and numerical methods, such as the Runge-Kutta method, to predict the number of patients with respiratory diseases based on weather data. To achieve this goal, a new chaotic equation will be derive and solved using the Runge-Kutta method. We will then use the results of our analysis to discuss the potential of this approach for predicting respiratory disease outbreaks and improving hospital planning. The significance of this research lies in the fact that it presents a novel chaotic system that can successfully predict the presence of respiratory diseases in patients, which has not been achieved in previous studies. This breakthrough holds the potential to greatly improve the diagnosis and treatment of respiratory conditions, as it allows for early identification of at-risk individuals and targeted interventions. As such, the findings of this study have the potential to significantly impact the field of healthcare and contribute to the betterment of public health.

The paper is divided into five sections, with the introduction being the first section. Section 2 will review the existing literature on the relationship between weather conditions and respiratory diseases, specifically influenza. Section 3 will cover chaos theory and the new chaotic equation that has been derived for this research. This section will describe the principles of chaos theory, the Lorenz equation, and the process of deriving the new chaotic equation. Section 4 will present the results of the study, including any analyses or simulations that were conducted using the new chaotic equation. The final section will provide conclusions based on the findings of the study and suggest directions for future research.

RELATED WORKS

A range of dynamic system behaviors are sensitive to initial conditions and can be unpredictable to some extent. In the early 20th century, Poincaré addressed the issue of weather forecasting. After Lorenz revisited this problem in the late 1960s, a significant portion of the scientific community began to focus on such phenomena, leading to the emergence of "Chaos Science" as a new branch of science. In 1963, Lorenz discovered new types of erratic oscillations while modeling fluid heat dissipation in the atmosphere to forecast weather patterns (Lorenz 1963). He gathered his previous solutions while taking a coffee break and returned to his computer to resolve the 12 ordinary differential equations he was using. When he returned, he found that the new solutions had reached a significantly different position than the previous ones. In other words, he discovered that the steady state exhibits new irregular oscillations with a significantly different appearance when the numerical integration is repeated with minimal variation in the initial conditions.

Lorenz, a meteorologist, was interested in mathematics and contributed to the development of the new field of chaos, a significant topic in the 20th century. He published his findings in a meteorology journal (Lorenz 1963). It took a decade for physicists and mathematicians to fully understand the significance of Lorenz's discovery. The Lorenz system has received significant attention and is considered the first example of how distributed systems can behave chaotically.

Following this, Lorenz developed equations for weather forecasting. In the field of chaos theory, numerous studies have been published in the last two decades about various systems, with Lorenz's system serving as a foundation for this research. This section therefore focuses on understanding the relationship between weather conditions and respiratory disease in order to develop a new chaotic system. In the next section, we will delve into the details of weather and respiratory diseases.

Weather Conditions and Respiratory Diseases

There are numerous published studies that describe the effect of weather conditions on respiratory infections, but no mathematical system has been developed to understand this association. These studies generally suggest that the relationship between infections and seasonal climate is causal. This was true to some extent when people lived and worked outdoors, with minimal protection from even the most extreme climatic conditions. However, the industrial revolution changed this. Many agricultural workers moved to factories and offices, and the widespread adoption of central heating and increasingly airtight, insulated buildings led to a further decoupling of daily and seasonal outdoor climate fluctuations. This separation is particularly noticeable in winter, when internal heating leads to a large deviation in the internal and external temperature and relative humidity (RH), but does not affect the absolute humidity (AH) (Quinn and Shaman 2017).

Nishimura et al. (2021) found that the average ambient temperature during daily working hours may have a stronger correlation with the number of patients transported by ambulance from outdoor sites than the daily average temperature or the daily highest temperature (Nishimura *et al.* 2021). The study results showed that patients transported from indoor environments are affected by previous environmental conditions for about 50 days, while those transported from outdoor sites are affected by a relatively shorter period of time (20 days), which may be due to heat adaptation. These findings provide a better understanding of the various factors that can lead to more accurate predictions of the number of heat-related patients based on weather forecasts.

A study by Lee et al. (2022) involving 525,579 individuals found that various weather and air quality factors affected the respiratory illnesses of people who visited emergency rooms (Lee *et al.* 2022). The majority of the patients with respiratory diseases had acute upper respiratory infections (J00-J06), influenza (J09-J11), and pneumonia (J12-J18), with PM10 temperature and steam pressure having the greatest effects. Pneumonia [J12–J18], acute upper respiratory infections [J00–J06], and chronic lower respiratory disorders [J40–J47] were the top three major causes of admission to the emergency room .

Bhimala et al. (2022) found that in different parts of India, specific humidity has a strong positive association, while maximum temperature has a negative correlation and minimum temperature has a positive correlation (Bhimala *et al.* 2022).

METHODOLOGY

This retrospective study aims to establish a chaotic equation that links weather and clinical data. To do so, the study first collected weather and patient data, and then applied Lorenz system to interpret the new variable. The stability of the new system was then evaluated using lyapunov analysis. To assess the correlation between the actual values and the results predicted by the new chaos equations, a NARX network was implemented to account for any delay effects and to predict the daily number of patients using real-time data.

Weather Data

Daily meteorological data, including maximum and minimum temperatures, relative humidity, pressure, and sunshine duration, were collected from the Meteorological Services Division. These parameters are illustrated in Figure 1.

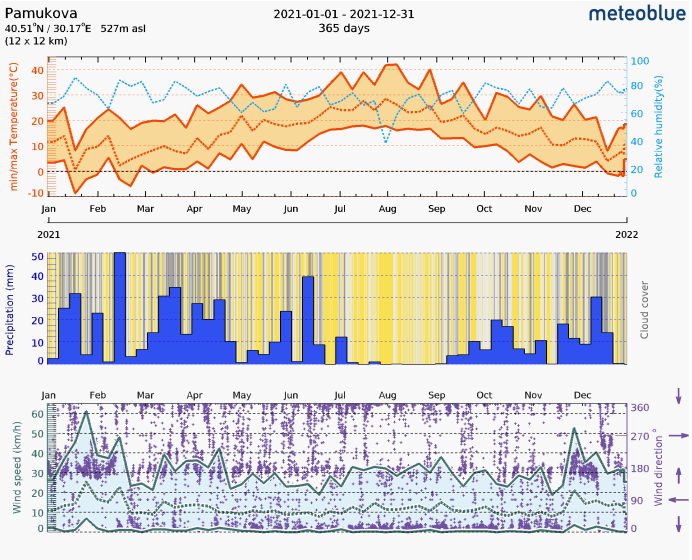

Figure 1 Weather data from Pamukova Region

Patient Data

The data for this study was collected from January 1, 2021 to December 31, 2021 with the ethical approval of Sakarya University (E-71522473-050.01.04-15185-157). The study group consisted of cases that occurred in the Pamukova District of Sakarya Province. A team of experienced medical professionals gathered the daily total of patients diagnosed with upper respiratory tract infections (J09-J18) from the Pamukova Family Medicine Center. Over the course of the study period, 10821 patients sought medical attention for upper respiratory illnesses.

Interpretation of New Variable

Edward Lorenz created the Lorenz system in 1963 as a more straightforward mathematical representation of atmospheric convection Lorenz (1963). The Lorenz chaotic system equations are well known and take the form of:

$$\begin{aligned} \dot{X} &= \alpha(Y - X) \\ \dot{Y} &= X(\beta - Z) - Y \\ \dot{Z} &= X * Y - \gamma Z \end{aligned} \tag{1}$$

With constant α = 10, β=28 and γ= 8/3. The initial conditions of the system are X(0) = 0, Y(0) = -1 and Z(0) = 0. We observe the chaotic behaviour, shown in Figure 2.

From this system, we assumed that there is an interpreted variable as a description of number of respiratory cases (w). This variable has the following:

1. Negative correlation with air pressure (Vitkina *et al.* 2019),
2. positive correlation with the average ambient temperature (Nishimura *et al.* 2021) and,
3. Negative correlation with the absolute humidity (Quinn and Shaman 2017).

The number of patients is also delayed due to the incubation period of diseases. Therefore, the variable is affected by the

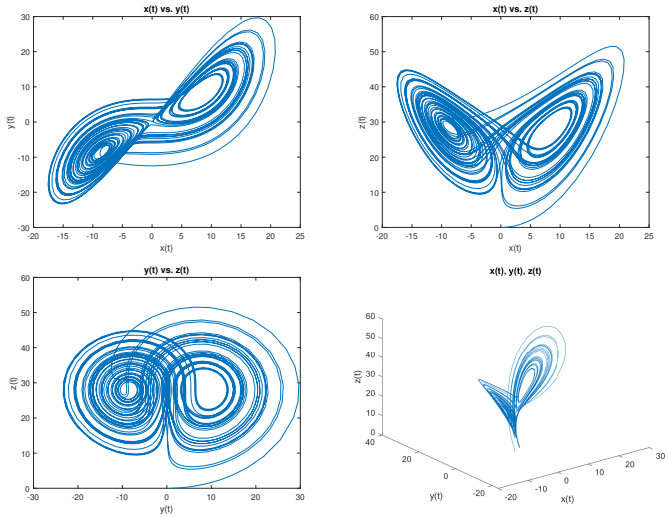

Figure 2 Phase portraits in the (x, y), (x, z), (y, z) and (x, y, z)

previous and current states. The newly found chaotic system are as follows:

$$\begin{aligned} \dot{X} &= \alpha(Y - X), \\ \dot{Y} &= X(\beta - Z) - Y, \\ \dot{Z} &= X * Y - \gamma Z \\ \dot{W} &= X * Y - \delta(\alpha * W + Y) - \delta * Z \end{aligned} \tag{2}$$

with constant α = 10, β=28, γ= 8/3, $\delta = 5$. The initial conditions of the system are X(0) = 10, Y(0) = -10, Z(0) = 25 and W(0)=0. The dynamic system simulation of the new chaotic system are shown in Figure 3.

System stability's analysis

Letting the system's derivatives equal to zero as:

$$\begin{aligned} 0 &= \alpha(Y - X), \\ 0 &= X(\beta - Z) - Y, \\ 0 &= X * Y - \gamma Z \\ 0 &= X * Y - \delta(\alpha * W + Y) - \delta * Z \end{aligned} \tag{3}$$

The equilibrium points are (0, 0.0000 - 8.4853i, 0.0000 + 8.4853i), (0, 0.0000 - 8.4853i, 0.0000 + 8.4853i), (0, -27, -27) and (0, -1.2600 - 0.8485i, -1.2600 + 0.8485i) and the eigenvalues of the first equilibrium point are: -50.0000 + 0.0000i, -2.6670 + 0.0000i, -1.2164 - 9.9045i, -9.7836 + 9.9045i; the first point is unstable. The eigenvalues of the second equilibrium point are: -50.0000 + 0.0000i, -2.6670 + 0.0000i, -1.2164 - 9.9045i and -9.7836 + 9.9045i; the second point is unstable. The eigenvalues of the third equilibrium point are: -50.0000, -2.6670, 8.2931 and -19.2931; the third point is unstable. The eigen values of the forth equilibrium point are: -50.0000 + 0.0000i, -2.6670 + 0.0000i, -4.9833 + 8.2108i, and -6.0167 - 8.2108i; the forth point is unstable.This analysis shows that the new system is unstable and may exhibit chaotic behavior, which can be confirmed by checking the Lyapunov exponents.

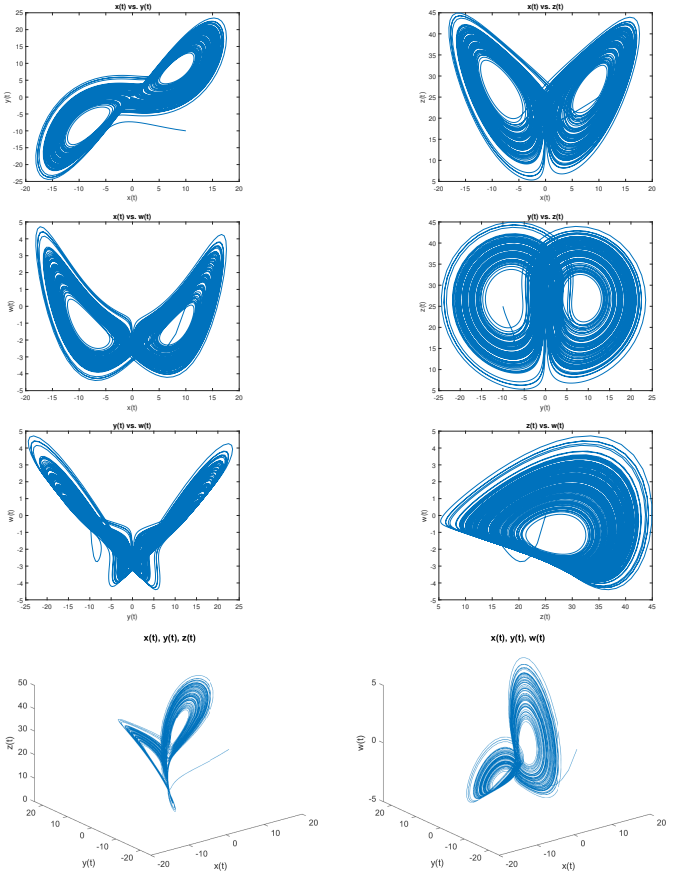

Figure 3 Phase portraits in the (x, y), (x, z), (x, w), (y, z), (y, w), (z, w), (x, y, z), and (x, y, w)

Lyapunov exponents analysis of Chaotic system

Lyapunov exponents are an important criterion in the analysis of the behavior of a dynamic system because they provide characteristic information about the system and serve as a measure of chaotic behavior (Abarbanel *et al.* 1991; Kinsner 2006; Aziz *et al.* 2021; Qiu *et al.* 2023). If the behavior of a dynamic system is sensitive to initial conditions, then as time progresses, orbits close to each other in the phase space will rapidly diverge. This indicates that the system is becoming dynamically unstable. However, it is often difficult to make this determination because most trajectories of the system are unknown. Nevertheless, it is possible to express the orbits that can be known.

Lyapunov superposition lambda gives a measure of the sensitivity to initial conditions and is defined as the average of the local separation degrees of neighboring curves within the phase space. If lambda is negative, different starting conditions tend to give the same output values, meaning that the development is not chaotic. If lambda is positive, different initial values give different output values, indicating that the movement is chaotic.
The fundamental characteristic of a chaotic system is its dependence on initial conditions. Even if the two different initial states are very close to each other, the orbits formed at these two points diverge from each other exponentially. Lyapunov exponents are used to measure the sensitive dependence of initial states in chaotic systems.

Lyapunov exponents are initially used to measure the distance between very small discrete trajectories. They are a generaliza-

tion of the eigenvalues and characteristic multipliers of a periodic solution at an equilibrium point and are used to determine the steady-state stability of semiperiodic and chaotic solutions. A dynamic system is considered chaotic if its sum contains at least one positive Lyapunov exponent. The Lyapunov exponents of a chaotic trajectory have at least one positive lambda, which distinguishes a strange attractor from other types of steady-state behavior.

Nonlinear Autoregressive Network with Exogenous Inputs (NARX)

To analyze results from chaotic systems and real data, a popular dynamic neural design for input-output modeling of nonlinear dynamic systems, the NARX network, is implemented. The NARX network is a time-delayed feedforward neural network for time series estimation. In theory, NARX networks can be used in place of traditional recurrent networks with no computational cost and are at least as effective as Turing machines (Lin *et al.* 1996; Siegelmann *et al.* 1997; Diaconescu 2008). Therefore, they can be used to predict chaotic equations (Diaconescu 2008; Martínez-García *et al.* 2008).

In this study, a NARX network with 3 inputs (maximum temperature, pressure, and humidity) and one output (number of patients) was used to analyze derived variables and real data. The network had 10 hidden layers and an incubation period of 5 days was included to account for any variations due to delays. The final structure of the NARX network is depicted in Figure 4.

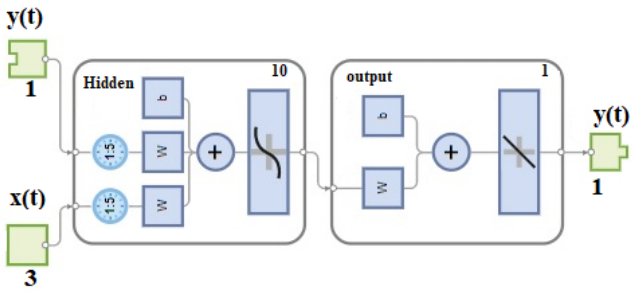

Figure 4 NARX Structure

RESULTS AND DISCUSSION

Results

Respiratory disorders, such as asthma and chronic obstructive pulmonary disease, are a major public health concern, as they can greatly impact an individual's quality of life and are a leading cause of morbidity and mortality worldwide. In this study, we aim to investigate the feasibility of using weather data to predict the prevalence of respiratory disorders. To accomplish this, we will utilize the Lorenz equation and numerical techniques, specifically the Runge-Kutta method, to derive and solve a new chaotic equation. The Runge-Kutta method is a numerical technique that is commonly used to solve differential equations. It is a widely used method that is known for its accuracy and stability, and has been applied to a variety of problems in science and engineering. In this study, we will use the Runge-Kutta method to solve the new chaotic equation that we will derive using the Lorenz equation and weather data.

Our objective is to use the Lorenz equation and the Runge-Kutta method to predict the prevalence of respiratory disorders based on weather data. By using these tools, we hope to gain a better understanding of the relationship between weather and respiratory disorders, and to develop more accurate and reliable methods for predicting the occurrence of these conditions. We believe that this research has the potential to significantly improve the management and treatment of respiratory disorders, and to ultimately improve the health and well-being of individuals affected by these conditions.

In order to give an example for the model detailed in the paper, a scenario is set with initial conditions and is expected to meet the actual data. In a three-dimensional system, the only possible case for Lyapunov exponents is the type (+, 0, -) to have chaotic behavior. For Lorenz Equation, they are $\lambda_1 > 0$, $\lambda_2 = 0$, *and* $\lambda_3 < 0$. In a four-dimensional system, the possible cases for Lyapunov exponents are the type (+, +, 0, -) and (+, 0, -, -). If type (+, +, 0, -), $\lambda_1 > 0$, $\lambda_2 > 0$, $\lambda_3 = 0$, *and* $\lambda_4 < 0$, is called hyperchaos.

The Lyapunov exponents of the system were analyzed to investigate its chaotic behavior. The results of the analysis are shown below and depicted in Figure 5. The Lyapunov exponents of the system are (+, 0, -, -)."

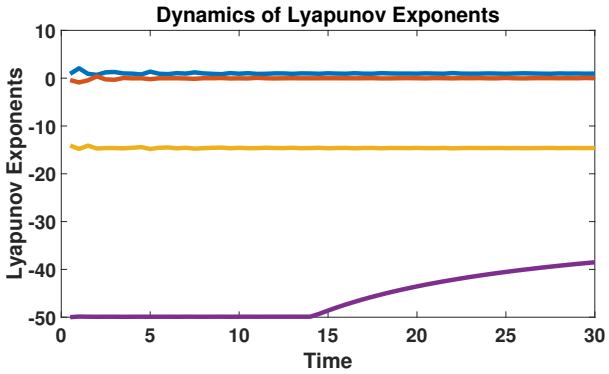

Figure 5 Lyapunov exponents

In this paper, we utilized the Lorenz equation and developed a new time series analysis, which is presented in Figure 6. However, as shown in Figure 7, the daily difference between the number of respiratory disease cases predicted by the chaotic equation and the actual number of cases is not similar to the difference between weather forecast and real weather data. This is due to the fact that the initial conditions for the chaotic equation and the weather data are not the same. To analyze the correlation between the real values and the results from the chaotic equation, we implemented a NARX network to account for any delay effects. The correlation between the number of cases predicted by the chaotic equation and the actual number of cases was found to be 90.16.

There is a well-established seasonality to the occurrence of influenza, with a marked peak in the colder winter months. However, in tropical regions, the seasonality of influenza is less well-defined, with detectable background activity throughout the year. In our study, we have developed a new chaotic model to better understand the patterns and underlying causes of respiratory diseases in these regions.

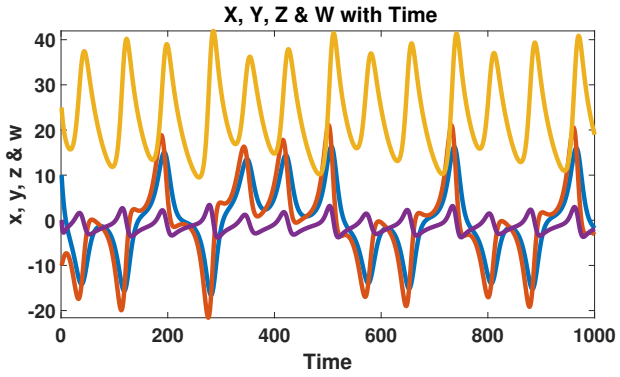

Figure 6 Time Series Analysis Results

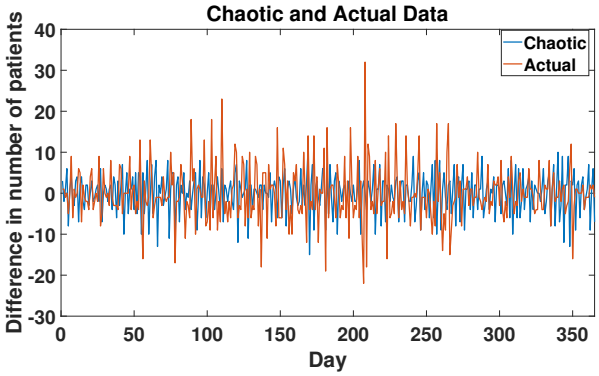

Figure 7 Actual and Equation Results

Discussion

This study used weather data to forecast the number of individuals who will have respiratory disease. This was achieved by developing a new chaos equation using patient data and weather predictions that have been gathered. The findings of this study agree with previous studies that have linked weather data to respiratory disease cases (Lee *et al.* 2022; Bhat *et al.* 2021).

The study of the relationship between weather patterns and respiratory illness led to the development of a novel chaotic system. According to the findings of this analysis, the system has Lyapunov exponents of (+, 0, -, -). A NARX network was then used to assess the created variables and real-world data, with a focus on counting the number of patients with respiratory illnesses. The daily projected patient count and the output of the new chaotic equation had a strong correlation of 90.16% after the chaotic system's equations were solved. As a result, the findings of this study are in line with those of other studies that have evaluated the effectiveness of time series in forecasting the occurrence of respiratory diseases (Shaman and Kohn 2009; Lee *et al.* 2022). This study reported a higher performance measure, with a correlation of 90.16% between real patient cases and predicted data.

Several methods have been identified in the literature for dealing with respiratory diseases. In a study (Lee *et al.* 2022), data from 525,579 participants was analyzed, and it was found that multiple variables of weather and air pollution influenced the respiratory diseases of patients who visited emergency departments. The majority of the patients with respiratory disease had acute upper respiratory infections. Similarly, another study (Xirasagar *et al.* 2006) found that the decline in temperature during colder months and the decrease in sunshine duration had a negative impact on respiratory diseases.

According to our research, predicting respiratory diseases from weather data could potentially be useful for hospital planning, as it could allow hospitals to anticipate increases in patient volume and adjust their staffing and resource allocation accordingly. It is important to have such a system that predict respiratory diseases from weather data.

CONCLUSIONS

There is a significant body of literature that explores the relationships between various fields, such as physics, mathematics, electrics, and electronics. These studies often involve the development and analysis of mathematical models that describe the behavior of chaotic systems. Scientists, engineers, and researchers may rely on these models in order to design and build new chaotic systems with complex and varied dynamic behaviors. However, the physical implementation of these models can be quite challenging due to the need to carefully consider and control initial conditions, as well as the impact of nonlinear effects. In other words, the real-world realization of chaotic systems based on these equations can be quite difficult and complex to achieve.

In this study, a new chaotic system was derived that investigates the connection between weather patterns and respiratory illness. To verify the chaotic behavior of the system, a Lyapunov analysis was performed. The results of this analysis indicated that the system had Lyapunov exponents of (+, 0, -, -). Next, the generated variables and real-world data were analyzed using a NARX network, specifically examining the number of patients suffering from respiratory illness. Upon resolving the equations of the chaotic system, it was found that there was a strong correlation of 90.16 between the daily anticipated patient count and the output of the new chaotic equation. It is anticipated that in the future, this model will be further refined and applied to different initial conditions depending on the local climate.

Conflicts of interest

The authors declare that there is no conflict of interest regarding the publication of this paper.

Availability of data and material

The data for this study was collected from January 1, 2021 to December 31, 2021 with the ethical approval of Sakarya University (E-71522473-050.01.04-15185-157). If you require raw data please contact corresponding author.

LITERATURE CITED

Abarbanel, H. D., R. Brown, and M. Kennel, 1991 Lyapunov exponents in chaotic systems: their importance and their evaluation using observed data. International Journal of Modern Physics B **5**: 1347–1375.

Akgül, A., E. E. Şahin, and F. Y. Şenol, 2022 Blockchain-based cryptocurrency price prediction with chaos theory, onchain analysis, sentiment analysis and fundamental-technical analysis. Chaos Theory and Applications **4**: 157 – 168.

Akgul, A., S. Hussain, and I. Pehlivan, 2016 A new three-dimensional chaotic system, its dynamical analysis and electronic circuit applications. Optik **127**: 7062–7071.

Ayres, J., B. Forsberg, I. Annesi-Maesano, R. Dey, K. Ebi, *et al.*, 2009 Climate change and respiratory disease: European respiratory society position statement. European Respiratory Journal **34**: 295–302.

Aziz, M. M. *et al.*, 2021 Stability, chaos diagnose and adaptive control of two dimensional discrete-time dynamical system. Open Access Library Journal **8**: 1.

Banerjee, S., L. Rondoni, and M. Mitra, 2012 *Applications of Chaos and Nonlinear Dynamics in Science and Engineering-Vol. 2*. Springer.

Bhat, G. S., N. Shankar, D. Kim, D. J. Song, S. Seo, *et al.*, 2021 Machine learning-based asthma risk prediction using iot and smartphone applications. IEEE Access **9**: 118708–118715.

Bhimala, K. R., G. K. Patra, R. Mopuri, and S. R. Mutheneni, 2022 Prediction of covid-19 cases using the weather integrated deep learning approach for india. Transboundary and Emerging Diseases **69**: 1349–1363.

Chen, G. and T. Ueta, 1999 Yet another chaotic attractor. International Journal of Bifurcation and chaos **9**: 1465–1466.

D'Amato, G., L. Cecchi, M. D'Amato, and I. Annesi-Maesano, 2014 Climate change and respiratory diseases.

D'Amato, G., C. Vitale, M. Lanza, A. Molino, and M. D'Amato, 2016 Climate change, air pollution, and allergic respiratory diseases: an update. Current opinion in allergy and clinical immunology **16**: 434–440.

de la Fraga, L. G., E. Tlelo-Cuautle, V. Carbajal-Gómez, and J. Munoz-Pacheco, 2012 On maximizing positive lyapunov exponents in a chaotic oscillator with heuristics. Revista mexicana de física **58**: 274–281.

Diaconescu, E., 2008 The use of narx neural networks to predict chaotic time series. Wseas Transactions on computer research **3**: 182–191.

Ditto, W. and T. Munakata, 1995 Principles and applications of chaotic systems. Communications of the ACM **38**: 96–102.

Duan, R.-R., K. Hao, and T. Yang, 2020 Air pollution and chronic obstructive pulmonary disease. Chronic diseases and translational medicine **6**: 260–269.

Gleick, J., 1987 The butterfly effect. Chaos: Making a New Science pp. 9–32.

Hilborn, R. C. *et al.*, 2000 *Chaos and nonlinear dynamics: an introduction for scientists and engineers*. Oxford University Press on Demand.

Holbrook, M. B., 2003 Adventures in complexity: An essay on dynamic open complex adaptive systems, butterfly effects, self-organizing order, coevolution, the ecological perspective, fitness landscapes, market spaces, emergent beauty at the edge of chaos, and all that jazz. Academy of Marketing Science Review **6**: 1–184.

Joshi, M., H. Goraya, A. Joshi, and T. Bartter, 2020 Climate change and respiratory diseases: a 2020 perspective. Current Opinion in Pulmonary Medicine **26**: 119–127.

Jun, M., 2022 Chaos theory and applications: the physical evidence, mechanism are important in chaotic systems. Chaos Theory and Applications **4**: 1–3.

Kennedy, M. P., 1995 Experimental chaos from autonomous electronic circuits. Philosophical Transactions of the Royal Society of London. Series A: Physical and Engineering Sciences **353**: 13–32.

Kia, B., 2011 Chaos computing: from theory to application. Technical report, Arizona State University.

Kinsner, W., 2006 Characterizing chaos through lyapunov metrics. IEEE Transactions on Systems, Man, and Cybernetics, Part C (Applications and Reviews) **36**: 141–151.

Kuhfittig, P. K. and T. W. Davis, 1990 Predicting the unpredictable. Cost Engineering **32**: 7.

Lee, E. S., J.-Y. Kim, Y.-H. Yoon, S. B. Kim, H. Kahng, *et al.*, 2022 A machine learning-based study of the effects of air pollution and weather in respiratory disease patients visiting emergency departments. Emergency Medicine International **2022**.

Lin, T., B. G. Horne, P. Tino, and C. L. Giles, 1996 Learning long-term dependencies in narx recurrent neural networks. IEEE Transactions on Neural Networks **7**: 1329–1338.

Lorenz, E. N., 1963 Deterministic nonperiodic flow. Journal of atmospheric sciences **20**: 130–141.

Martínez-García, J. A., A. M. González-Zapata, E. J. Rechy-Ramírez, and E. Tlelo-Cuautle, 2008 On the prediction of chaotic time series using neural networks. Chaos Theory and Applications **4**: 94–103.

Mirsaeidi, M., H. Motahari, M. Taghizadeh Khamesi, A. Sharifi, M. Campos, *et al.*, 2016 Climate change and respiratory infections. Annals of the American Thoracic Society **13**: 1223–1230.

Nishimura, T., E. A. Rashed, S. Kodera, H. Shirakami, R. Kawaguchi, *et al.*, 2021 Social implementation and intervention with estimated morbidity of heat-related illnesses from weather data: A case study from nagoya city, japan. Sustainable Cities and Society **74**: 103203.

Qiu, H., X. Xu, Z. Jiang, K. Sun, and C. Cao, 2023 Dynamical behaviors, circuit design, and synchronization of a novel symmetric chaotic system with coexisting attractors. Scientific Reports **13**: 1893.

Quinn, A. and J. Shaman, 2017 Health symptoms in relation to temperature, humidity, and self-reported perceptions of climate in new york city residential environments. International journal of biometeorology **61**: 1209–1220.

Rikitake, T., 1958 Oscillations of a system of disk dynamos. In *Mathematical Proceedings of the Cambridge Philosophical Society*, volume 54, pp. 89–105, Cambridge University Press.

Rössler, O. E., 1976 An equation for continuous chaos. Physics Letters A **57**: 397–398.

Shaman, J. and M. Kohn, 2009 Absolute humidity modulates influenza survival, transmission, and seasonality. Proceedings of the National Academy of Sciences **106**: 3243–3248.

Siegelmann, H. T. and S. Fishman, 1998 Analog computation with dynamical systems. Physica D: Nonlinear Phenomena **120**: 214–235.

Siegelmann, H. T., B. G. Horne, and C. L. Giles, 1997 Computational capabilities of recurrent narx neural networks. IEEE Transactions on Systems, Man, and Cybernetics, Part B (Cybernetics) **27**: 208–215.

Sprott, J. C., 1994 Some simple chaotic flows. Physical review E **50**: R647.

Van der Pol, B. and J. Van Der Mark, 1927 Frequency demultiplication. Nature **120**: 363–364.

Vitkina, T. I., L. V. Veremchuk, E. E. Mineeva, T. A. Gvozdenko, M. V. Antonyuk, *et al.*, 2019 The influence of weather and climate on patients with respiratory diseases in vladivostok as a global health implication. Journal of Environmental Health Science and Engineering **17**: 907–916.

Xirasagar, S., H.-C. Lin, and T.-C. Liu, 2006 Seasonality in pediatric asthma admissions: the role of climate and environmental factors. European journal of pediatrics **165**: 747–752.

Yavari, M., A. Nazemi, and M. Mortezaee, 2022 On chaos control of nonlinear fractional chaotic systems via a neural collocation optimization scheme and some applications. New Astronomy **94**: 101794.

How to cite this article: Mansour, M., Donmez, T. B., Kutlu, M., and Freeman, C. Respiratory Diseases Prediction from a Novel Chaotic System. *Chaos Theory and Applications*, 5(1), 20-26, 2023.

CHAOS
Theory and Applications
in Applied Sciences and Engineering

e-ISSN: 2687-4539
RESEARCH ARTICLE
Vol.5 / No.1 / 2023 / pp.27-33
https://doi.org/10.51537/chaos.1210461

Analysis of Nonlinear Mathematical Model of COVID-19 via Fractional-Order Piecewise Derivative

Muhammad Sinan [*,1], **Kamal Shah** [β,2], **Thabet Abdeljawad** [α,3] **and Ali Akgül** [§,4]

*School of Mathematical Sciences, University of Electronic Science and Technology of China, Chengdu 611731, China, βDepartment of Mathematics and Sciences, Prince Sultan University, Riyadh 11586, Saudi Arabia, αDepartment of Mathematics, University of Malakand, Chakdara Dir (Lower), Khyber Pakhtunkhawa, Pakistan, §Department of Computer Science and Mathematics, Lebanese American University, Beirut, Lebanon; Siirt University, Art and Science Faculty, Department of Mathematics, 56100 Siirt, Türkiye; Near East University, Mathematics Research Center, Department of Mathematics, Near East Boulevard, PC: 99138, Nicosia / Mersin-10, Türkiye.

ABSTRACT Short memory and long memory terms are excellently explained using the concept of piecewise fractional order derivatives. In this research work, we investigate dynamical systems addressing COVID-19 under piecewise equations with fractional order derivative (FOD). Here, we study the sensitivity of the proposed model by using some tools from the nonlinear analysis. Additionally, we develop a numerical scheme to simulate the model against various fractional orders by using Matlab 2016. All the results are presented graphically.

KEYWORDS
Nonlinear dynamical system
Crossover behavior
Mathematical biology
Sensitivity analysis

INTRODUCTION

Fractional calculus has been recognized as a powerful tool to investigate various dynamical problems with more detail and a realistic approach. The foundation of this branch was laid by Newton and some known mathematicians of that time. Later on Reimann, Liouville, Hadamard, Hilfer and other researchers developed this branch further by introducing various differential and integral operators (Machado *et al.* 2011). The great advantage of using fractional calculus instead of classical in the description of real-world problems is its global nature. By fractional derivatives, we can describe global dynamics for various evolutionary processes in a more realistic way. Also, the mentioned operators are keeping a greater degree of freedom as compared to ordinary operators of derivatives which are local in nature, (see some detail in (Hilfer *et al.* 2008) and (Agarwal *et al.* 2010)).

Keeping the mentioned characteristics in mind researchers have increasingly used the concept of fractional calculus in the mathematical modeling of various phenomena and processes. In this regard, we can find literature full of such types of articles, books, and monographs addressing the applications of fractional calculus. Here we remark that fractional derivative has not a unique definition. There have been introduced various definitions by researchers including singular and non-singular operators (Rahman *et al.* 2021). Recently in this connection, see more work as (Ahmad *et al.* 2021c; Alqahtani *et al.* 2021; Ojo and Goufo 2022, 2023). Both forms have been used extensively in various research problems. Both operators have merits and sometimes some de-merits which have been discussed by researchers. For instance, authors have investigated fractal fractional chaotic attractor behavior in (Saifullah *et al.* 2021), a physical model in (Ahmad *et al.* 2021b), and using the Caputo-Fabrizio derivative in (Ahmad *et al.* 2021c).

On the other hand, for epidemiological purposes, the said concept has been used very well. Large numbers of models have been investigated under the concept of fractional order derivatives and integrals. As we know that infectious diseases have greatly affected our society from ancient times. Due to this disease, millions of people have lost their lives in the past as well as in the recent two-three years. Currently, the outbreak of COVID-19 has greatly destroyed the world and more than fifty million people have died within two years all over the globe. The said infection has also affected the economic situation of various countries around the globe. Further, to control the disease researchers, physicians and authorities are working day and night to overcome or control this disease from further spreading.

Manuscript received: 26 November 2022,
Revised: 18 February 2023,
Accepted: 22 February 2023.

[1] sinanmathematics@gmail.com
[2] kamalshah408@gmail.com
[3] tabdeljawad@psu.edu.sa
[4] aliakgul00727@gmail.com (**Corresponding Author**)

In this regards various procedures have been introduced in the last two years to overcome the infection. Some work done on mathematical models of COVID can be seen as (Atangana and İğret Araz 2020), (Arfan *et al.* 2021), and (Abdo *et al.* 2020). Among one which is very important of vaccine which has been prepared and is now available in the market. Further, to aware people of the individual measures to save their lives and their family. Various measures for safety have been implemented by various countries including keeping social distance, regularly washing mouth, hands, etc, and wearing a face mask in gatherings, avoiding joining the huge crowd.

One important tool from a research perspective to investigate the transmission dynamics of the disease in the community through a scientific approach is devoted to mathematical modeling. In this regards various models have been introduced to study the mentioned process, for instance, authors investigated the time fractal-Klein-Gordon equation in (Saifullah *et al.* 2022), the complex behavior of multi-structure dynamical system (Ahmad *et al.* 2021a), Zika virus model in (Zhou *et al.* 2017) and some heat problems in(Doungmo Goufo 2016). For this purpose, various differential operators have been used properly. Along the same line fractional calculus has been used extensively. In the same fashion authors (Doungmo Goufo 2016) have discussed the dynamics of the KDV-Berger equation. Also in (Doungmo Goufo 2015), the authors have applied the concept of fractal-fractional to investigate the cellulose degradation model.

Applications of the newly introduced ABC derivative have been discussed in (Atangana 2020). The existence and uniqueness of the epidemiological model has been studied in (Shah *et al.* 2023). Some authors investigated different TB models under the concept of the fractional derivative with simulation in (Shatanawi *et al.* 2021). Authors (Nawaz *et al.* 2022) established some computational and theoretical analysis for TB model by using ABC derivative of fractional order.

We should keep in mind that many evolutionary processes often suffer from abrupt changes in their dynamics, which can be determined by ordinary derivatives and even fractional derivatives also. For such a situation, we need to use a fractional type derivative with piecewise nature which has the ability to clarify the crossover behavior of the dynamics more properly. In this regard recently some authors have introduced the concept of piecewise derivative to detect the said behavior in the dynamical problems (Atangana and Araz 2021). For further details on piecewise derivatives, recent contributions can be seen as (Shah *et al.* 2022a,b,c).

Motivated by the said analysis, literature, and features of fractional calculus, we will investigate the following models of COVID-19 under the global piecewise derivative of fractional order. Our concerned model is given by

$$\begin{aligned}
{}_0^{\mathbf{pABC}}\mathcal{D}_t^{\chi}\mathscr{S}(t) &= \beta-\xi\mathscr{S}(t)\mathscr{I}(t)-(\tau+\theta)\mathscr{S}(t)+\eta\mathscr{R}(t),\\
{}_0^{\mathbf{pABC}}\mathcal{D}_t^{\chi}\mathscr{E}(t) &= \xi\mathscr{S}(t)\mathscr{I}(t)-(\delta+\tau+\theta)\mathscr{E}(t),\\
{}_0^{\mathbf{pABC}}\mathcal{D}_t^{\chi}\mathscr{I}(t) &= \delta\mathscr{E}(t)-(\theta+\tau+\Delta+\omega)\mathscr{I}(t),\\
{}_0^{\mathbf{pABC}}\mathcal{D}_t^{\chi}\mathscr{V}(t) &= \theta\mathscr{I}(t)-(\tau+\kappa)\mathscr{V}(t)+\theta\mathscr{E}(t)+\theta\mathscr{S}(t),\\
{}_0^{\mathbf{pABC}}\mathcal{D}_t^{\chi}\mathscr{R}(t) &= \Delta\mathscr{I}(t)+\kappa\mathscr{V}(t)-(\tau+\eta)\mathscr{R}(t).
\end{aligned} \tag{1}$$

Here we remark in determinacy form the model (8) is given as

$$\begin{aligned}
\frac{d\mathscr{S}(t)}{dt} &= \beta-\xi\mathscr{S}(t)\mathscr{I}(t)-(\tau+\theta)\mathscr{S}(t)+\eta\mathscr{R}(t),\\
\frac{d\mathscr{E}(t)}{dt} &= \xi\mathscr{S}(t)\mathscr{I}(t)-(\delta+\tau+\theta)\mathscr{E}(t),\\
\frac{d\mathscr{I}(t)}{dt} &= \delta\mathscr{E}(t)-(\theta+\tau+\Delta+\omega)\mathscr{I}(t),\\
\frac{d\mathscr{V}(t)}{dt} &= \theta\mathscr{I}(t)-(\tau+\kappa)\mathscr{V}(t)+\theta\mathscr{E}(t)+\theta\mathscr{S}(t),\\
\frac{d\mathscr{R}(t)}{dt} &= \Delta\mathscr{I}(t)+\kappa\mathscr{V}(t)-(\tau+\eta)\mathscr{R}(t).
\end{aligned} \tag{2}$$

The complete detailed description and explanations of compartments and parameters are given in Tables 2 and 3 respectively. We obtained the basic reproduction number (R_0) using the next-generation matrix on the disease-free equilibrium point and investigated the global sensitivity analysis of the basic reproduction number (R_0). Then, we focused on some numerical techniques based on the Euler method to simulate the given model under the concept of piecewise fractional order derivatives. We use some real values of parameters to present results graphically.

PRELIMINARIES

Here we recall some definitions results, lemmas from (Doungmo Goufo 2015).

Definition 0.1. If $f(t)\in\mathscr{H}^1(0,T)$ and $\chi\in(0,1]$, then the **ABC** derivative is defined as

$${}_0^{\mathbf{ABC}}D_t^{\chi}\mathbf{u}(t)=\frac{\mathbf{ABC}(\chi)}{1-\chi}\int_0^t E_{\chi}\left[\frac{-\chi}{1-\chi}(t-\tau)^{\chi}\right]\frac{d}{d\tau}\mathbf{u}(\tau)d\tau,\varepsilon \tag{3}$$

Definition 0.2. Let $\mathbf{u}(t)\in L[0,T]$, then the fractional integral in **ABC** sense as:

$${}_0^{\mathbf{ABC}}I_t^{\chi}\mathbf{u}(t)=\frac{1-\chi}{\mathbf{ABC}(\chi)}\mathbf{u}(t)+\frac{\chi}{\mathbf{ABC}(\chi)\Gamma(\chi)}\int_0^t(t-\zeta)^{\chi-1}\mathbf{u}(\zeta)d\zeta. \tag{4}$$

Definition 0.3. Let, $\mathbf{u}(t)$ is a differentiable function at interval $[0,t_1]$ and $[t_1,t]$, then the piecewise derivative is defined as:

$${}_0^{\mathbf{pABC}}D\mathbf{u}(t)=\begin{cases}\frac{d\mathbf{u}}{dt}, & 0<t<t_1\\ {}_0^{\mathbf{pABC}}D_t^{\chi}\mathbf{u}. & t_1<t<t_2\end{cases}=\begin{cases}g(t,\mathbf{u}(t)),\\ t\in[0,t_2]\end{cases} \tag{5}$$

Definition 0.4. Suppose, we consider the generic piecewise fractional order differential equation with fractional order χ, such that

$${}_0^{\mathbf{pABC}}\mathcal{D}_t^{\chi}\mathbf{u}(t)=\rho(t,\mathbf{u}(t)),\ \text{with}\ \mathbf{u}(0)=\mathbf{u}_0. \tag{6}$$

For the differential equation (6) we propose a numerical Euler's scheme that is

$$\mathbf{u}(t_{n+1})=\begin{cases}y_n+hf(t_{n-1},\mathbf{u}(t_{n-1})), & 0<t<t_1\\ \mathbf{u}(t_1)+\frac{(1-\chi)}{\mathbf{ABC}(\chi)}f(t_n,\mathbf{u}_n)+\frac{h^{\chi}(1-\chi)}{\mathbf{ABC}(\emptyset)}f(t_n,\mathbf{u}_n), & t_1<t<t_2,\quad 0<\chi<1.\end{cases} \tag{7}$$

MATHEMATICAL MODEL OF COVID-19

We investigate the mathematical model given in (2) by using the Caputo and Atangana-Baleanu piecewise differential operators. We formulated the proposed model in the aforementioned operators form with $0 < \chi \leq 1, t \in [0, T], 0 \leq t \leq T, T < \infty$ as

$$\left.\begin{aligned}
{}^{\mathbf{pABC}}_{0}\mathcal{D}_t^{\chi}\mathscr{S}(t) &= \beta - \xi\mathscr{S}(t)\mathscr{I}(t) - (\tau+\theta)\,\mathscr{S}(t) + \eta\mathscr{R}(t),\\
{}^{\mathbf{pABC}}_{0}\mathcal{D}_t^{\chi}\mathscr{E}(t) &= \xi\mathscr{S}(t)\mathscr{I}(t) - (\delta+\tau+\theta)\,\mathscr{E}(t),\\
{}^{\mathbf{pABC}}_{0}\mathcal{D}_t^{\chi}\mathscr{I}(t) &= \delta\mathscr{E}(t) - (\theta+\tau+\Delta+\omega)\,\mathscr{I}(t),\\
{}^{\mathbf{pABC}}_{0}\mathcal{D}_t^{\chi}\mathscr{V}(t) &= \theta\mathscr{I}(t) - (\tau+\kappa)\,\mathscr{V}(t) + \theta\mathscr{E}(t) + \theta\mathscr{S}(t),\\
{}^{\mathbf{pABC}}_{0}\mathcal{D}_t^{\chi}\mathscr{R}(t) &= \Delta\mathscr{I}(t) + \kappa\mathscr{V}(t) - (\tau+\eta)\,\mathscr{R}(t).
\end{aligned}\right\} \tag{8}$$

In more explicit form the model (8) can also be write as

$$\left.\begin{aligned}
&{}^{\mathbf{pABC}}_{0}\mathcal{D}_t^{\chi}(\mathscr{S}(t))\\
&= \begin{cases} \frac{d\mathscr{S}(t)}{dt} = \mathscr{H}_1(\mathscr{S},\mathscr{E},\mathscr{I},\mathscr{V},\mathscr{R},t), & 0 < t \leq t_1,\\ {}^{\mathbf{ABC}}_{0}\mathcal{D}_t^{\chi}(\mathscr{S}(t)) = \mathscr{H}_1(\mathscr{S},\mathscr{E},\mathscr{I},\mathscr{V},\mathscr{R},t), & t_1 < t \leq T. \end{cases}\\
&{}^{\mathbf{pABC}}_{0}\mathcal{D}_t^{\chi}(\mathscr{E}(t))\\
&= \begin{cases} \frac{d\mathscr{E}(t)}{dt} = \mathscr{H}_2(\mathscr{S},\mathscr{E},\mathscr{I},\mathscr{V},\mathscr{R},t), & 0 < t \leq t_1,\\ {}^{\mathbf{ABC}}_{0}\mathcal{D}_t^{\chi}(\mathscr{E}(t)) = \mathscr{H}_2(\mathscr{S},\mathscr{E},\mathscr{I},\mathscr{V},\mathscr{R},t), & t_1 < t \leq T. \end{cases}\\
&{}^{\mathbf{pABC}}_{0}\mathcal{D}_t^{\chi}(\mathscr{I}(t))\\
&= \begin{cases} \frac{d\mathscr{I}(t)}{dt} = \mathscr{H}_3(\mathscr{S},\mathscr{E},\mathscr{I},\mathscr{V},\mathscr{R},t), & 0 < t \leq t_1,\\ {}^{\mathbf{ABC}}_{0}\mathcal{D}_t^{\chi}(\mathscr{I}(t)) = \mathscr{H}_3(\mathscr{S},\mathscr{E},\mathscr{I},\mathscr{V},\mathscr{R},t), & t_1 < t \leq T. \end{cases}\\
&{}^{\mathbf{pABC}}_{0}\mathcal{D}_t^{\chi}(\mathscr{V}(t))\\
&= \begin{cases} \frac{d\mathscr{V}(t)}{dt} = \mathscr{H}_4(\mathscr{S},\mathscr{E},\mathscr{I},\mathscr{V},\mathscr{R},t), & 0 < t \leq t_1,\\ {}^{\mathbf{ABC}}_{0}\mathcal{D}_t^{\chi}(\mathscr{V}(t)) = \mathscr{H}_4(\mathscr{S},\mathscr{E},\mathscr{I},\mathscr{V},\mathscr{R},t), & t_1 < t \leq T. \end{cases}\\
&{}^{\mathbf{pABC}}_{0}\mathcal{D}_t^{\chi}(\mathscr{R}(t))\\
&= \begin{cases} \frac{d\mathscr{R}(t)}{dt} = \mathscr{H}_5(\mathscr{S},\mathscr{E},\mathscr{I},\mathscr{V},\mathscr{R},t), & 0 < t \leq t_1,\\ {}^{\mathbf{ABC}}_{0}\mathcal{D}_t^{\chi}(\mathscr{R}(t)) = \mathscr{H}_5(\mathscr{S},\mathscr{E},\mathscr{I},\mathscr{V},\mathscr{R},t), & t_1 < t \leq T. \end{cases}
\end{aligned}\right\} \tag{9}$$

EQUILIBRIUM POINT AND BASIC REPRODUCTION NUMBER (R_0)

The Disease–Free equilibrium point is computed as:

$$E^0 = \left(\mathscr{S}^0, 0, 0, \mathscr{V}^0, \mathscr{R}^0\right). \tag{10}$$

Where,

$$\begin{aligned}
\mathscr{S}^0 &= \frac{\beta\left(\eta\,\tau+\eta\,\kappa+\tau\kappa+\tau^2\right)}{\eta\,\tau^2+\tau^2\xi+\tau^2\kappa+\tau^3-\theta\eta\,\kappa+\eta\,\tau\xi+\eta\,\tau\kappa+\eta\,\xi\kappa+\tau\xi\kappa},\\
\mathscr{V}^0 &= \frac{\theta\,\beta(\eta+\tau)}{\eta\,\tau^2+\tau^2\xi+\tau^2\kappa+\tau^3-\theta\eta\,\kappa+\eta\,\tau\xi+\eta\,\tau\kappa+\eta\,\xi\kappa+\tau\xi\kappa},\\
\mathscr{R}^0 &= \frac{\theta\,\beta\kappa}{\eta\,\tau^2+\tau^2\xi+\tau^2\kappa+\tau^3-\theta\eta\,\kappa+\eta\,\tau\xi+\eta\,\tau\kappa+\eta\,\xi\kappa+\tau\xi\kappa}.
\end{aligned} \tag{11}$$

The basic reproduction number at disease-free equilibrium point for the model (8) is computed such that considering the equation:

$$\left.\frac{dZ}{dt}\right|_{E^0} = \mathbf{f} - \mathbf{v}. \tag{12}$$

The non–linear and linear terms from the infected classes in matrix f and v, respectively:

$$f = \begin{pmatrix} \xi\mathscr{S}\mathscr{I} \\ 0 \end{pmatrix}, \quad v = \begin{pmatrix} (\delta+\tau+\theta)\,\mathscr{E}(t) \\ (\theta-\tau-\Delta-\omega)\,\mathscr{I}(t) - \delta\mathscr{E}(t) \end{pmatrix}. \tag{13}$$

Now, the jacobian matrix of f and v is given by:

$$\mathscr{F} = \begin{pmatrix} 0 & \xi\mathscr{S}^0 \\ 0 & 0 \end{pmatrix}, \quad \mathscr{V} = \begin{pmatrix} \theta+\delta+\tau & 0 \\ -\delta & \theta+\tau+\Delta+\omega \end{pmatrix}. \tag{14}$$

Calculating the inverse of matrix $\mathscr{V}$ and the next generation matrix G, such that:

$$\mathscr{V}^{-1} = \begin{pmatrix} \frac{1}{\theta+\delta+\tau} & 0 \\ \frac{\delta}{(\theta+\delta+\tau)\,(\theta+\tau+\Delta+\omega)} & \frac{1}{\theta+\tau+\Delta+\omega} \end{pmatrix}. \tag{15}$$

Thus, the non-zero and largest eigenvalue is the basic reproduction number R_0 is:

$$R_0 = \frac{\delta\,\xi\mathscr{S}^0}{(\theta+\delta+\tau)\,(\theta+\tau+\Delta+\omega)}. \tag{16}$$

Where,

$$\mathscr{S}^0 = \frac{\beta\left(\eta\,\tau+\eta\,\kappa+\tau\,\kappa+\tau^2\right)}{\eta\,\tau^2+\tau^2\xi+\tau^2\kappa+\tau^3-\theta\eta\,\kappa+\eta\,\tau\xi+\eta\,\tau\,\kappa+\eta\,\xi\kappa+\tau\xi\kappa}.$$

SENSITIVITY ANALYSIS

It is vital to understand the relative relevance of the many elements involved in COVID-19 transmissions and prevalence in order to determine how best to decrease human mortality and morbidity as a result of the virus. The endemic equilibrium point is directly connected to R_0, and the initial illness transmission is directly related to R_0. The infectious human percentage, $\mathscr{I}(t)$, is particularly noteworthy since it reflects persons who may get clinically sick and is proportional to the overall number of COVID-19 fatalities. The reproductive number, R_0, and sensitivity indices to the model parameters are calculated. These indices indicate the importance of each parameter in disease transmission and prevalence. To assess the resilience of model predictions to parameter values, sensitivity analysis is widely performed (since there are usually errors in data collection and presumed parameter values). Using the explicit formula for R_0, we derive an analytical expression for the sensitivity of R_0

$$\mathbf{s}^{R_0}_{(\mathbf{p})} = \frac{\mathbf{p}}{R_0}\left[\frac{\partial R_0}{\partial \mathbf{p}}\right]. \tag{17}$$

Now, according to the above relation, we have

$$\mathbf{s}^{R_0}_{\beta} = \frac{\beta}{R_0}\left[\frac{\delta\,\xi(\eta+\tau)(\tau+\kappa)}{(\theta+\delta+\tau)(\theta+\tau+\Delta+\omega)\phi_1}\right], \tag{18}$$

$$\mathbf{s}_{\tau}^{R_0} = \frac{\tau}{R_0}\left[\frac{\delta\,\beta\,\xi\,(\eta+2\,\tau+\kappa)}{(\theta+\delta+\tau)\,(\theta+\tau+\Delta+\omega)\,\phi_1} - \frac{\delta\,\beta\,\xi\,\phi_2}{(\theta+\delta+\tau)\,(\theta+\tau+\Delta+\omega)^2\,\phi_1} - \frac{\delta\,\beta\,\xi\,\phi_2}{(\theta+\delta+\tau)^2\,(\theta+\tau+\Delta+\omega)\,\phi_1} - \frac{\delta\,\beta\,\xi\,\phi_2\,(2\,\eta\,\tau+\eta\,\xi+2\,\tau\,\xi+\eta\,\kappa+2\,\tau\,\kappa+\xi\,\kappa+3\,\tau^2)}{(\theta+\delta+\tau)\,(\theta+\tau+\Delta+\omega)\,{\phi_1}^2}\right],$$

where

$$\phi_1 = \eta\,\tau^2+\tau^2\,\xi+\tau^2\,\kappa+\tau^3-\theta\,\eta\,\kappa+\eta\,\tau\,\xi+\eta\,\tau\,\kappa+\eta\,\xi\,\kappa+\tau\,\xi\,\kappa,$$
$$\phi_2 = \eta\,\tau+\eta\,\kappa+\tau\,\kappa+\tau^2.$$

$$\mathbf{s}_{\eta}^{R_0} = \frac{\eta}{R_0}\left[\frac{\theta\,\delta\,\beta\,\tau\,\xi\,\kappa\,(\tau+\kappa)}{(\theta+\delta+\tau)\,(\theta+\tau+\Delta+\omega)\,{\Phi_1}^2}\right],$$

$$\mathbf{s}_{\kappa}^{R_0} = \frac{\kappa}{R_0}\left[\frac{\theta\,\delta\,\beta\,\tau\,\xi\,\kappa\,(\tau+\kappa)}{(\theta+\delta+\tau)\,(\theta+\tau+\Delta+\omega)\,{\Phi_1}^2}\right],$$

$$\mathbf{s}_{\theta}^{R_0} = \frac{\theta}{R_0}\left[\frac{\delta\,\beta\,\eta\,\xi\,\kappa\,(\eta+\tau)\,(\tau+\kappa)}{(\theta+\delta+\tau)\,(\theta+\tau+\Delta+\omega)\,{\Phi_1}^2} - \frac{\Phi_2}{(\theta+\delta+\tau)^2\,(\theta+\tau+\Delta+\omega)\,\Phi_1} - \frac{\Phi_2}{(\theta+\delta+\tau)\,(\theta+\tau+\Delta+\omega)^2\,\Phi_1}\right],$$

where

$$\Phi_1 = \eta\,\tau^2+\tau^2\,\xi+\tau^2\,\kappa+\tau^3-\theta\,\eta\,\kappa+\eta\,\tau\,\xi+\eta\,\tau\,\kappa+\eta\,\xi\,\kappa+\tau\,\xi\,\kappa,$$
$$\Phi_2 = \delta\,\beta\,\xi\,(\eta+\tau)\,(\tau+\kappa).$$

$$\mathbf{s}_{\xi}^{R_0} = \frac{\xi}{R_0}\left[\frac{\delta\,\beta\,(\eta+\tau)\,(\tau+\kappa)\,(\eta\,\tau^2+\tau^2\,\kappa+\tau^3-\theta\,\eta\,\kappa+\eta\,\tau\,\kappa)}{(\theta+\delta+\tau)\,(\theta+\tau+\Delta+\omega)\,{\Phi_1}^2}\right],$$

$$\mathbf{s}_{\delta}^{R_0} = \frac{\delta}{R_0}\left[\frac{\beta\,\xi\,(\theta+\tau)\,(\eta+\tau)\,(\tau+\kappa)}{(\theta+\delta+\tau)^2\,(\theta+\tau+\Delta+z)\,\Phi_1}\right],$$

$$\mathbf{s}_{\Delta}^{R_0} = -\frac{\Delta}{R_0}\left[\frac{\delta\,\beta\,\xi\,(\eta+\tau)\,(\tau+\kappa)}{(\theta+\delta+\tau)\,(\theta+\tau+\Delta+\omega)^2\,\Phi_1}\right],$$

$$\mathbf{s}_{\omega}^{R_0} = -\frac{\omega}{R_0}\left[\frac{\delta\,\beta\,\xi\,(\eta+\tau)\,(\tau+\kappa)}{(\theta+\delta+\tau)\,(\theta+\tau+\Delta+\omega)^2\,\Phi_1}\right].$$

Table 1 Sensitivity of the R_0 versus proposed parameters

Parameter	Sensitivity Index	Value	Sign
β	$\mathbf{s}_{(\beta)}^{R_0}$	1.0000	+ve
η	$\mathbf{s}_{(\eta)}^{\mathcal{R}_0}$	-0.0006	-ve
θ	$\mathbf{s}_{(\theta)}^{\mathcal{R}_0}$	-3.4078	-ve
δ	$\mathbf{s}_{(\delta)}^{\mathcal{R}_0}$	0.9434	+ve
ω	$\mathbf{s}_{(\omega)}^{\mathcal{R}_0}$	-0.0001	-ve
τ	$\mathbf{s}_{(\tau)}^{\mathcal{R}_0}$	0.0010	+ve
κ	$\mathbf{s}_{(\kappa)}^{\mathcal{R}_0}$	-0.0004	-ve
ξ	$\mathbf{s}_{(\xi)}^{\mathcal{R}_0}$	1.5554	+ve
Δ	$\mathbf{s}_{(\Delta)}^{\mathcal{R}_0}$	-0.0909	-ve

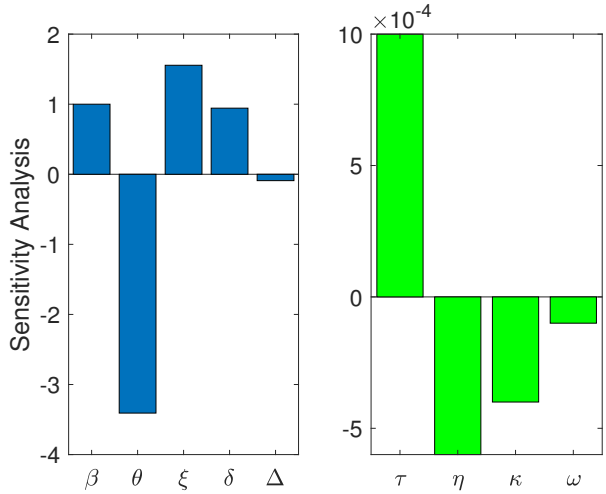

Figure 1 Plot of Sensitivity Analysis with a graphical representation of sensitivity indices $\mathbf{s}_{(\mathbf{p})}^{R_0}$ bases on the expression (17).

In Table (1), the sensitivity indices are provided for each parameter associated with basic reproduction number (R_0) computed based on the expression (17). There is a positive and negative effect of each parameter in the basic reproduction number (R_0) and thus the parameters with positive signs increase the basic reproduction number (R_0) and negative decreases, respectively. Considering the Table (1) and Figure (1), we observed that with the increase in the value parameters β, ξ, δ, and τ cause growth in basic reproduction number (R_0) while decay by parameters θ, Δ, η, κ, and ω. Thus, having negative indices must be minimized in the environment.

NUMERICAL SCHEME

Consider the model (8), we use the proposed Euler's scheme from the Definition (7) and implement on the given problem, such that

$$\mathscr{S}(t_{n+1}) = \begin{cases} \mathscr{S}_n + hf(t_{n-1}, \mathscr{S}(t_{n-1})), & 0 < t < t_1 \\ z_1, & t_1 < t < t_2, 0 < \chi < 1. \end{cases} \tag{19}$$

where, $z_1 = \mathscr{S}(t_1) + \frac{(1-\chi)}{\mathbf{ABC}(\chi)} f(t_n, \mathscr{S}_n) + \frac{h^\chi (1-\chi)}{\mathbf{ABC}(\chi)} f(t_n, \mathscr{S}_n)$.

$$\mathscr{E}(t_{n+1}) = \begin{cases} \mathscr{E}_n + hf(t_{n-1}, \mathscr{E}(t_{n-1})), & 0 < t < t_1 \\ z_2, & t_1 < t < t_2, 0 < \chi < 1. \end{cases} \tag{20}$$

where, $z_2 = \mathscr{E}(t_1) + \frac{(1-\chi)}{\mathbf{ABC}(\chi)} f(t_n, \mathscr{E}_n) + \frac{h^\chi (1-\chi)}{\mathbf{ABC}(\chi)} f(t_n, \mathscr{E}_n)$.

$$\mathscr{I}(t_{n+1}) = \begin{cases} \mathscr{I}_n + hf(t_{n-1}, \mathscr{I}(t_{n-1})), & 0 < t < t_1 \\ z_3, & t_1 < t < t_2, 0 < \chi < 1. \end{cases} \tag{21}$$

where, $z_3 = \mathscr{I}(t_1) + \frac{(1-\chi)}{\mathbf{ABC}(\chi)} f(t_n, \mathscr{I}_n) + \frac{h^\chi (1-\chi)}{\mathbf{ABC}(\chi)} f(t_n, \mathscr{I}_n)$.

$$\mathscr{V}(t_{n+1}) = \begin{cases} \mathscr{V}_n + hf(t_{n-1}, \mathbf{u}(t_{n-1})), & 0 < t < t_1 \\ z_4, & t_1 < t < t_2, 0 < \chi < 1. \end{cases} \tag{22}$$

where, $z_4 = \mathscr{V}(t_1) + \frac{(1-\chi)}{\mathbf{ABC}(\chi)} f(t_n, \mathscr{V}_n) + \frac{h^\chi (1-\chi)}{\mathbf{ABC}(\chi)} f(t_n, \mathscr{V}_n)$.

$$\mathscr{R}(t_{n+1}) = \begin{cases} \mathscr{R}_n + hf(t_{n-1}, \mathscr{R}(t_{n-1})), & 0 < t < t_1 \\ z_5, & t_1 < t < t_2, 0 < \chi < 1. \end{cases} \tag{23}$$

where, $z_5 = \mathscr{R}(t_1) + \frac{(1-\chi)}{\mathbf{ABC}(\chi)} f(t_n, \mathscr{R}_n) + \frac{h^\chi (1-\chi)}{\mathbf{ABC}(\chi)} f(t_n, \mathscr{R}_n)$.

NUMERICAL INTERPRETATION AND DISCUSSION

Here we apply the aforesaid scheme to simulate the results for different fractional order under piecewise derivative to see the crossover behavior in the transmission dynamics of the disease and the effect of vaccination.

In Figures 2-6, we have presented the approximate solutions corresponding to piecewise derivatives using various fractional orders. We have taken here $t_1 = 5$ and $T = 120$. The crossover effect is clearly observed near the point $t_1 = 5$, and the dynamics after that point shows variation in behavior. This multi-behavior of the dynamics is known as crossover. This effect cannot be determined by using a usual derivative of fractional order. As the vaccination procedure increases more people are giving vaccines, and the security from the infection is also increasing, and hence recovered class is growing up.

Table 2 Table of description and Initial Condition of Compartment of Population.

Symbols	Description of Compartment	Initial Condition
$\mathscr{S}(t)$	Susceptible Human Population	$\mathscr{N} - (\mathscr{E} + \mathscr{I} + \mathscr{V} + \mathscr{R})$
$\mathscr{E}(t)$	Exposed Human Population	10
$\mathscr{I}(t)$	Infected Human Population	20
$\mathscr{V}(t)$	Vaccinated Human Population	30
$\mathscr{R}(t)$	Recovered Human Population	50
$\mathscr{N}$	Total Population	200

Table 3 Table of description and values of Parameters.

Symbol	Description of Parameter	Value
τ	Natural Death Rate	$\frac{1}{67.7 \times 365}$
β	Recruitment Rate	$\tau \times N$
ξ	Transmission rate	0.1784
θ	Vaccination Rate	0.5
η	Lose of Immunity in Recovered Population	0.1
δ	Rate of Infection of Exposed Population	0.03
Δ	Recovery Rate of Infected Population	0.05
κ	Recovery Rate of Vaccinated Population.	0.15
ω	Death Rate of Infected Population due to COVID–19 Infection	0.32

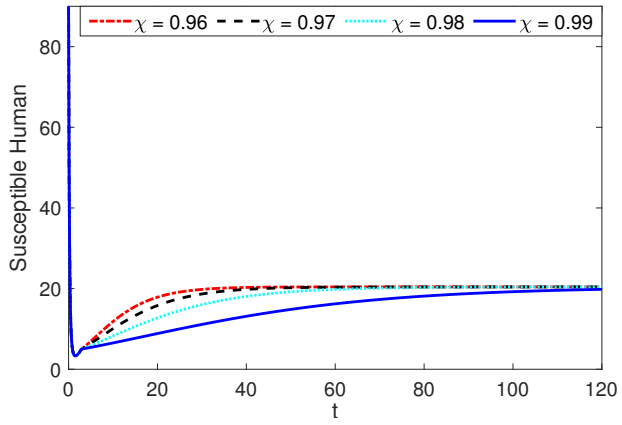

Figure 2 Plot of susceptible class at various fractional order derivatives.

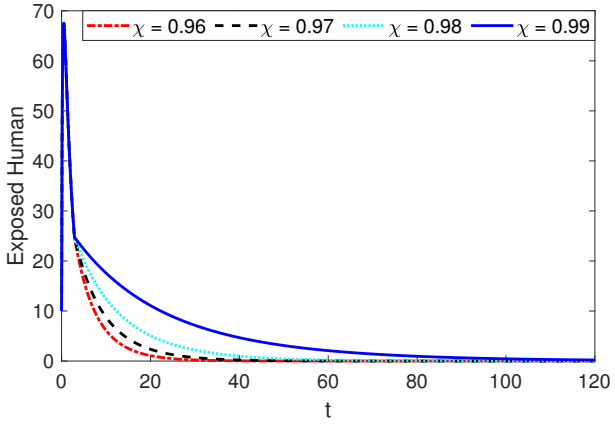

Figure 3 Plot of exposed class at various fractional order derivatives.

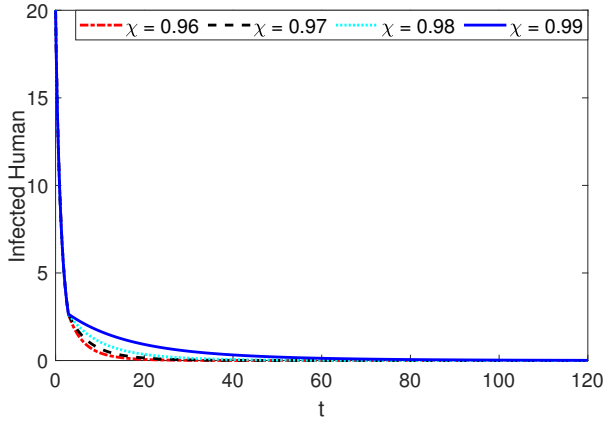

Figure 4 Plot of infected class at various fractional order derivatives.

CONCLUSION

We have extended the concept of piecewise ABC fractional order derivative concept to a dynamical system of COVID-19 with a vaccinated class. We investigated global sensitivity analysis of parameters associated with the basic reproduction number (R_0) of the given model and as a result, we have some potential parameters on which the basic reproduction number (R_0) depends. Due to both increase and decrease, there is an associated increase and decrease in (R_0). We present the sensitivity indices graphically using a bar chart for justification. We have also simulated the results by using some real values for the parameters and initial data. We see that at point $t_1 = 5$, the behavior of the dynamics has shown variation. This is due to the piecewise derivative. Such effect is called crossover and can be well explained by using piecewise derivative as compared to ordinary or usual fractional order. Hence we concluded that piecewise derivative can be used as a powerful tool to investigate the transmission dynamics of infectious diseases that suffer from abrupt changes in their dynamical evolution.

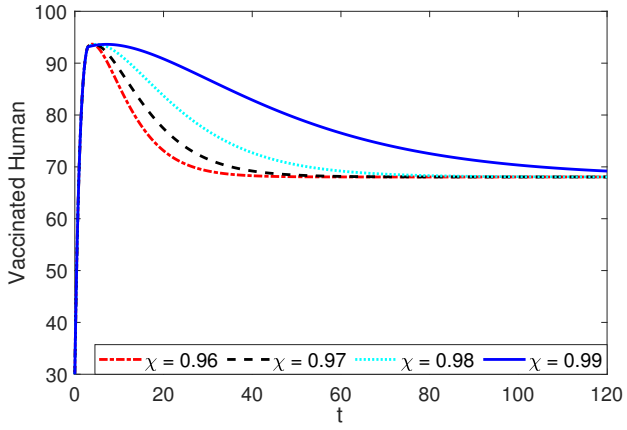

Figure 5 Plot of recovered class at various fractional order derivatives.

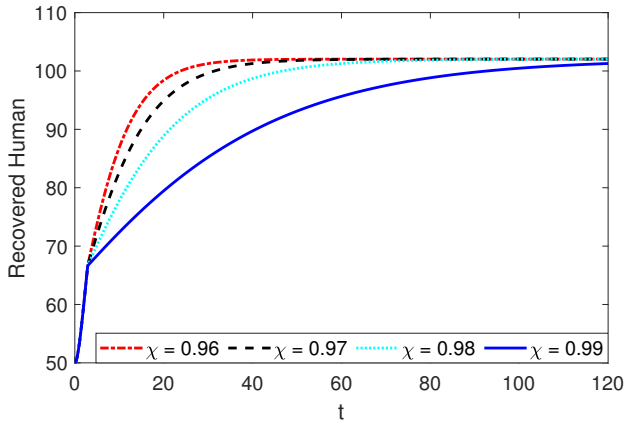

Figure 6 Plot of vaccinated class at various fractional order derivatives.

Acknowledgments

The authors Kamal Shah and Thabet Abdeljawad would like to thank Prince Sultan University for support through the TAS research lab.

Conflicts of interest

The authors declare that there is no conflict of interest regarding the publication of this paper.

Availability of data and material

Not applicable.

LITERATURE CITED

Abdo, M. S., K. Shah, H. A. Wahash, and S. K. Panchal, 2020 On a comprehensive model of the novel coronavirus (covid-19) under mittag-leffler derivative. Chaos, Solitons & Fractals **135**: 109867.

Agarwal, R. P., V. Lakshmikantham, and J. J. Nieto, 2010 On the concept of solution for fractional differential equations with uncertainty. Nonlinear Analysis: Theory, Methods & Applications **72**: 2859–2862.

Ahmad, S., A. Ullah, and A. Akgül, 2021a Investigating the complex behaviour of multi-scroll chaotic system with caputo fractal-fractional operator. Chaos, Solitons & Fractals **146**: 110900.

Ahmad, S., A. Ullah, A. Akgül, and M. De la Sen, 2021b A study of fractional order ambartsumian equation involving exponential decay kernel. AIMS Math **6**: 9981–9997.

Ahmad, S., A. Ullah, M. Partohaghighi, S. Saifullah, A. Akgül, *et al.*, 2021c Oscillatory and complex behaviour of caputo-fabrizio fractional order hiv-1 infection model. Aims Math **7**: 4778–4792.

Alqahtani, R. T., S. Ahmad, and A. Akgül, 2021 Dynamical analysis of bio-ethanol production model under generalized nonlocal operator in caputo sense. Mathematics **9**: 2370.

Arfan, M., H. Alrabaiah, M. U. Rahman, Y.-L. Sun, A. S. Hashim, *et al.*, 2021 Investigation of fractal-fractional order model of covid-19 in pakistan under atangana-baleanu caputo (abc) derivative. Results in Physics **24**: 104046.

Atangana, A., 2020 Extension of rate of change concept: from local to nonlocal operators with applications. Results in Physics **19**: 103515.

Atangana, A. and S. İ. Araz, 2021 New concept in calculus: Piecewise differential and integral operators. Chaos, Solitons & Fractals **145**: 110638.

Atangana, A. and S. İğret Araz, 2020 Mathematical model of covid-19 spread in turkey and south africa: theory, methods, and applications. Advances in Difference Equations **2020**: 1–89.

Chitnis, N., J. M. Hyman, and J. M. Cushing, 2008 Determining important parameters in the spread of malaria through the sensitivity analysis of a mathematical model. Bulletin of mathematical biology **70**: 1272–1296.

Doungmo Goufo, E. F., 2015 A biomathematical view on the fractional dynamics of cellulose degradation. Fractional Calculus and Applied Analysis **18**: 554–564.

Doungmo Goufo, E. F., 2016 Application of the caputo-fabrizio fractional derivative without singular kernel to korteweg-de vries-burgers equation. Mathematical Modelling and Analysis **21**: 188–198.

Grace, S., R. Agarwal, P. Wong, and A. Zafer, 2012 On the oscillation of fractional differential equations. Fractional Calculus and Applied Analysis **15**: 222–231.

Hajiseyedazizi, S. N., M. E. Samei, J. Alzabut, and Y. ming Chu, 2021 On multi-step methods for singular fractional q-integro-differential equations. Open Mathematics **19**: 1378–1405.

Hilfer, R. *et al.*, 2008 Threefold introduction to fractional derivatives. Anomalous transport: Foundations and applications pp. 17–73.

Machado, J. T., V. Kiryakova, and F. Mainardi, 2011 Recent history of fractional calculus. Communications in nonlinear science and numerical simulation **16**: 1140–1153.

Nawaz, Y., M. S. Arif, and W. Shatanawi, 2022 A new numerical scheme for time fractional diffusive seair model with non-linear incidence rate: An application to computational biology. Fractal and Fractional **6**: 78.

Ojo, M. M. and E. F. D. Goufo, 2022 Modeling, analyzing and simulating the dynamics of lassa fever in nigeria. Journal of the Egyptian Mathematical Society **30**: 1.

Ojo, M. M. and E. F. D. Goufo, 2023 The impact of covid-19 on a malaria dominated region: A mathematical analysis and simulations. Alexandria Engineering Journal **65**: 23–39.

Rahman, F., A. Ali, and S. Saifullah, 2021 Analysis of time-fractional ϕ 4-equation with singular and non-singular kernels. International Journal of Applied and Computational Mathematics **7**: 192.

Saifullah, S., A. Ali, and E. F. D. Goufo, 2021 Investigation of complex behaviour of fractal fractional chaotic attractor with mittag-leffler kernel. Chaos, Solitons & Fractals **152**: 111332.

Saifullah, S., A. Ali, and Z. A. Khan, 2022 Analysis of nonlinear time-fractional klein-gordon equation with power law kernel. AIMS Math **7**: 5275–5290.

Shah, K., B. Abdalla, T. Abdeljawad, and R. Gul, 2023 Analysis of multipoint impulsive problem of fractional-order differential equations. Boundary Value Problems **2023**: 1–17.

Shah, K., T. Abdeljawad, B. Abdalla, and M. S. Abualrub, 2022a Utilizing fixed point approach to investigate piecewise equations with non-singular type derivative. AIMS Math **7**: 14614–14630.

Shah, K., T. Abdeljawad, and A. Ali, 2022b Mathematical analysis of the cauchy type dynamical system under piecewise equations with caputo fractional derivative. Chaos, Solitons & Fractals **161**: 112356.

Shah, K., T. Abdeljawad, and H. Alrabaiah, 2022c On coupled system of drug therapy via piecewise equations. Fractals **30**: 2240206.

Shatanawi, W., M. S. Abdo, M. A. Abdulwasaa, K. Shah, S. K. Panchal, *et al.*, 2021 A fractional dynamics of tuberculosis (tb) model in the frame of generalized atangana–baleanu derivative. Results in Physics **29**: 104739.

Zhou, H., J. Alzabut, and L. Yang, 2017 On fractional langevin differential equations with anti-periodic boundary conditions. The European Physical Journal Special Topics **226**: 3577–3590.

How to cite this article: Sinan, M., Shah, K., Abdeljawad, T., and Akgul, A. Analysis of Nonlinear Mathematical Model of COVID-19 via Fractional-Order Piecewise Derivative. *Chaos Theory and Applications*, 5(1), 27-33, 2023.

CHAOS
Theory and Applications
in Applied Sciences and Engineering

e-ISSN: 2687-4539
RESEARCH ARTICLE
Vol.5 / No.1 / 2023 / pp.34-51
https://doi.org/10.51537/chaos.1249532

Computational Complexity-based Fractional-Order Neural Network Models for the Diagnostic Treatments and Predictive Transdifferentiability of Heterogeneous Cancer Cell Propensity

Yeliz Karaca *,[1]
*University of Massachusetts Chan Medical School (UMASS), 55 Lake Avenue North, Worcester, MA 01655, USA.

ABSTRACT Neural networks and fractional order calculus are powerful tools for system identification through which there exists the capability of approximating nonlinear functions owing to the use of nonlinear activation functions and of processing diverse inputs and outputs as well as the automatic adaptation of synaptic elements through a specified learning algorithm. Fractional-order calculus, concerning the differentiation and integration of non-integer orders, is reliant on fractional-order thinking which allows better understanding of complex and dynamic systems, enhancing the processing and control of complex, chaotic and heterogeneous elements. One of the most characteristic features of biological systems is their different levels of complexity; thus, chaos theory seems to be one of the most applicable areas of life sciences along with nonlinear dynamic and complex systems of living and non-living environment. Biocomplexity, with multiple scales ranging from molecules to cells and organisms, addresses complex structures and behaviors which emerge from nonlinear interactions of active biological agents. This sort of emergent complexity is concerned with the organization of molecules into cellular machinery by that of cells into tissues as well as that of individuals to communities. Healthy systems sustain complexity in their lifetime and are chaotic, so complexity loss or chaos loss results in diseases. Within the mathematics-informed frameworks, fractional-order calculus based Artificial Neural Networks (ANNs) can be employed for accurate understanding of complex biological processes. This approach aims at achieving optimized solutions through the maximization of the model's accuracy and minimization of computational burden and exhaustive methods. Relying on a transdifferentiable mathematics-informed framework and multifarious integrative methods concerning computational complexity, this study aims at establishing an accurate and robust model based upon integration of fractional-order derivative and ANN for the diagnosis and prediction purposes for cancer cell whose propensity exhibits various transient and dynamic biological properties. The other aim is concerned with showing the significance of computational complexity for obtaining the fractional-order derivative with the least complexity in order that optimized solution could be achieved. The multifarious scheme of the study, by applying fractional-order calculus to optimization methods, the advantageous aspect concerning model accuracy maximization has been demonstrated through the proposed method's applicability and predictability aspect in various domains manifested by dynamic and nonlinear nature displaying different levels of chaos and complexity.

KEYWORDS
Computational complexity
Complex systems
Artificial Intelligence (AI)
Chaos theory
Fractional calculus
Fractional-order derivatives
Mittag-Leffler functions
Heavy-tailed distributions
Computational biocomplexity
Nonlinearity and uncertainty
Multilayer perceptron algorithm (MLP)
Neural networks
Transdifferentiable mathematics-informed framework
Complex order optimization
Mathematical biology
Data-driven fractional-order biological modeling
Cancer cell propensity.

INTRODUCTION

Universal order and complex universe, correspondingly, require solutions and models to address the complexity challenge by self-organization, harmonization and synchronization. Complex-fractional models in complex dynamical processes, therefore, have extensive schemes made up of hierarchical, spatial as well as topological structures that have assorted likely granularities of the particular system by differential equations. On the other hand, complex order fractional derivatives govern complex-fractional systems in which memory and nonlinearity are seen as the two aspects of complex-fractional systems with complex variables, which point out the significance of the modeling of memory-intense systems. Complex-order systems which functions within a universal order manifests multiple dynamical interactive components grounded on multiscale spatial and temporal fields, which points towards the integration for the construction of an operational whole on a holistic spectrum. Fractional calculus (FC), owing to its ability of reflecting the systems' actual state properties, exhibiting unforeseeable variations, makes the generalization of integration and differentiation possible. In that regard, it can provide a new added value for the enhanced description of the characteristics concerning different complex systems. When it is necessary to summon solutions for the complex models, simulations, technological advances have enabled the integration of fractional calculus and Artificial Intelligence (AI) applications particularly for the managing

Manuscript received: 9 February 2023,
Revised: 18 February 2023,
Accepted: 26 February 2023.

[1] yeliz.karaca@ieee.org (**Corresponding Author**)

of uncertainty and making critical multi-stage and multi-criteria decisions within the framework of mathematical modeling. Formation and validation of hypothesis can, hence, be minimized in terms of time, with the acceleration of experiments and numerical simulations along with the substantial volume of data analyses, which have become precise, reliable and trustworthy.

Fractional-order calculus (FOC), being based on fractional-order thinking, concerns the differentiation and integration of non-integer orders, which enables improved understanding of complex and dynamic systems with or without time delays. Certain complex systems in nature may not always be likely to be characterized by classical integer-order calculus models; therefore, a fractional-order system-based model is capable of describing the system performance in a more accurate manner. The processing as well as control of complex elements are also enhanced whilst making the performance more optimal owing to FOC. The fractal processes' discontinuous nature necessitates a reinvestigation of equations of motion including fractional operators. In this regard, fractional calculus paves the way for modeling the impact of an erratic background in a system with its description merging with nonlinear dynamics.

Fractional thinking as a sort of in-between thinking is situated between the integer-order moments, and there, fractional moments are needed as empirical integer moments cannot converge. Between the integer dimensions, there exist fractal dimensions whose significance is seen when data possess no characteristic scale length. The non-integer operators that are required to define dynamics with long-time memory and spatial heterogeneity are at stake between the integer value operators local in time and space. Taking all these into account, it can be said that the modern inclination of science requires the understanding and even embracing of complexity where complex phenomena oblige us to find new ways of thinking. Fractional calculus is one way to provide framework towards such thinking (West 2016; West *et al.* 2003). Fractional differential equations are also beneficial means to characterize and show the dynamics of complex phenomena with spatial heterogeneous characteristics and long memory. The fractional derivative of real order is seen as the degree of structural heterogeneity between the homogeneous and also in homogeneous spheres in which complexity usually arise with respect to systems made up of elements interacting with one another which may be intrinsically hard in terms of modeling (Lopes and Tenreiro Machado 2019).

Fractional-order differential and integral equations enable the conventional integral and differential equations' generalization by extending the related conceptions with respect to different biological phenomena. Correspondingly, adeptness in computational complexity ensures an interconnected, integrative and multifarious angle towards problems; which is the cause of applicable sets of ideas and implementations to be implemented for the identification of the subtle features of complex dynamic systems. One significant point to bear in mind is to acknowledge the varying degrees of problems in order that the models can be established in a way that can be adjustable and fitting the matter into the right data, as handled in various disciplines like neuroscience (Singhal *et al.* 2010), biology (Magin 2010) and so on.

Mathematical-informed frameworks with computer-assisted proofs are used so that it becomes possible to be equipped with reliable and accurate understanding in complex heterogeneity and dynamic structure of temporally and spatially multiple transient states. There still exist means in mathematics awaiting to construct their way in theoretical biology as is in the case of fractional, or non-integer order calculus whose application emerges as a powerful and strategic approach of modeling in the light of forthcoming opportunities and challenges in mathematical medicine. Fractional mathematical oncology, in this regard, deals with memory effects, heterogeneous scales and dormant periods with respect to the onset and development of tumors in a straightforward way (Valentim *et al.* 2021). Biological phenomena and problems, inherently characterized by nonlinearity and uncertainty, modeled by ordinary or partial differential equations with integer order, are possible to be described well through the employing of ordinary and partial differential equations. The variables, attributes, parameters, initial conditions as well as observation states in the model are to be considered for computational purposes. At each instance of time, it is possible to measure the correct information by a non-integer order derivative.

One relevant study on that subject matter is (Ziane *et al.* 2020) aims at applying the local fractional homotopy analysis method (LEHAM) in order to get the non-differentiable solution of two non-linear partial differential equations (PDEs) concerning the Cantor sets' biological population model. The proposed method is demonstrated to be effective and powerful in terms of solving those PDEs with LFHAM being applied for the solution of other nonlinear PDEs with local fractional derivative. Another study is on biomathematical modeling (Carletti and Banerjee 2019), distinguishing demographic noise and environmental noise. The authors present a technique for simulating and modeling demographic noise that goes in backward direction. Neurological phenomena, on the other hand, have layered, multi-phase and multi-functional materials like those of brain tissue with interconnected networks.

In order to enhance the comprehension how the brain provides its functions, robust mathematical-informed as well as feedback engineering frameworks which use basic scientific concepts to interpret and direct the experiments investigating brain's responses to different stimuli, diseases and treatment courses thereof are required. In neuroscience, one of the related studies (Lewis *et al.* 2016) is concerned with the ratio processing system (RPS) tuned to the holistic magnitudes suited for grounding fraction learning difficulties about symbolic fractions. The proposed premise is the capability to represent ratio/fraction magnitudes stated by the RPS could upkeep a more profound grasping of fractions as relative magnitudes, which shows the critical importance of RPS about learning with regard to fractions. In short, fractional dynamics could be applicable both for the oculomotor system and for the motor control systems.

A fractional derivative's physical meaning is said to be an open problem and for the modeling of various memory related phenomena, a memory process is made up of two stages: short has permanent retention and the second one is ruled by a simple model of fractional derivative. The fractional model is shown to fit the test data of memory related phenomena in different fields like mechanics and biology perfectly though the numerical least square model. Thus, the physical meaning concerning fractional order is found to be an index of memory based on that scheme (Du *et al.* 2013). Fractional Calculus (FC), refers to the calculus of derivatives and integrals of arbitrary complex order or real order has wide-ranging domains of application. Different studies are available in the literature addressing the solution of varying fractional order biological disease models in environments displaying uncertainty. The application of Caputo operator to convey non-integer derivative of fractional order can be found in (Khan *et al.* 2020), handling of chaos control and synchronization of a biological snap oscillator through a new fractional model is addressed with regard to bio-

engineering in (Sommacal *et al.* 2008), biology (Toledo-Hernandez *et al.* 2014), (Tokhmpash 2021), signal processing (Gutierrez *et al.* 2010), image processing (Debnath 2003), electronics (Krishna and Reddy 2008) robotics (Singh *et al.* 2021), control theory (Panda and Dash 2006), (Garrappa 2015). Numerical parameters, variables and radiation elements are used for the treatment model's simulation. It has been concluded that the model is capable of simulating the treatment process of cancer and make the prediction of the results of other protocols related to radiation.

Regarding the broad class of functions, the Riemann–Liouville definition is employed in the process of the problem formulation, with the Grünwald-Letnikov definition being referred to for achieving some numerical solutions. The use of Riemann-Liouville fractional calculus' operators is considered in (Rodríguez-Germá *et al.* 2008) for the reduction of linear ordinary or PDEs with variable coefficients to more simple problems through certain commutative differential relations. Thus, it has been aimed to avoid the singularities in the original equations and the case of Bessel differential equations is used as the related example. The efficiency of the technique employing Riemann-Liouville operators of fractional calculus has been shown by (Rodríguez-Germá *et al.* 2008). Regarding the derivatives of Riemann-Liouville and Caputo derivatives, Riemann-Liouville derivative as one of mostly employed fractional derivatives and some important features of the Caputo derivative are discussed in (Li *et al.* 2011) which provides benefits for the understanding of fractional calculus as well as modeling of fractional equations in the fields of science and engineering.

Mittag-Leffler (ML) functions, with their various properties and one to five and more parameters, are inclined towards modification on a complex plane with the extension of particular fractional-calculus operators owing to their use in the various direct applications and involvements in fractional calculus and fractional differential equations concerning biology, physics, applied sciences and engineering. Among the studies in the literature, the following work can be referred to: (Fernandez and Husain 2020), (Pang *et al.* 2018).

Fractional order calculus theory, employed for addressing varying orders of derivatives and integrals, lends itself to diverse kinds of definitions for fractional order derivatives with Riemann–Liouville, Caputo and Grünwald–Letnikov being the most frequently used ones. On the other hand, fractional calculus affords tools that can describe and deal with complex phenomena as well as its connection to the inherent properties that are nonlinear complex considering the memory effects and apparently chaotic behavior. In view of that, the fractional order derivative notion is ubiquitous in different areas, offering diverse and varying methods concerning fractional order derivative (FOD) (KARCI *et al.* 2014).

It is noted that fractional derivatives have the capability of improving the machine learning algorithms' accuracy, with computing power, if and when utilized for spectral data, signals and images. Given these, fractional derivatives and, successively, fractional calculus have proved to provide a framework to be able to enhance optimization tasks. One example of work handled within that view is by (Raubitzek *et al.* 2022) providing exemplary applications to segment MRI brain scans, for stroke, to be applied as input for a machine learning algorithm. Another work addresses practical software optimization methods to implement fractional-order backward difference, sum, and differintegral operator, which are dependent on the Grünwald–Letnikov definition regarding the evaluation of fractional-order differential equations in embedded systems owing to their more convenient form in contrast with Caputo and Riemann–Liouville definitions (Matusiak 2020).

The work of (Viola and Chen 2022) provides an evaluation of a fractional-order self-optimizing control architecture for the purpose of process control. As a consequence, the related controller is stated to enhance the system closed-loop response under different operating conditions while reducing convergence time of the real-time derivative-free optimization algorithm through fractional-order stochasticity. Furthermore, another paper is related to the optimization techniques of image analysis algorithms. The authors optimize the Grünvald - Letnikov fractional - order backward difference for the estimation of the position of the marker in a sequence of images, and through the mathematical foundation of the fractional order derivative optimization tool of the study, it is observed that process or load linked with the optimized algorithm was reduced by 35% and more (Jachowicz *et al.* 2022).

Conducting predictions reliant on mathematical models with regard to processes and datasets related to biology requires the parameters concerning machine learning. Moreover, the fitting of the parameters to experimental data is challenging as it is important and essential to find the model parameters' optimal values during when the model parameters' different values may exhibit consistent aspects with the data, called the identifiability. For ANNs, learning is a noteworthy stage concerning convergence rate, as obtained potentially by the use of fractional-order gradient in data science.

One respective study, (Gomolka 2018), utilizes a model of a neural network with a new backpropagation rule by making use of a fractional order derivative mechanism. Another study, (Kadam *et al.* 2019) addresses the ANN approximation of fractional derivative operators. The study (Mall and Chakraverty 2018) develops an ANN technique to find solution of FDEs and shows the advantage of them in terms of describing various real-world application problems of physical systems. A MLP architecture and error back propagation algorithm are used to minimize the error function and modify the weights and biases as parameters. ANN output is said to yield a suitable approximate solution of FDE and the accuracy of the method is put forth as such. (Wu *et al.* 2017) investigates in depth the ML stability of a class of fractional-order neural networks in the field of neurodynamics. The results established are dependent on the FDE theories of FDE and differential equation with generalized piecewise constant arguments with the derived criteria improving and extending the respective results. Finally, (Niu *et al.* 2021) provides the discussion of an optimal randomness case study for a stochastic configuration network (SCN) machine-learning method having heavy-tailed distributions along with the discussion of the employment of fractional dynamics in analytics concerning big data to quantify variability due to the complex systems' generation.

Complex systems are marked by order and homogeneity as well as the hierarchy of subsystems and different levels in space and time. Therefore, the observation of the interconnection with respect to different biological elements such as cells, molecules and tissues, with a focus on their qualitative properties, is required. Considering this intricate complexity, it would not be adequate to characterize and identify only the discrete biological components of the system. Thus, mathematical models play a noteworthy role for the complex problems' solution and the viable applications to biological data so that it can be possible to attain a thorough understanding of the emergent interactions between heterogeneous biological components and their related pathways. In this way, it can be ensured to reveal the correlations between different observable phenomena characterized by heterogeneity and dynamic properties in an accurate and robust way.

Life is endowed with many diverse and peculiar attributes, which invokes the investigation of its origin that is not possible to obtained from scratch, referring to its molecular constituents. These complex systems in life do not only evolve through time, they also have a past which is jointly responsible for the present behaviors. On the other hand, the evolution of its forms cannot be predicted; in that sense, evolution, as a universal process and dynamics, brings about diverse phenomenology of life with its related theory leading to rich phenomenology of life on earth for modern biology and mathematical bioengineering which has been subject to modifications due to its nature over the years. The complexity of living systems can be expressed in cells and tissues' structures and functions, which means biological functions of each element are embedded in a three-dimensional alignment of the cells of each tissue, extracellular matrices and anatomical organization. Biocomplexity, alternatively, with multiple scales ranging from molecules to cells and organisms addresses complex structures and behaviors that emerge from nonlinear interactions of active biological agents. Due to this complexity of biological systems and elements, chaos theory seems to be one of the most applicable areas of life sciences in view of nonlinear dynamic and complex systems of living and non-living environment.

Biocomplexity, with multiple scales that range from molecules to cells and organisms, is concerned with complex structures and behaviors emerging from nonlinear interactions of active biological agents. This alignment of emergent complexity deals with the organization of molecules into cellular machinery through that of cells into tissues as well as that of individuals to communities. As healthy systems keep up their complexity in their lifetime and are chaotic, disease is seen as an outcome when the loss of complexity or the loss of chaos occurs. Furthermore, mathematical models enable researchers to dig into the degree of complexity concerning processes, routes and the way these are interconnected. One of the related studies in this domain is (Tzoumas *et al.* 2018) on the sensor selection to determine the minimum number of state variables which are required to be measured for the monitoring of the evolution of the biological system. The authors focus on the solution of different problems of sensor selection and consider biologically motivated discrete-time fractional-order systems. The work (Blazewicz and Kasprzak 2012) addresses the progress of research in computational biology based on computer science and operational research, presenting the different issues around complexity as inspired by computational biology.

Algorithms and complexity along with their conceptual aspects become significant on the condition that their definition is done vis-*á*-vis formal computational models (Du and Ko 2011). Since computing is proven to be critical to be able to deal with exhaustive data tasks and achieve scalable solutions to complex problems, researchers and developers should be familiar with impacts of computational complexity to better grasp and design efficient algorithms in computational biology. Algorithmic (computational) complexity, known as running time, is a way of comparing the efficiency of an algorithm. For a given task, an algorithm doing the completion of a task is considered to be more complex if more steps are the case.

It is possible to express the algorithmic complexity with the *Big O* notation varying in relation to the size of the input. The measurement of complexity is considered based on the duration it takes for a program to run in relation to the size of the input (time complexity) or to the memory it is to take up (space complexity). One related work (Sidelnikov *et al.* 2018) investigates the application of dynamic deep neural networks for non-linear equalization in long haul transmission systems. The optimum dimensions are identified by extensive numerical analysis and computational complexity of the systems are calculated as a function of system length. The authors demonstrate performance at a considerably lower cost of computation.

Neural networks and fractional order calculus are known to be efficient to identify systems, which concerns the capability to approximate nonlinear functions. One of the relevant studies (Aguilar *et al.* 2020) is concerned with a fractional gradient descent method. By using the Caputo derivative, the authors made the evaluation of the fractional-order gradient of the error. The performance of the proposed fractional-order backpropagation algorithm was shown on certain datasets. The study (Boroomand and Menhaj 2009) on neural networks for the identification of the problem proposes a new approach to the neural networks. In another relevant study (Xue *et al.* 2020), a fractional order gradient descent with momentum method was used for updating the weights of neural network for the purpose of data classification. The error analysis of the study put forth the effectiveness of the algorithm in accelerating the convergence speed of gradient descent method, which also improves the performance with validity and accuracy.

Different computing techniques have been developed for optimized solutions regarding fractional order systems. Computational complexity, accordingly, proves to be significant to analyze problems as their complexity increases in size. Measuring the extent of the work required for the different problems' solution, computational complexity can provide a practical classification tool from the powerful lenses where the patterns can be observed both on a distinctive level and as a whole. In line with a novel mathematics-informed framework and multi-staged integrative method regarding computational complexity, there is no existing previous work as this work in the literature, obtained from such an interconnected and inclusive perspective with the methods proposed. With its novel mathematics-informed framework and multifarious integrative methods concerning computational complexity, this study has the aim of establishing a robust, reliable as well as accurate model depending upon the integration of fractional-order derivative and ANN for the purposes of diagnosis and differentiability prediction purposes for heterogeneous cancer cell that displays various transient and dynamic biological properties.

The other aim of the present work is to reveal the importance of computational complexity so that the fractional-order derivative with the least complexity could be obtained to be able to attain the optimized solution. Accordingly, the subsequent steps were integrated and applied: first of all, the Caputo fractional-order derivative with three-parametric Mittag-Leffler function (MLF) (α, β, γ) was applied to the cancer cell dataset. Hence, the new fractional models with changeable degrees were formed by enabling data fitting with the fitting algorithm MLF which has three parameters, depending upon the heavy-tailed distributions. Afterwards, the new datasets (mfc_cancer cell and the mfr_cancer cell dataset) were generated. As the following step, classical derivative (calculus) was applied to the cancer cell dataset, and from this application, the cd_ cancer cell datasets were generated. After that, the performance of the new dataset, obtained from the application of the first step and the performance of the dataset obtained from the application of the second step as well as of the cancer cell dataset was compared by the multilayer perceptron (MLP) algorithm application. As the following step, the fractional order derivatives models that could be the most optimal for the disease were produced. Last but not least, computational complexity was

employed to achieve the Caputo fractional-order derivative (FOD) that has the least complexity, for the purpose of obtaining the optimized solution as a result.

This multifarious scheme, by the application of fractional-order calculus (FOC) to optimization methods and the experimental results, have allowed us to highlight the advantage of the maximization of the model's accuracy and the minimization of the cost functions. This corroborates the applicability of the proposed method in different domains which are characterized by nonlinear and dynamic nature with varying levels of complexity. Multistage integrative models can capture the regular and significant attributes on temporal and spatial scales, besides fractional-order differential and integral equations demonstrate the generalization of classical calculus by the extension of the conceptions concerned with biological processes and systems.

The rest of the study is structured in the following manner. Section 2 is on Biocomplexity, Biological Dataset, Related Method and Methodology with the subheading, 2.1 Complex Heterogenous Cancer Cell Dataset of the Study and 2.2 Method and Methodology. Subsequently, Section 3 addresses Experimental Results and Discussion: Computation- related Application of Caputo Fractional-Order Derivatives with Three-Parametric Mittag-Leffler Functions, ANN algorithm and Computational Complexity. Finally, Section 4, provides the Concluding Remarks and Future Directions of this work.

BIOCOMPLEXITY, BIOLOGICAL DATASET, RELATED METHOD AND METHODOLOGY

Complex Heterogenous Cancer Cell Dataset of the Study

Biocomplexity addresses the complex interactions within and among different systems are evident; and thus, biocomplexity necessitates an integrated exploration of coupled human-natural systems by looking into the reasons for and consequences of biological dynamics so that it can provide the related mathematical models of complex biological phenomena to comprehend them, and to interpret and guide quantitative experimental processes. Accordingly, an accurate interpretation of the data entails the grasping of many emergent and dynamic properties that are due to the interchange of various varying biological elements in complex heterogeneous biological systems. Given such complexity, only identifying and characterizing the individual biological components in the system would not be sufficient. To address these challenges, mathematical modeling, which enables researchers to look into the degree of complexity, along with statistical techniques are important to investigate problems. If the disruptions concerning the processes and the way the interaction occurs is understood well, then it will also be possible to identify the factors that have impact on the disease. Consequently, the present study handles a complex biological dataset concerned with cancer cell, which manifests complex, heterogeneous and dynamic properties, with an undeniable effect on health and life quality, being one of the most frequent reasons for mortality.

Regarding the aims of diagnosis and differentiability prediction concerning the heterogeneous cancer cell, 30 different columns were employed. The other related details with respect to the heterogenous biocomplex cancer cell dataset with attributes computed unit-wise can be found in the following reference (Murphy 1994). Biocomplexity with a quantitative and integrative approach refers to the study of the emergence of complex and self-organized behaviors based on the interacting of numerous simple agents. This kind of an emergent complexity is representative of the different levels of organization concerning molecules and tissues. Biocomplexity, arises from biological, environmental, chemical, behavioral, physical and social interactions, encompassing the presence of multiple scales (Michener *et al.* 2001).

If one is to have a thorough understanding of the correct interpretation of data, knowing the dynamic and emerging characteristics is important. Robust, accurate and appropriate mathematical modeling serves the investigation of problems due to the fact that mathematical models allow the exploration of the way complexity processes and disruptions regarding these processes affecting the course of the disease, which also has critical impact on its prediction. This study deals with biological dataset, namely cancer cell, which shows heterogeneous, dynamic as well as complex characteristics which need to be taken under careful control in order to prevent possible detrimental effects for the future.

Method and Methodology

Algorithm based on Heavy-tailed distribution for Data Fitting with the ML Functions

Three-parametric ML functions $(\alpha,\ \beta,\ \gamma)$ Being among the domains of mathematical analysis, special function is linked with different topics (Garrappa 2015). MLF is also one of the important classes of special functions with its extensions [46]. For benefits of fractional calculus and fractional exponential functions, (Karaca and Baleanu 2022a), (Camargo *et al.* 2012) and (Fernandez and Husain 2020) can be referred to. (Baleanu and Karaca 2022) can be referred to for the details concerning the original function of ML relying on different parameters with different extensions.

The Basic Theory Behind Heavy- tailed Distributions

Pareto distribution: a power-law probability distribution

The Pareto distribution is known as a power-law probability distribution which is employed to describe different observable phenomena concerning science, social life, control and so forth (Newman 2005). Pareto distribution (P_D) as a random variable (Arnold 2014) is followed by the Pareto distribution provided it owns the tail's array as such according to Eq. (1):

$$P_D(V) = \begin{cases} 1 - \frac{(b)}{V} & V \leq b \\ 0. & V < b \end{cases} \tag{1}$$

a and b respectively show the scale and shape parameters with 1 and 1 values.

Weibull distribution: a continuous probability distribution

The Weibull distribution is employed to describe a particle size distribution (Almalki and Nadarajah 2014). The Weibull W_D as a random variable (Baleanu and Karaca 2022) follows the Weibull along with the tail formula as obtained in line with Eq. 2 (Kharazmi 2016)

$$W_D(V) = exp^{(\frac{V}{k})^{\zeta}} \tag{2}$$

k and ζ refer for shaping and scaling the parameters (Gorenflo *et al.* 2020).

Cauchy distribution: a continuous probability distribution

The Cauchy distribution refers to the spread of the ratio of normally distributed two independent random variables with a mean of zero (Steck 1958). The Cauchy distribution (C_D) as a random variable (Arnold and Beaver 2000) is followed with the tail formula whose formulation can be provided according to Eq. 3:

$$C_D(V) = \frac{1}{\pi} arctan\left(\frac{2(V-\mu)}{\beta}\right) + \frac{1}{2} \tag{3}$$

b and u respectively with 1 and 0 values represent the scale and location parameters. Mittag-Leffler (ML) distribution: probability distributions on the half line $[0, \infty)$.

Shown as $E_\alpha(y)$, the ML distribution states its reliance upon the cumulative density function (cdf) or distribution function, given based on Eq. 4 (Chakraborty and Ong 2017).

$$f(x;\ \alpha) = 1 - E_\alpha(-y^\alpha) = \sum_{k=1}^{\infty}(1)^{k-1}(k\,\alpha).x^{k\,\alpha-1} \Big/ \{\Gamma(\alpha k+1),$$
$$x > 0,\ \ 0 < \alpha \leq 1 \tag{4}$$

The ML distribution has different shapes and distributional properties (see (Mainardi and Gorenflo 2000), (Mittag-Leffler 1903), (Pillai and Functions 1990), (Karaca and Baleanu 2022a) for further related details.

The comparison of these four distributions is conducted in relation with their performances, by using log likelihood value (MLE) and the Akaike Information Criterion (AIC). The respective definitions can be presented in the following manner:

$AIC = -21nL + 2k$, and k shows the number of parameter(s) and L shows the maximum log-likelihood with regard to a particular dataset. Moreover, the other related applications of the were done as well. (please see ref. ((D'Agostino 2017), (Fan and Gijbels 2018)) for further details). Relatively high (small) values of log likelihood (AIC) may hint better fittings, as overviewed in Table 1 for different relevant distributions, which clearly yield the best of the fit. In addition, the performance of the likelihood ratio test is also provided in order that different distributions can be differentiated (see Table 1).

Figure 3 shows the functions along with the four related heavy tailed distributions. The computations were conducted by Matlab with the pattern of $[\ ] = gml\_fun(\ )$, made for the evaluation pertaining to the MLF (Petrás 2011), (Karaca and Baleanu 2022a).

The biological datasets handled in this study were fit as per the three-parametric MLF $(\alpha,\ \beta,\ \gamma)$. Algorithm 1 (see Section 3.1) is based on heavy-detailed distributions, having been applied on the cancer cell dataset to identify the optimized three-parametric MLF, found with heavy-tailed distributions. As a result, the optimized MLF $(\alpha,\ \beta,\ \gamma)$ were obtained, which is an important stage to explore the complex attributes.

The Basic Theory Behind the Fractional Calculus

Fractional calculus (FC) may be considered to be a natural extension of traditional integer order calculus because this area of mathematics is concerned with the investigation and application of the concepts of integral and non-integer differential calculus (Karaca and Baleanu 2022c). The main publications on the subject matter were seen in the early 20th centur (Tenreiro Machado *et al.* 2010).

The basic notions can be seen in classical materials by (Oldham and Spanier 1974), (Ross 1977). More recent ones can be found in the works of (David *et al.* 2011), (De Oliveira and Tenreiro Machado 2014), (Kochubei *et al.* 2019), (Valentim *et al.* 2021). Mathematical biology, with an interdisciplinary approach, looks into cancer-related phenomena via mathematical models in an inclusive way. Encompassing wide-ranging domains from biology to materials science, mathematical biological enables the comprehension of biological systems that cause disease.

By this virtue, fractional-order models can enable a better understanding related to oncological biological particularities, which contributes potentially to critical multi-stage decision-making including early diagnosis techniques, tumor evolution and treatment procedures as well as therapies tailored depending on the patient.

FC regarded as a generalization of integer order calculus, with the related core notions are presented by depending on more basic conjectures. Factorials, for example, make up only natural numbers, so this has constricting factors for its domains of applications (Herrmann 2011). Gamma function is introduced for any as factorial generalization, indicated as in (Karaca and Baleanu 2022a) can be generalized as well through the replacement of its factorial component with a gamma function, producing the following in accordance with Eq. (5).

$$e^z = \sum_{n=0}^{\infty}\frac{z^n}{\Gamma(1+n)} \tag{5}$$

and hence, the MLF for $\Re(z) > 0$ is introduced as follows, (Mittag-Leffler 1903) based on Eq (6).

$$E_\alpha(z) = \sum_{n=0}^{\infty}\frac{z^n}{\Gamma(1+n\alpha)'} \tag{6}$$

as extended to concede the three parameters for $\Re(z) > 0$ (Wiman 1905) according to Eq (7).

$$E_{\alpha,\beta}(z) = \sum_{n=0}^{\infty}\frac{z^n}{\Gamma(n\alpha+\beta)} \tag{7}$$

For the purpose of representing the solution of several fractional problems related to mathematics and physics, the MLF is critical, as the exponential functions are for integer calculus. This is because numerous simple functions are the specific cases of this generalization, so a number ofstudies have investigated the related particularities along with its uses (Camargo *et al.* 2012); (Gorenflo *et al.* 2020).

Fractional-Order Derivatives

Fractional-order derivative models are employed for the accurate modeling of the systems that require different analytical and numerical methods along with their related their applications to new and complex problems. Being a critical function with extensive domains of application, MLF is employed as a fractional differential method. The following power series are usedto define the MLF in line with the following references (Karaca and Baleanu 2022a), (Gutierrez *et al.* 2010) Eq. (8).

It, as an entire function, ensures a simple generalization of the exponential function whose reduction and convergence can be found in more detail in (Mainardi and Gorenflo 2000). The complex plane denotations and approaches related to the MLF, can be found in (Baleanu and Karaca 2022), (Mainardi 2020).

Caputo Fractional-Order Derivatives

The Caputo Fractional-order derivative is employed to model phenomena, considering the significant interactions of past and problems that have nonlocal properties based on equations having memory. The related definition is addressed as per Eq. 9 (Gutierrez *et al.* 2010), which is used to solve the differential equations:

$$D_\alpha^m\ f(t) = \frac{1}{\Gamma(m\alpha)}\int_0^t \frac{f^{(m)}(\tau)}{(t-\tau)^{\alpha+1-m}}d\tau, \tag{8}$$

Being similar to Caputo fractional derivative (CFD), Grünwald-Letnikov fractional derivative is related to most of the analytic functions, and there is a insignificantly different aspect identified when the constant function is addressed. For a constant, the Caputo fractional derivative equals to 0. However, the Riemann–Liouville counterpart does not equal to 0. Caputo fractional derivative is generally used to address the initial value FODE (Gutierrez *et al.* 2010).

The important implications about fractional integral and derivatives of the power function $(t-t_0)^{\beta}$ for, $\beta > -1$ are the case and for the Caputo's derivative, Eq. 16 is employed in the following way:

$$D_{t_0}^{\alpha}(t-t_0)^{\beta} = \begin{cases} 0 & \beta \in 0, 1, ..., m-1 \\ \frac{\Gamma(\beta+1)}{\Gamma(\beta-\alpha+1)}(t-t_0)^{\beta-\alpha} & \beta > m-1 \\ non\ existing & otherwise \end{cases}$$

D^m and $f^{(m)}$ signify the integer-order derivatives (Garrappa *et al.* 2019).

When compared with the Riemann–Liouville, the Laplace transform for the Caputo's derivative is initialized with the standard initial values shown in terms of integer-order derivatives (Ouyang and Wang 2016).

Artificial Neural Networks Algorithm

As a series of algorithms attempting to recognize the underlying patterns in a set of data, neural networks, systems of neurons, whether they be organic or artificial in nature, mimic the way the human brain operations through different processes. Since neural networks, rooted in artificial intelligence, can be adaptive in changing input, the network generates the best possible result without the need of redesigning the output criteria. As a special type of machine learning algorithms, Artificial Neural Networks (ANNs) are modeled by mimicking the human brain, and they enjoy predictive and solution abilities.

ANNs can learn from the data of the past, just like the neurons in the human nervous system learn from the past data, and can provide responses in prediction or classification forms. ANN is a self-learning network, conducts the learning from sample data sets and signals; and as nonlinear models, they manifest a complex relationship between the inputs and outputs to discover a new pattern. Accordingly, Multi-layered perceptron (MLP) is a type of network in which multiple layers of a group of perceptron are together loaded in order to make a model. In a multi-layered perceptron, the arrangement of the perceptrons is seen in interconnected layers (Karaca 2016).

The use of the MLP networks, with at least three layers, signifies there is a training set of input-output pairs (for further details on the weight coefficients, please refer to (Karaca and Cattani 2018), (Karaca *et al.* 2020), (Karaca and Baleanu 2022b)). For its related steps and architecture, please see (Mia *et al.* 2015), (Alsmadi *et al.* 2009) and (Abdul Hamid *et al.* 2011). The input signal propagates via the network layer by layer. The signal-flow of the network with two hidden layer is provided in Figure 1. Multilayer feed forward back propagation algorithm is utilized for network training and network performance testing.

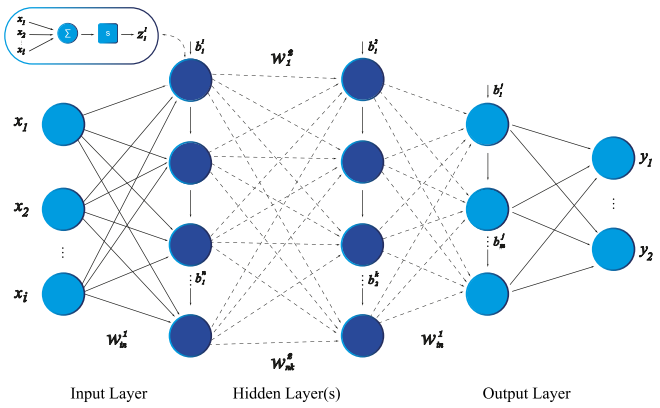

Figure 1 The configuration depiction of the MLP algorithm

The back-propagation algorithm involves the subsequent steps (Karaca and Baleanu 2020), (Karaca and Cattani 2018) and (Zhang and Wu 2008).

Step 1. Initialization: The algorithm at first is to be initialized regarding that one does not know any previous information. The thresholds and synaptic weights are picked among a uniform distribution. Sigmoid shows the activation function.

Step 2. The network should be presented by epochs of training examples to conduct computations of forward and backward.

Step 3. The preferred response vector is $d(n)$ in the output layer of computation nodes, which is a forward computation, if the input vector to the layer of sensory nodes is $x(n)$. The computation of the network's local fields and signals related to function is done by proceeding forward via the network through each of the layers. If the sigmoid function is employed, then equation provided below is considered to obtain the output signal:

$$y_j^{(l)} = \varphi_j(v_j(n))$$

If l=1, meaning that the j neuron is in the first hidden layer, then this is obtained:

$$y_j^{(0)} = x_j(n)$$

Here, $x_j(n)$ refers to the jth element of the input vector $x(n)$.

Let, L refers to the depth of network. If the neuron j is in the output layer, that is to say, $l = L$ then

$$y_j^{(L)} = o_j(n)$$

Hence, the error signal will be:

$$e(n) = d_j(n) - o_j(n)$$

$d_j(n)$ refers to the jth element of the vector of preferred response $d(n)$.

Step 4. The following equation in backward computation shows the local gradients of the network (Haykin 2009).

$$\delta_j^l(n) = \begin{cases} e_j^L(n)\varphi_j'(n)(v_j^L(n)) & output\ layer\ L \\ \\ \theta_j'(v_j^i(n))\sum_k \delta_k^{(i+1)}(n) w_{kj}^{(i+1)}(n) & hidden\ layer\ L \end{cases}$$

$\varphi_j'(\bullet)$ refers to differentiation concerning the argument. The network's synaptic weights in layer l need to be adapted to as per the generalized data rule. If η is the training-rate parameter and α signifies the momentum constant, the following is to be obtained:

$$w_{ji}^l(n+1) = w_{ji}^{(l)}(n) + \infty[w_{ji}^{(l)}(n-1)] + \eta\ \delta_i^{(l)}(n) y_i^{(l-1)}(n)$$

Step 5. Last but not least, the computations regarding the forward and backward need to be iterated till the stopping criterion chosen can be fulfilled. The learning-rate parameters and momentum are adjusted through reducing the related values as the number of iterations goes up.

In the current study, MLP algorithm was applied to the cancer cell dataset (768×9) for the purposes of diagnosis and differentiability concerning the disease classification and prediction.

Computational Complexity

Computational complexity serves the goal of classifying and comparing the practical aspect of problem solutions regarding finite combinatorial objects (Stockmeyer 1987). Technically, *Big-O notation*, used to describe the complexity of algorithms, presents the approximation or placing of an upper bound on the *resource requirements* for an algorithm. The *complexity* of the algorithm signifies the computational complexity and technically speaking, computational (algorithmic) complexity can be applied both to *space* and *time* (storage and memory) resource necessities. As a matter of fact, many individuals focus their attention on the *running time* of an algorithm (Arora and Barak 2009), (Chivers *et al.* 2015). Algorithmic complexity is denoted by the term of "*on the order of*", which indicates the approximate cost of the algorithm considering the aforementioned resource requirements. "*on the order of*" is written in an abbreviated form in capital "*O*". This gives us the more recognized term, that is to say the *Big-O notation* (Karaca *et al.* 2022).

Computational complexity measures how much work is required for the solution of different problems and providing a practical classification tool beside dealing with complex problems through the powerful lenses from which the patterns can be observed both on a distinctive level and as a whole, considering the resource usage. Concerning the temporal aspect, computational time complexity denotes the change in an algorithm's runtime, and this process is dependent on the variation in the size of the input data. When it comes to spatial properties, space complexity is the description of the amount of additional memory a related algorithm needs to have, which is dependent on the input data's size.

Big-O notation is: O (formula)

Big-O notation depends on the input parameters for whose details (Karaca *et al.* 2022) can be referred to. Figure 2 depicts the order of growth concerning the algorithms stated in *Big-O* notation.

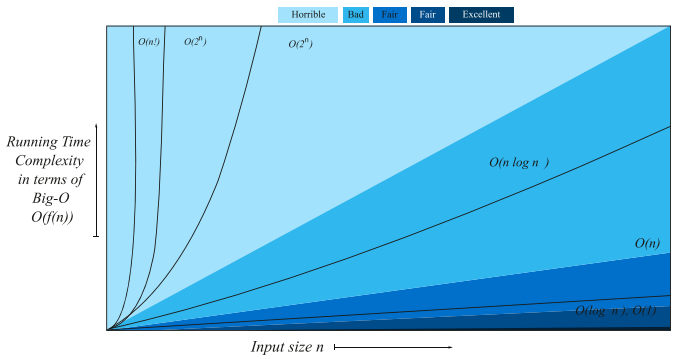

Figure 2 The order of growth pertaining to algorithms stated in *Big-O* notation

Big-O notation is a notation which is utilized to represent algorithmic complexity. It is expedient to contrast with various algorithms because the notation actually yields the conveying of the algorithm scales. That is to say, the input size becomes larger, and this is often referred to as the *order of growth* (see Figure 2) (Chivers *et al.* 2015).

Complexity of the Fast Fourier Transform (FFT) Computation

The problem related to the Fourier transform (FT) is because of its sine/cosine its complex exponential form or regression model form, necessitating $O(n^2)$ operations to compute all the Fourier coefficients. This does not apply for the short time series, though. Notwithstanding, for quite long time series, this situation may be an exhaustive computational process although performed on developed computers of the current era.

FFT is known to be an important improvement for the reduction of the complexity of the FT computation from $O(n^2)$ to $O(n\ log\ n)$, (Al Na'mneh and Pan 2007). The core notion behind this is that: assume that there is a time series $y_1, ..., y_n$ and one would like to calculate the complex Fourier coefficient z_1. It requires the following computation with the formula:

$$z_0 = \sum_{t=0}^{n-1} y_t,$$

Which is proportional to the data mean. In the case that data are de-trended or de-meaned, then this value will be 0. The next Fourier coefficient will be:

$$z_1 = \sum_{t=0}^{n-1} y_1 exp(-2\pi i.1.t/n)$$

$$= y_0 exp(-2\pi i.1.0/n) + y_1 exp(-2\pi i.1.1/n) + ...$$

Let us suppose that one would like to calculate the new coefficient . Then, this shall necessitate the computation as such:

$$z_2 = y_0\ exp(-2\pi i.2.0/n) + y_1\ exp(-2\pi i.2.1/n) + ...$$

In the 2^{nd} term, the exponential in the sum for z_2 is the same that in the 3^{rd} term in the sum for z_1, equaling to $exp(-2\pi i.1.2/n)$. There exists no need to calculate this exponential quantity two times, so one may calculate it for the first time when we assume recovering from memory is speedier compared to computing that from the very beginning. The FFT algorithm, therefore, can be regarded as an intricate bookkeeping algorithm being able to monitor such symmetries in the Fourier coefficients' computational processes.

EXPERIMENTAL RESULTS AND DISCUSSION: COMPUTATION-RELATED APPLICATION OF CAPUTO FODS WITH THREE-PARAMETRIC ML FUNCTIONS $(\alpha,\ \beta,\ \gamma)$, ANN ALGORITHM AND COMPUTATIONAL COMPLEXITY

Mathematics-informed modeling of complex systems by FODs relying upon FC plays a critical role for one to achieve the related syntheses robustly and effectively. Correspondingly, the current study has aimed at establishing an accurate model depending upon the integration of FOD and ANN for the diagnosis and differentiability pertaining to the prediction of disease which exhibits transient biological features. One other goal has been to illustrate the benefit of computational complexity to obtain the FOD that has the least complexity to be able to obtain the solution which is optimized. For this particular purpose, the proposed integrative multifarious approach has followed the below stated stages:
i) Caputo fractional derivative along with MLF that had three parameters $(\alpha,\ \beta,\ \gamma)$ was applied to the cancer cell dataset. In this way, it was possible to establish the new fractional models which had distinct degrees through the conducting of data fitting with the fitting algorithm MLF with three parameters $(\alpha,\ \beta,\ \gamma)$ dependent on Heavy-tailed distributions (see Algorithm 1). Through the algorithm, it was possible to obtain the optimized ML $(\alpha,\ \beta,\ \gamma)$ functions, which enabled us to find the best fitting MLF with three parameters $(\alpha,\ \beta,\ \gamma)$ in the cancer cell dataset. As a result, the new datasets, namely the mfc_cancer cell dataset and mfr_cancer cell dataset were obtained.
ii) The classical derivatives were applied to the cancer cell dataset (the raw dataset); and obtained the cd_cancer cell datasets.
iii) The performances of the new dataset (in line with step i), the dataset obtained from the classical derivative (calculus) application (in line with step ii) and the cancer cell dataset were compared by the MLP algorithm application. Consequently, the most optimal fractional order derivative model for the disease was engendered.
iv) In order to attain the Caputo FOD with the optimized solution and the least complexity, computational complexity was addressed. Computational complexity with the Caputo FOD (ML with three functions) and classical derivative (calculus) was calculated comparatively through the identification of the complexity concerning the cancer cell dataset. *Big O* was used to identify the derivatives which had the maximum and minimum level of complexity. The experimental results obtained from the multifarious approach with an integrative scheme corroborate and reveal the applicability of the proposed scheme. It is, consequently, shown that the Caputo FOD with the least complexity produced the most successful end result as per the output derived from that MLP algorithm.

MATLAB (MATLAB 2022) and Phyton (Van Rossum and Drake Jr 1995) were used for the obtaining of all the analyses, results and visual depictions of the study.

Computation-related Application of ML Functions with Heavy-tailed distributions' Algorithm for Optimized Cancer Cell Data Fitting

Algorithm 1 was applied to the cancer cell dataset so that it could be possible to make the identification of the optimized MLF with three parameters $(\alpha,\ \beta,\ \gamma)$ to fit the data possible. Hence, it was possible to obtain the optimized ML $(\alpha,\ \beta,\ \gamma)$ functions. To put it differently, this application enabled the finding of the best fitting MLF with three parameters in the cancer cell dataset.

Algorithm 1 has been benefited from for the fitting with three parameters related to MLF based on heavy-tailed distributions. The related steps for Algorithm 1 can be referred to in (Karaca and Baleanu 2022a).

Algorithm 1 was applied to the cancer cell dataset (569×25) for the nine attributes in units (see the details related to the dataset in the following reference (Murphy 1994)).

For the analyses, negative log likelihood: -log L was taken for the log likelihood value. The best fit distribution was generated (retrieved from the AIC, SD, MAE, MAPE, SSE, MSE and RMSE calculations). The lowest of the two values was taken and the best fitting distribution was achieved in order that the ML functions representing the data most in the most suitable way were obtained (Step 4 carried out based on Algorithm 1). The lowest value for each distribution was taken; and conducted computations for all the nine attributes. As an exemplary view, the presentations for one attribute, which is the Smoothness, are shown in Table 1). Hence, the lowest value obtained is marked bold in the respective tables. The illustrations of the figures based on the computations gained from the above mentioned attribute provided in the table indicating the distribution beside the related peak points (see Figure 3).

Table 1 depicts the smoothness attribute showing the lowest value taken for each of the heavy-tailed distributions.

The depictions regarding the calculations gained from the attributes provided in Table 1 for the Smoothness attribute the four related heavy-tailed distributions and its peak points are indicated in Figure 3. Two approaches are applicable to handle each of the cancer cell data set attribute to perform the aforementioned analysis. The former one is as such: based on the results which are obtained from each distribution as per Algorithm 1, the most accurate distribution is obtained based on the results as attained with the lowest value. The latter one has to do with the addressing of the results based on α, β and γ values depending on the results produced by the 4 heavy-tailed distributions together with the eight statistical values while performing the comparison of the connected attributes inherently (for further details Table 1 can be referred to); and in addition, the most accurate distribution is achieved based on the outcomes gained with the minimum value. Should there be extreme points within the distribution, those extreme values would not be considered for the analyses conducted in the current work.

The best outcome for ML function with three parameters was found to be MLF (10, 2, 2) for the cancer cell dataset.

Computation-related Application of Caputo FODs to Cancer Cell Dataset

Algorithm 2 provides the steps of fractional derivatives with non-integer orders for the cancer cell dataset, concerned with the identification of the order degree to find the most significant attribute.
Algorithm 2: Application of the Caputo FODs on cancer cell dataset that has non-integer orders.
Step 1: Establish non-integer orders $(y = orders = [0.1,\ 0.2,\ 0.3,\ ...,\ 0.9])$.
Step 2: All of the orders are applied to the attributes specifically in the dataset, as a result of which values were obtained for the y order fractional derivatives, identified in Step 1.
Step3: Obtain 3D graphs of 3 types of derivatives as grid and surface $(x,\ y,\ z) = (for\ each\ attribute\ of\ the\ data\ u,\ alpha,\ derivative\ of\ all\ the\ data)$.

Figure 4 presents the application steps of CFOD on the cancer cell dataset. The most significant orders were obtained based on the application of the procedures indicated in Figure 3, and for the related orders, CFOD models were identified, as detailed with the outcomes derived accordingly.

Table 1 Smoothness attribute computation concerning the cancer cell dataset for MLF depending upon Heavy-tailed distributions

Distributions	α	β	γ	-log L	AİC	SD	MAE	MAPE	SSE	MSE	RMSE
Mittag-Leffler	0.5	0.5	0.5	631.09718	1264.1944	0.008366	0.329849	0.534995	61.909033	0.108803	0.329853
Cauchy dist.	0.5	0.5	0.5	834.76194	1671.5239	0.008366	0.230607	0.374042	30.260861	0.053183	0.230613
Pareto dist.	0.5	0.5	0.5 Inf	Inf	0.008366	0	0	0	0	0	
Weibull dist.	0.5	0.5	0.5	350.9032	703.8064	0.008366	0.539741	0.875463	165.77254	0.29134	0.539759
Mittag-Leffler	3	1	1	816.59675	1635.1935	0.002348	0.238082	0.234318	32.252786	0.056683	0.238083
Cauchy dist.	3	1	1	1054.8973	2111.7946	0.002348	0.156618	0.154142	13.957155	0.024529	0.156618
Pareto dist.	3	1	1	18.14285	38.285699	0.002348	0.968628	0.95332	533.86979	0.93826	0.968638
Weibull dist.	3	1	1	578.14566	1158.2913	0.002348	0.362015	0.356292	74.5705	0.131055	0.362016
Mittag-Leffler	5	1	3	808.74844	1619.4969	0.000352	0.241388	0.240808	33.154539	0.058268	0.241388
Cauchy dist.	5	1	3	1047.1228	2096.2456	0.000352	0.158772	0.15839	14.343667	0.025209	0.158772
Pareto dist.	5	1	3	2.738101	7.476202	0.000352	0.9952	0.992808	563.55062	0.990423	0.9952
Weibull dist.	5	1	3	570.37073	1142.7415	0.000352	0.366994	0.366112	76.63567	0.134685	0.366994
Mittag-Leffler	5	1	7	810.58361	1623.1672	0.00082	0.240611	0.239266	32.941402	0.057894	0.240611
Cauchy dist.	5	1	7	1048.9504	2099.9009	0.00082	0.158263	0.157378	14.251833	0.025047	0.158263
Pareto dist.	5	1	7	6.378511	14.757021	0.00082	0.988854	0.983328	556.38788	0.977835	0.988855
Weibull dist.	5	1	7	572.1984	1146.3968	0.00082	0.365817	0.363773	76.145014	0.133823	0.365818
Mittag-Leffler	7	2	1	807.37739	1616.7548	0	0.24197	0.24197	33.314695	0.05855	0.24197
Cauchy dist.	7	2	1	1045.7534	2093.5068	0	0.159155	0.159154	14.412869	0.02533	0.159155
Pareto dist.	7	2	1	0.00272	2.005439	0	0.999995	0.999993	568.99456	0.99999	0.999995
Weibull dist.	7	2	1	569.00136	1140.0027	0	0.367879	0.367878	77.005408	0.135335	0.367879
Mittag-Lefflerr	7	2	2	807.37874	1616.7575	1e-06	0.24197	0.241968	33.314536	0.058549	0.24197
Cauchy dist.	7	2	2	1045.7548	2093.5095	1e-06	0.159154	0.159153	14.412801	0.02533	0.159154
Pareto dist.	7	2	2	0.005439	2.010879	1e-06	0.99999	0.999986	568.98912	0.999981	0.99999
Weibull dist.	7	2	2	569.00272	1140.0054	1e-06	0.367878	0.367876	77.00504	0.135334	0.367878
Mittag-Lefflerr	7	2	4	807.38147	1616.7629	1e-06	0.241968	0.241966	33.314217	0.058549	0.241968
Cauchy dist.	7	2	4	1045.7575	2093.515	1e-06	0.159153	0.159152	14.412663	0.02533	0.159153
Pareto dist.	7	2	4	0.010879	2.021757	1e-06	0.999981	0.999971	568.97824	0.999962	0.999981
Weibull dist.	7	2	4	569.00544	1140.0109	1e-06	0.367876	0.367872	77.004304	0.135333	0.367876
Mittag-Leffler	7	2	8	807.3869	1616.7738	3e-06	0.241966	0.241961	33.31358	0.058548	0.241966
Cauchy dist.	7	2	8	1045.7629	2093.5259	3e-06	0.159152	0.159149	14.412387	0.025329	0.159152
Pareto dist.	7	2	8	0.021757	2.043515	3e-06	0.999962	0.999943	568.95649	0.999924	0.999962
Weibull dist.	7	2	8	569.01088	1140.0218	3e-06	0.367872	0.367865	77.002832	0.13533	0.367872
Mittag-Leffler	10	2	2	807.37603	1616.7521	0	0.241971	0.241971	33.314854	0.05855	0.241971
Cauchy dist.	10	2	2	1045.7521	2093.5041	0	0.159155	0.159155	14.412938	0.02533	0.159155
Pareto dist.	10	2	2	5e-06	2.000011	0	1	1	568.99999	1	1
Weibull dist.	10	2	2	569	1140	0	0.367879	0.367879	77.005775	0.135335	0.367879
Mittag-Leffler	10	2	5	807.37603	1616.7521	0	0.241971	0.241971	33.314853	0.05855	0.241971
Cauchy dist.	10	2	5	1045.7521	2093.5041	0	0.159155	0.159155	14.412938	0.02533	0.159155
Pareto dist.	10	2	5	1.4e-05	2.000027	0	1	1	568.99997	1	1
Weibull dist.	10	2	5	569.00001	1140	0	0.367879	0.367879	77.005774	0.135335	0.367879
Mittag-Leffler	10	2	7	807.37604	1616.7521	0	0.241971	0.241971	33.314853	0.05855	0.241971
Cauchy dist.	10	2	7	1045.7521	2093.5041	0	0.159155	0.159155	14.412938	0.02533	0.159155
Pareto dist.	10	2	7	1.9e-05	2.000038	0	1	1	568.99996 1	1	
Weibull dist.	10	2	7	569.00001	1140	0	0.367879	0.367879	77.005774	0.135335	0.367879

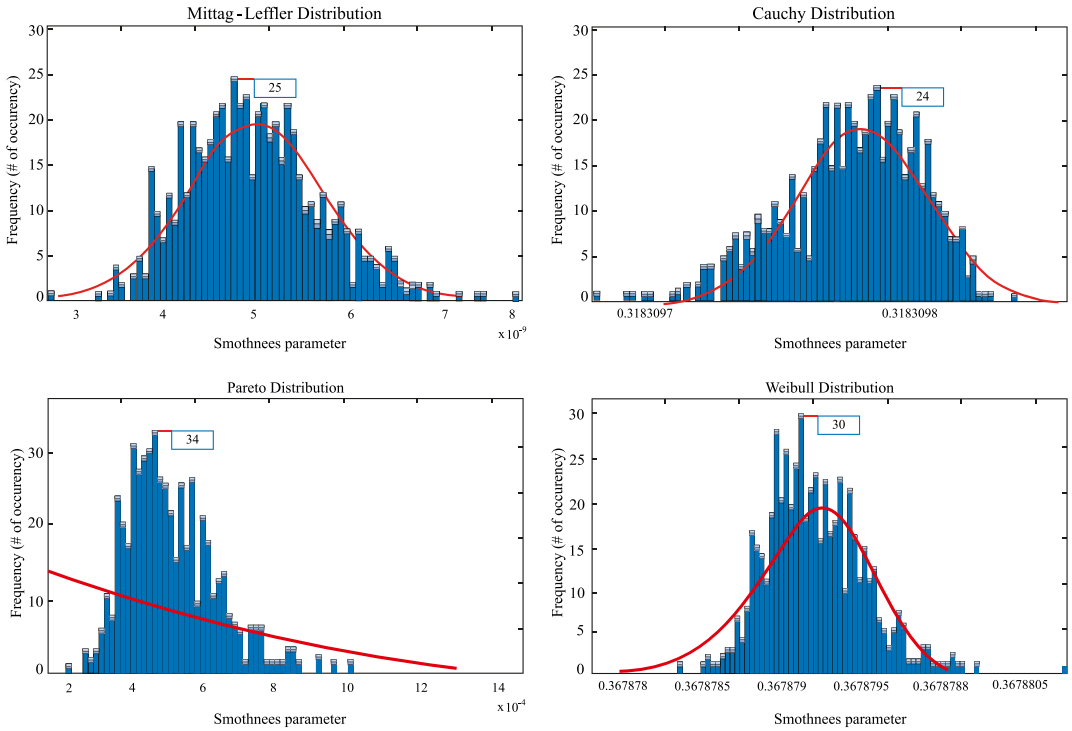

Figure 3 Smoothness attribute computation based on cancer cell dataset for MLF depending upon Heavy-tailed distributions.

The computation-related application of CFODs and classical derivative, both with $(y = orders = [0.1,\ 0.2,\ 0.3, ...,\ 0.9])$, for all of the related parameters were conducted for the cancer cell dataset. As an example to depict the computations in a clear way, Figure 4 is presented for three parameters (the radius parameter, the symmetry parameter and the smoothness parameter). Figure 4 shows the computational application of CFODs and classical derivative, both with $y(= orders)$, for 3 parameters for the cancer cell dataset. CFOD and classical derivative models were identified for the related orders. The computation-related application of CFODs and classical derivative, for all the parameters were carried out concerning the cancer cell dataset. To illustrate, for depicting the computations in a evident manner, Figure 4 provides the three parameters including radius, symmetry and smoothness). Figure 4 shows the computation-related application of CFODs and classical derivative, both with $y(= orders)$, for the cancer cell dataset. CFOD and classical derivative models were identified for these orders.

Computation-related Application of ANN Algorithm to Cancer Cell Dataset and Optimized Results Diagnostic Treatments and Predictive Transdifferentiability

The computation-related application of CFODs and classical derivative obtained in Figure 4 for all the parameters for the cancer cell dataset generates the significant attributes in newly obtained datasets. CFOD and classical derivative models were found and determined for the related orders depending upon the model. Table 2 shows the parameters of that MLP algorithm, employed in the present study.

Figure 5 presents the application of CFODs with MLF parameters MLF (10, 2, 2) to the cancer cell dataset, besides the new datasets (mfc_cancer cell dataset and mfr_cancer cell dataset), as taken from the significant attributes from the related application, with MLP algorithm application, to the new dataset ensuring performance of the orders with respect to the disease diagnosis as well as differentiability.

Figure 6 presents the application of classical derivative to the cancer cell dataset, besides that of the MLP algorithm application to the new dataset (cd_cancer cell dataset), which provides the orders' performance with respect to the disease diagnosis and differentiability.

CFODs indicate the condition of higher conditions concerning regularity in terms of differentiability. The related derivative needs to be calculated initially for the fractional derivative of a function in the sense of Caputo.

Table 3 presents the outcomes generated by CFODs; and the classical derivative application is contrasted with the outcomes of classical derivative showing that CFOD (with order 0.8) provides us with better results. The result that MLP algorithm application cancer cell dataset based on CFOD and classical calculus yielding the respective highest accuracy results is presented for the related orders: for order 0.2 (79.4376%); for order 0.5 (80.1406%); for order 0.8 (83.4798%) and for order 1 (79.9649%) in Table 3. It is observed that the results obtained by CFOD application with changing orders produces more accurate outcomes. As a consequence, the CFOD for differentiable functions generated accuracy rates with more robustness. Hence, the definition for CFODs is performed for differentiable functions while functions without any first-order derivative may own fractional derivatives with all orders which equal to lower than 1.

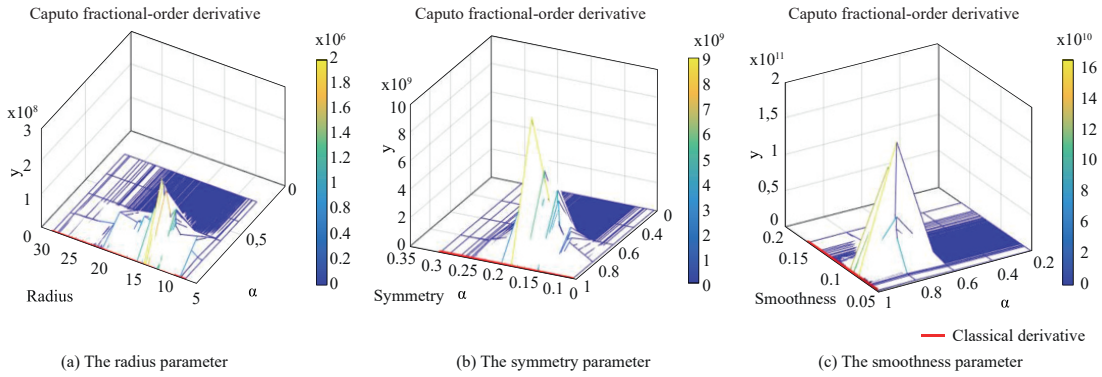

(a) The radius parameter (b) The symmetry parameter (c) The smoothness parameter

Figure 4 Computation-related application of CFODs and Classical derivative for the three parameters (a) The radius (b) The symmetry and (c) The smoothness for the cancer cell dataset.

Table 2 MLP algorithm's Network Parameters

Network Properties	Values
Adoption learning function	Learngdm
Training Properties	Levenberg- Marquart ('trainlm')
Transfer function	Tansig
Performance	Mean squared error (MSE)
Epoch number	1000
Hidden layer number	3
Test dataset	(85x1)
Training dataset	(399x1)
Validation dataset	(85x1)
Output	Cancer

Table 3 The optimized outcomes derived from CFODs with three-parametric MLF and classical derivatives for the mfc_cancer cell dataset with MLP algorithm

Fractional Differential Type/Order	Percentage of Correct Classification (Accuracy)	Sensitivity	Precision	Specificity	F1-score	Multiclass Classification (MCC)	Area Under ROC Curve the (AUC)
Caputo/0.2	79.4376	100	75.3165	44.8113	85.9206	0.58095	0.72406
Caputo/0.5	80.1406	96.9188	77.2321	51.8868	85.9627	0.57669	0.76685
Caputo/0.8	83.4798	98.0392	80.0915	58.9623	88.1612	0.65292	0.79883
Caputo/1	79.9649	99.1597	76.1290	47.6415	86.1314	0.58548	0.74041
Dataset	80.6678	96.9188	77.7528	53.3019	86.2843	0.58816	0.77370

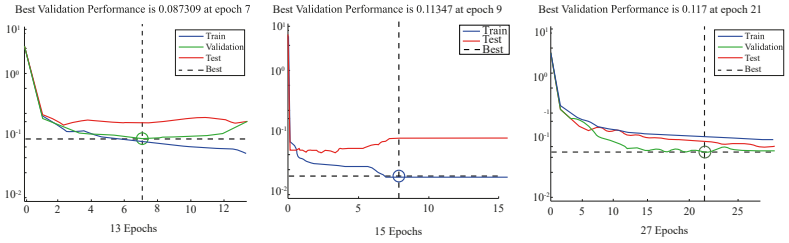

(a) Best validation performance (MSE) for mfc_cancer cell dataset

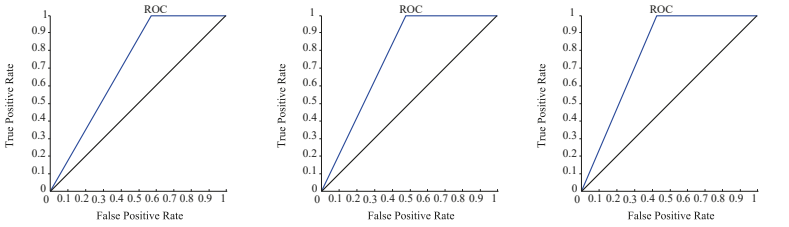

(b) ROC analyses for mfc_cancer cell dataset

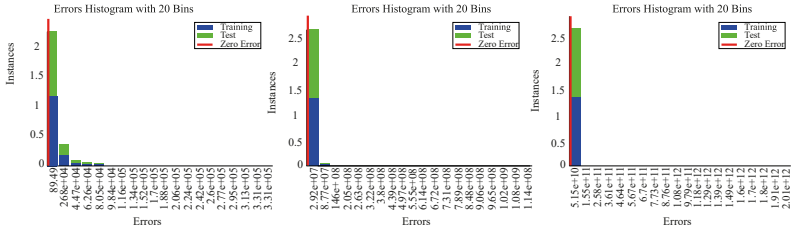

(c) Error histogram for mfc_cancer cell dataset

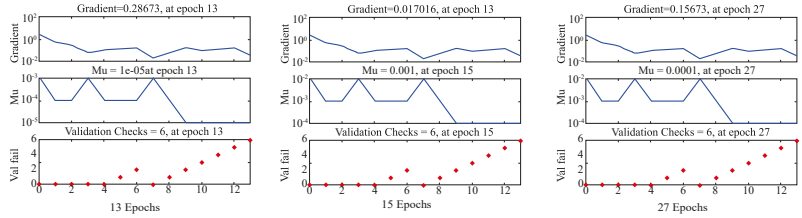

(d) Training state for mfc_cancer cell dataset

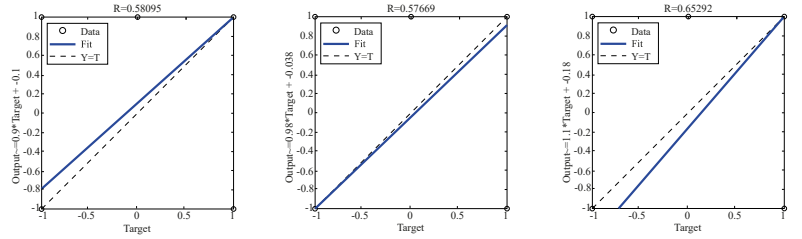

(e) Linear regression graphs for mfc_cancer cell dataset

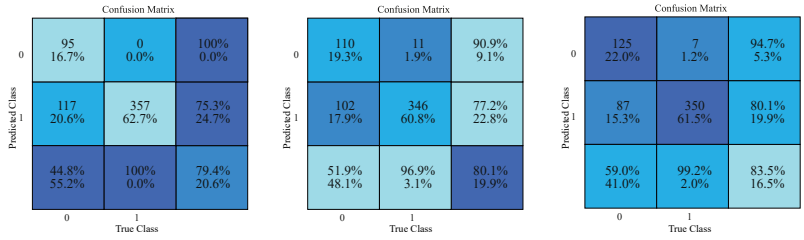

(f) Confusion matrix for mfc_cancer cell dataset

Figure 5 The MLP algorithm application to the mfc_cancer cell dataset (a) Best validation performance analyses (b) ROC analyses (c) Error Histograms with 20 Bins (d) Training state analyses (e) Linear regression graphs and (f) Confusion matrices

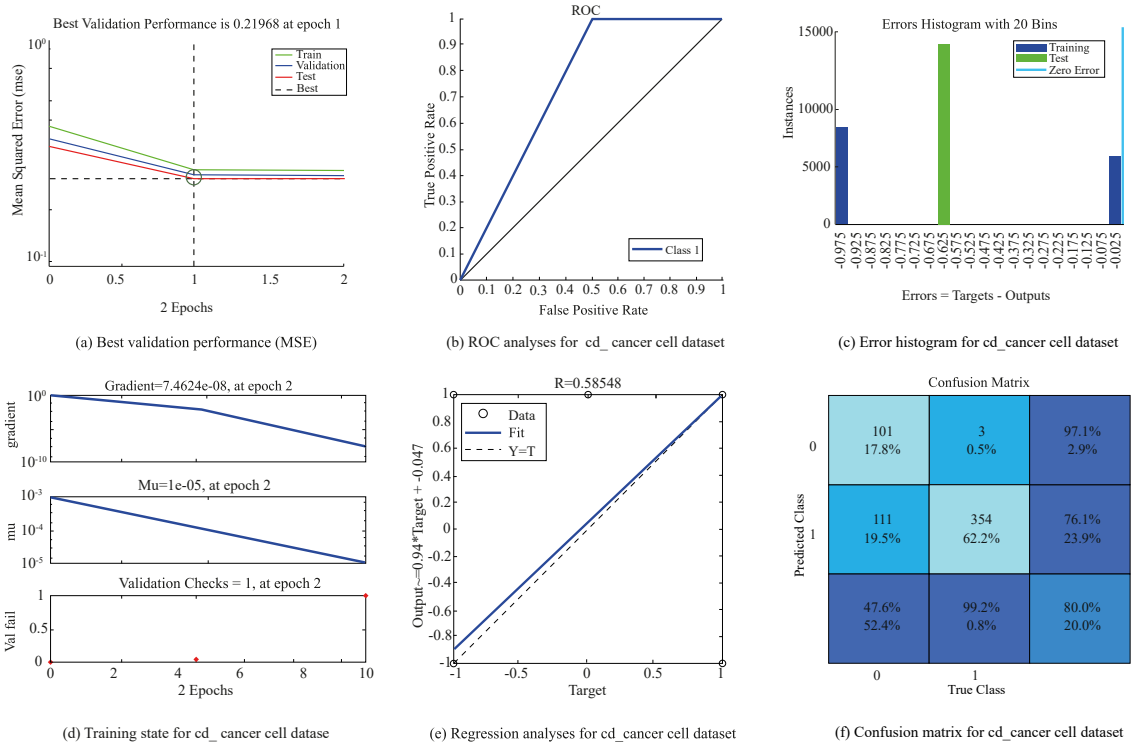

(a) Best validation performance (MSE)

(b) ROC analyses for cd_ cancer cell dataset

(c) Error histogram for cd_cancer cell dataset

(d) Training state for cd_ cancer cell datase

(e) Regression analyses for cd_cancer cell dataset

(f) Confusion matrix for cd_cancer cell dataset

Figure 6 The MLP algorithm application to the cd_cancer cell dataset (a) Best validation performance analyses (b) ROC analyses (c) Error Histograms with 20 Bins (d) Training state analyses (e) Linear regression graphs and (f) Confusion matrices

The Application of Computational Complexity based on Caputo FOD to the cancer cell dataset

Computational complexity, is utilized to classify the computational problems. As it is not possible to address some matters in computational biology in a computational sense, it could be limiting to search for the optimal solution for some practical reasons. Consequently, those kinds of matters are addressed through heuristics and approximations to be able to overcome the computational requirements that bring about solutions which are suboptimal. Yet, when essential complexity of an algorithm is investigated, it can also be possible to identify the algorithm's efficiency.

Bearing that in mind, during the conducting of the complexity computations for the three-parametric ML function, CFOD and classical derivative, FFT, integration, gamma function and m^{th} derivative were shown in *Big O* form.

The computational complexity application for the MLF with three parameters is as per Eq. 10.

$$E^{\gamma}_{\alpha,\beta}(x) = \sum_{n=0}^{\infty} \frac{\Gamma(\gamma+n)}{\Gamma(\gamma)\Gamma(n\alpha+\beta)} \cdot \frac{x^n}{n!} \quad \alpha, \beta, \delta > 0, \; x \in \mathbb{R}^N \tag{9}$$

$$O(E^{\gamma}_{\alpha,\beta}(x)) = O\left(\frac{\Gamma(\gamma+n)}{\Gamma(\gamma)\Gamma(n\alpha+\beta)} \cdot \frac{x^n}{n!}\right) \tag{10}$$

The application of the computational complexity for CFOD based on the 3 parametric ML function can be seen according to Eq.11.

$$\begin{aligned} O(D^{\alpha} f(t)) &= O\left(\frac{1}{\Gamma(m-\alpha)} \int_0^t \frac{f^{(m)}(\tau)}{(t-\tau)^{(\alpha+1-m)}} d\tau \right) \\ O(D^{\alpha} f(t)) &= O(log(m\alpha)^{-2}.N^2.O_{ML}(N)^m) \\ O(D^{\alpha} f(t)) &= O(log(1\alpha)^{-2}.N^2.O_{ML}(N)) \end{aligned} \tag{11}$$

The outcomes of the computational complexity application depending on the CFOD and classical derivatives to the cancer cell dataset are presented in Table 4.

While carrying out the complexity computations with regard to three-parametric MLF $(\alpha,\ \beta,\ \gamma)$, CFOD, classical derivative, FFT, integration, gamma function and m^{th} derivative are handled in the form of *Big O*.

The outcomes regarding the application of computational complexity based on Caputo FOD and classical derivatives to the cancer cell dataset are presented in Table 4.

CFOD is $\alpha \leq 1$, then α the value goes down. The complexity, in the meantime, goes up logarithmically. When this condition is at stake, $\alpha = 1$, then it belongs to the category of trivial.

As per the complexity outcomes obtained for CFOD related to the computational complexity as obtained (presented in Table 4), as it can be observed, the lowest complexity order is for 0.8 and the highest complexity is the case for order 0.2.

The lowest order, namely 0.8, with the least complexity of CFOD, provides the most successful outcome as 83.80% in the diagnostic and classification purpose of disease related to cancer cell by the ANN algorithm.

Table 4 Outcomes of the computational complexity application depending on theCaputo FOD and classical derivativeto the cancer cell dataset.

	Order	Cancer cell dataset (N=24)	
Caputo FOC (for Eq.11)	(α)**= 0.2**	(N/log(0.8))2*(log(-18*N-4)/N)	= 2.9294e+03+1.5142e+03i
	(α)**= 0.5**	(N/log(0.5))2*(log(-18*N-4)/N)	= 3.0360e+02+1.5693e+02i
	(α)**= 0.8**	(N/log(0.2))2*(log(-18*N-4)/N)	= 56.3116+29.1080i
	(α)**= 1**	(N/log(0))2*(log(-18*N-4)/N)	= 0

CONCLUDING REMARKS AND FUTURE DIRECTIONS

Computational complexity which concerns the way needed resources are employed for the answer and solution of the problem is important to address the computational problems in complex and nonlinear systems. Since it could not be to address some of the problems in computational biology in a computational perspective, it could be restricting to seek the optimal solution due to practical reasons. As a result, sometimes those problems are addressed by heuristics and approximations so that one can overcome the computational requirements; yet, such an approach may result in solutions which are suboptimal. When the essential complexity of an algorithm is explored, the efficiency of the algorithm is able to be assessed through computational complexity. As uncertainties in the complex processes bring about computational complexity, fractional-order models are employed in a widespread way to describe the real processes and phenomena. Fractional-order calculus concerns the integration and differentiation of non-integer orders and it is dependent on fractional-order thinking. The aim is to enable a better grasp of complex and dynamic systems, to improve the processing and control of complex elements and to make the optimization performance more optimal.

Dynamic complexity arises from the latent factors and the interactions between factors which may have a significant influence on the systems' performance. It is not possible to characterize some particular complex systems in nature by classical integer-order calculus models; so a fractional-order system based model which is capable of describing the system performance more accurately is needed. Different levels of complexity are one of the most characteristic features of biological systems; therefore, the rules of how complex behaviors and patterns emerge and the novel physical as well as chemical properties and functions with relation to biological entities need to be holistically understood. The behavior of high-level structures is also more than the whole of the direct interactions between one single component. Biocomplexity, as an integrative approach and philosophy, addresses the emergence of complex and self-organized behaviors which are based on the interaction of many simple agents. This sort of an emergent complexity represents the organization of molecules into cellular machinery, including the organization of cells into tissues and to the organization of individuals into communities.

It should also be noted that biocomplexity arises from many different interactions including biological, environmental, chemical, behavioral, physical and social ones, with the presence of multiple scales. Within the mathematics-informed framework based on FOC and ANNs, the integrative approaches can be employed for reliable and accurate comprehension of different complex biological processes that make up spatio-temporal scales. This line of methods has the aim of achieving optimized solutions through maximizing the accuracy of the model and minimizing the computational cost. In this way, capturing the significant and regular attributes on those spatio-temporal scales can provide the generalization of classical calculus by the extension of the conceptions related to biological processes and systems. Computational complexity also comes to the foreground since it is used to measure the extent of work required for the solution of different problems while providing us with a practical classification tool when one deals with complex problems. Accordingly, the present study has aimed at constructing a robust as well as an accurate model reliant upon the integration of FOD as well as ANN for the diagnostic and predictive differentiability aims for cancer cell propensity.

We have also attempted to show the importance of computational complexity to obtain the FOD with the lowest complexity so that it could be possible to obtain the optimized solution. Based on the experimental results obtained from this study, the CFOD has yielded the most accurate results for order 0.8 in terms of diagnosis and differentiability of the disease, which also has shown its critical role, suggesting the selection of the appropriate alternative mathematical models can be established in advance so that we can take uncertain situations under control and conduct the management effectively. The results also highlight the advantages of CFOD since it allows the conventional initial and boundary conditions to be encompassed in the formulation of the problem as well as its derivative for the constant as zero. On the flipside, the functions that lack differentiable properties do not have fractional derivative, that is to say, Caputo derivative's application areas remain has to be decreased. Furthermore, other fractional order derivatives (Riemann–Liouville, Grünwald-Letnikov and so forth) can be applied and compared with the machine learning methods with respect to different datasets. In view of these, the multifarious scheme with the related integrative steps, based on the application of FOC to the optimization means and the experimental results, have enabled us to emphasize the benefits of model accuracy maximization and cost function minimization.

Considering these elements and approach addressed in this study, the below directions can be stated for future investigation:

- The integrated method of fractional-order calculus and Artificial Intelligence (AI) methods can have a facilitating role for the prediction of future occurrence of manifold phenomena while comparing the predicted data with the actual data to validate with high-performance computing.
- Fractional order and fractional derivatives along with the generalization of integer calculus order, addressing the varying orders of derivatives and integrals as used in this study, can provide a viable framework to enhance optimization tasks focusing on complex order optimization.
- The increased capability of machine learning algorithms with computing power and accuracy for spectral data, signals, images and so forth in connection with the inherent properties

help the managing of memory effects and apparently chaotic behavior in critical multi-stage decision-making processes.
- The promoting of new methods to enhance performance outcomes can be suggested to take strategic actions to yield optimal results for accurate prediction of future in areas characterized by dynamic complexity where "know-why" research activities are required to develop models that merge phenomenological and data-oriented approaches in other applicable domains.
- The sophisticated integrative and multi scale approach used with computer-assisted proofs focusing on computational bio complexity fosters inter- and trans disciplinary work through the employment of computational power and combined expertise of different complex realms.

All in all, the experimental results obtained enable the diagnosis and differentiability in cancer cell prediction based on computational complexity, fractional order derivatives and ANN. Taken together, the scheme proposed with a multi-stage approach and/or novel methods in this study has demonstrated the proposed method's applicability and satisfactory predictive aspect in different domains characterized by dynamic, chaotic, heterogeneous and nonlinear nature displaying varying levels of complexity, which is of crucial value in terms of timely detection and taking action toward appropriate and tailored treatments.

Conflicts of interest

The author declares that there is no conflict of interest regarding the publication of this paper.

Availability of data and material

Not applicable.

LITERATURE CITED

Abdul Hamid, N., N. Mohd Nawi, R. Ghazali, and M. N. Mohd Salleh, 2011 Accelerating learning performance of back propagation algorithm by using adaptive gain together with adaptive momentum and adaptive learning rate on classification problems. In *Ubiquitous Computing and Multimedia Applications: Second International Conference, UCMA 2011, Daejeon, Korea, April 13-15, 2011. Proceedings, Part II 2*, pp. 559–570, Springer.

Aguilar, C. Z., J. Gómez-Aguilar, V. Alvarado-Martínez, and H. Romero-Ugalde, 2020 Fractional order neural networks for system identification. Chaos, Solitons & Fractals **130**: 109444.

Al Na'mneh, R. and W. D. Pan, 2007 Five-step fft algorithm with reduced computational complexity. Information processing letters **101**: 262–267.

Almalki, S. J. and S. Nadarajah, 2014 Modifications of the weibull distribution: A review. Reliability Engineering & System Safety **124**: 32–55.

Alsmadi, M., K. B. Omar, and S. A. Noah, 2009 Back propagation algorithm: the best algorithm among the multi-layer perceptron algorithm .

Arnold, B. C., 2014 Pareto distribution. Wiley StatsRef: Statistics Reference Online pp. 1–10.

Arnold, B. C. and R. J. Beaver, 2000 The skew-cauchy distribution. Statistics & probability letters **49**: 285–290.

Arora, S. and B. Barak, 2009 *Computational complexity: a modern approach*. Cambridge University Press.

Baleanu, D. and Y. Karaca, 2022 Mittag-leffler functions with heavy-tailed distributions' algorithm based on different biology datasets to be fit for optimum mathematical models' strategies. In *Multi-Chaos, Fractal and Multi-fractional Artificial Intelligence of Different Complex Systems*, pp. 117–132, Elsevier.

Blazewicz, J. and M. Kasprzak, 2012 Complexity issues in computational biology. Fundamenta Informaticae **118**: 385–401.

Boroomand, A. and M. B. Menhaj, 2009 Fractional-based approach in neural networks for identification problem. In *2009 Chinese Control and Decision Conference*, pp. 2319–2322, IEEE.

Camargo, R. F., E. C. de Oliveira, and J. Vaz, 2012 On the generalized mittag-leffler function and its application in a fractional telegraph equation. Mathematical Physics, Analysis and Geometry **15**: 1–16.

Carletti, M. and M. Banerjee, 2019 A backward technique for demographic noise in biological ordinary differential equation models. Mathematics **7**: 1204.

Chakraborty, S. and S. Ong, 2017 Mittag-leffler function distribution-a new generalization of hyper-poisson distribution. Journal of Statistical distributions and applications **4**: 1–17.

Chivers, I., J. Sleightholme, I. Chivers, and J. Sleightholme, 2015 An introduction to algorithms and the big o notation. Introduction to Programming with Fortran: With Coverage of Fortran 90, 95, 2003, 2008 and 77 pp. 359–364.

D'Agostino, R., 2017 *Goodness-of-fit-techniques*. Routledge.

David, S., J. Linares, and E. Pallone, 2011 Cálculo de ordem fracionária: apologia histórica, conceitos básicos e algumas aplicações. Revista Brasileira de Ensino de Física **33**: 4302–4302.

De Oliveira, E. C. and J. A. Tenreiro Machado, 2014 A review of definitions for fractional derivatives and integral. Mathematical Problems in Engineering **2014**.

Debnath, L., 2003 Recent applications of fractional calculus to science and engineering. International Journal of Mathematics and Mathematical Sciences **2003**: 3413–3442.

Du, D.-Z. and K.-I. Ko, 2011 *Theory of computational complexity*, volume 58. John Wiley & Sons.

Du, M., Z. Wang, and H. Hu, 2013 Measuring memory with the order of fractional derivative. Scientific reports **3**: 3431.

Fan, J. and I. Gijbels, 2018 *Local polynomial modelling and its applications*. Routledge.

Fernandez, A. and I. Husain, 2020 Modified mittag-leffler functions with applications in complex formulae for fractional calculus. Fractal and Fractional **4**: 45.

Garrappa, R., 2015 Numerical evaluation of two and three parameter mittag-leffler functions. SIAM Journal on Numerical Analysis **53**: 1350–1369.

Garrappa, R., E. Kaslik, and M. Popolizio, 2019 Evaluation of fractional integrals and derivatives of elementary functions: Overview and tutorial. Mathematics **7**: 407.

Gomolka, Z., 2018 Backpropagation algorithm with fractional derivatives. In *ITM web of conferences*, volume 21, p. 00004, EDP Sciences.

Gorenflo, R., A. A. Kilbas, F. Mainardi, S. V. Rogosin, *et al.*, 2020 *Mittag-Leffler functions, related topics and applications*. Springer.

Gutierrez, R. E., J. M. Rosário, and J. Tenreiro Machado, 2010 Fractional order calculus: basic concepts and engineering applications. Mathematical problems in engineering **2010**.

Haykin, S., 2009 *Neural networks and learning machines, 3/E*. Pearson Education India.

Herrmann, R., 2011 *Fractional calculus: an introduction for physicists*. World Scientific.

Jachowicz, R. E., P. Duch, P. W. Ostalczyk, and D. J. Sankowski, 2022 Fractional order derivatives as an optimization tool for object detection and tracking algorithms. IEEE Access **10**: 18619–

18630.
Kadam, P., G. Datkhile, and V. A. Vyawahare, 2019 Artificial neural network approximation of fractional-order derivative operators: analysis and dsp implementation. In *Fractional Calculus and Fractional Differential Equations*, pp. 93–126, Springer.
Karaca, Y., 2016 Case study on artificial neural networks and applications. Applied Mathematical Sciences **10**: 2225–2237.
Karaca, Y. and D. Baleanu, 2020 A novel r/s fractal analysis and wavelet entropy characterization approach for robust forecasting based on self-similar time series modeling. Fractals **28**: 2040032.
Karaca, Y. and D. Baleanu, 2022a Algorithmic complexity-based fractional-order derivatives in computational biology. In *Advances in Mathematical Modelling, Applied Analysis and Computation: Proceedings of ICMMAAC 2021*, pp. 55–89, Springer.
Karaca, Y. and D. Baleanu, 2022b Artificial neural network modeling of systems biology datasets fit based on mittag-leffler functions with heavy-tailed distributions for diagnostic and predictive precision medicine. In *Multi-Chaos, Fractal and Multi-fractional Artificial Intelligence of Different Complex Systems*, pp. 133–148, Elsevier.
Karaca, Y. and D. Baleanu, 2022c Computational fractional-order calculus and classical calculus ai for comparative differentiability prediction analyses of complex-systems-grounded paradigm. In *Multi-Chaos, Fractal and Multi-fractional Artificial Intelligence of Different Complex Systems*, pp. 149–168, Elsevier.
Karaca, Y., D. Baleanu, and R. Karabudak, 2022 Hidden markov model and multifractal method-based predictive quantization complexity models vis-á-vis the differential prognosis and differentiation of multiple sclerosis' subgroups. Knowledge-Based Systems **246**: 108694.
Karaca, Y. and C. Cattani, 2018 Computational methods for data analysis. In *Computational Methods for Data Analysis*, De Gruyter.
Karaca, Y., M. Moonis, and D. Baleanu, 2020 Fractal and multifractional-based predictive optimization model for stroke subtypes' classification. Chaos, Solitons & Fractals **136**: 109820.
KARCI, A. *et al.*, 2014 Fractional order derivative and relationship between derivative and complex functions. Mathematical Sciences and Applications E-Notes **2**: 44–54.
Khan, H., A. Khan, M. Al Qurashi, D. Baleanu, and R. Shah, 2020 An analytical investigation of fractional-order biological model using an innovative technique. Complexity **2020**: 1–13.
Kharazmi, O., 2016 Generalized weighted weibull distribution. Journal of Mathematical Extension **10**: 89–118.
Kochubei, A., Y. Luchko, V. E. Tarasov, and I. Petráš, 2019 *Handbook of fractional calculus with applications*, volume 1. de Gruyter Berlin, Germany.
Krishna, B. and K. Reddy, 2008 Active and passive realization of fractance device of order 1/2. Active and passive electronic components **2008**.
Lewis, M. R., P. G. Matthews, and E. M. Hubbard, 2016 Neurocognitive architectures and the nonsymbolic foundations of fractions understanding. In *Development of mathematical cognition*, pp. 141–164, Elsevier.
Li, C., D. Qian, Y. Chen, *et al.*, 2011 On riemann-liouville and caputo derivatives. Discrete Dynamics in Nature and Society **2011**.
Lopes, A. M. and J. Tenreiro Machado, 2019 The fractional view of complexity.
Magin, R. L., 2010 Fractional calculus models of complex dynamics in biological tissues. Computers & Mathematics with Applications **59**: 1586–1593.
Mainardi, F., 2020 Why the mittag-leffler function can be considered the queen function of the fractional calculus? Entropy **22**: 1359.
Mainardi, F. and R. Gorenflo, 2000 On mittag-leffler-type functions in fractional evolution processes. Journal of Computational and Applied mathematics **118**: 283–299.
Mall, S. and S. Chakraverty, 2018 Artificial neural network approach for solving fractional order initial value problems. arXiv preprint arXiv:1810.04992 .
MATLAB, 2022 *version 9.12.0 (R2022a)*. The MathWorks Inc., Natick, Massachusetts.
Matusiak, M., 2020 Optimization for software implementation of fractional calculus numerical methods in an embedded system. Entropy **22**: 566.
Mia, M. M. A., S. K. Biswas, M. C. Urmi, and A. Siddique, 2015 An algorithm for training multilayer perceptron (mlp) for image reconstruction using neural network without overfitting. International Journal of Scientific & Technology Research **4**: 271–275.
Michener, W. K., T. J. Baerwald, P. Firth, M. A. Palmer, J. L. Rosenberger, *et al.*, 2001 Defining and unraveling biocomplexity. BioScience **51**: 1018–1023.
Mittag-Leffler, G., 1903 Sur la nouvelle fonction ea (x). Comptes rendus de l'Académie des Sciences **137**: 554–558.
Murphy, P. M., 1994 Uci repository of machine learning databases. http://www. ics. uci. edu/˜ mlearn/MLRepository. html .
Newman, M. E., 2005 Power laws, pareto distributions and zipf's law. Contemporary physics **46**: 323–351.
Niu, H., Y. Chen, and B. J. West, 2021 Why do big data and machine learning entail the fractional dynamics? Entropy **23**: 297.
Oldham, K. and J. Spanier, 1974 *The fractional calculus theory and applications of differentiation and integration to arbitrary order*. Elsevier.
Ouyang, Y. and W. Wang, 2016 Comparison of definition of several fractional derivatives. In *2016 International Conference on Education, Management and Computer Science*, pp. 553–557, Atlantis Press.
Panda, R. and M. Dash, 2006 Fractional generalized splines and signal processing. Signal Processing **86**: 2340–2350.
Pang, D., W. Jiang, and A. U. Niazi, 2018 Fractional derivatives of the generalized mittag-leffler functions. Advances in Difference Equations **2018**: 1–9.
Petrás, I., 2011 *Fractional derivatives, fractional integrals, and fractional differential equations in Matlab*. IntechOpen.
Pillai, R. and O. M.-L. Functions, 1990 Related distributions. Ann. Inst. Statist. Math **42**: 157–161.
Raubitzek, S., K. Mallinger, and T. Neubauer, 2022 Combining fractional derivatives and machine learning: A review. Entropy **25**: 35.
Rodríguez-Germá, L., J. J. Trujillo, and M. Velasco, 2008 Fractional calculus framework to avoid singularities of differential equations. Fract. Cal. Appl. Anal **11**: 431–441.
Ross, B., 1977 Fractional calculus. Mathematics Magazine **50**: 115–122.
Sidelnikov, O., A. Redyuk, and S. Sygletos, 2018 Equalization performance and complexity analysis of dynamic deep neural networks in long haul transmission systems. Optics express **26**: 32765–32776.
Singh, A. P., D. Deb, H. Agrawal, K. Bingi, and S. Ozana, 2021 Modeling and control of robotic manipulators: A fractional calculus point of view. Arabian Journal for Science and Engineering **46**: 9541–9552.
Singhal, G., V. Aggarwal, S. Acharya, J. Aguayo, J. He, *et al.*, 2010 Ensemble fractional sensitivity: a quantitative approach to neuron selection for decoding motor tasks. Computational intelli-

gence and neuroscience **2010**: 1–10.
Sommacal, L., P. Melchior, A. Oustaloup, J.-M. Cabelguen, and A. J. Ijspeert, 2008 Fractional multi-models of the frog gastrocnemius muscle. Journal of Vibration and Control **14**: 1415–1430.
Steck, G. P., 1958 *A uniqueness property not enjoyed by the normal distribution*. Sandia Corporation.
Stockmeyer, L., 1987 Classifying the computational complexity of problems. The journal of symbolic logic **52**: 1–43.
Tenreiro Machado, J., V. Kiryakova, and F. Mainardi, 2010 A poster about the old history of fractional calculus. Fractional Calculus and Applied Analysis **13**: 447–454.
Tokhmpash, A., 2021 *Fractional Order Derivative in Circuits, Systems, and Signal Processing with Specific Application to Seizure Detection*. Ph.D. thesis, Northeastern University.
Toledo-Hernandez, R., V. Rico-Ramirez, G. A. Iglesias-Silva, and U. M. Diwekar, 2014 A fractional calculus approach to the dynamic optimization of biological reactive systems. part i: Fractional models for biological reactions. Chemical Engineering Science **117**: 217–228.
Tzoumas, V., Y. Xue, S. Pequito, P. Bogdan, and G. J. Pappas, 2018 Selecting sensors in biological fractional-order systems. IEEE Transactions on Control of Network Systems **5**: 709–721.
Valentim, C. A., J. A. Rabi, and S. A. David, 2021 Fractional mathematical oncology: On the potential of non-integer order calculus applied to interdisciplinary models. Biosystems **204**: 104377.
Van Rossum, G. and F. L. Drake Jr, 1995 *Python tutorial*, volume 620. Centrum voor Wiskunde en Informatica Amsterdam, The Netherlands.
Viola, J. and Y. Chen, 2022 A fractional-order on-line self optimizing control framework and a benchmark control system accelerated using fractional-order stochasticity. Fractal and Fractional **6**: 549.
West, B. J., 2016 *Fractional calculus view of complexity: tomorrow's science*. CRC Press.
West, B. J., M. Bologna, and P. Grigolini, 2003 *Physics of fractal operators*, volume 10. Springer.
Wiman, A., 1905 Über den fundamentalsatz in der teorie der funktionen e a (x) .
Wu, A., L. Liu, T. Huang, and Z. Zeng, 2017 Mittag-leffler stability of fractional-order neural networks in the presence of generalized piecewise constant arguments. Neural Networks **85**: 118–127.
Xue, H., Z. Shao, and H. Sun, 2020 Data classification based on fractional order gradient descent with momentum for rbf neural network. Network: Computation in Neural Systems **31**: 166–185.
Zhang, Y.-D. and L. Wu, 2008 Weights optimization of neural network via improved bco approach. Progress In Electromagnetics Research **83**: 185–198.
Ziane, D., M. Hamdi Cherif, D. Baleanu, and K. Belghaba, 2020 Non-differentiable solution of nonlinear biological population model on cantor sets. Fractal and Fractional **4**: 5.

How to cite this article: Karaca, Y. Computational Complexity-based Fractional-Order Neural Network Models for the Diagnostic Treatments and Predictive Transdifferentiability of Heterogeneous Cancer Cell Propensity. *Chaos Theory and Applications*, 5(1), 34-51, 2023.

CHAOS
Theory and Applications
in Applied Sciences and Engineering

e-ISSN: 2687-4539
RESEARCH ARTICLE
Vol.5 / No.1 / 2023 / pp.52-58
https://doi.org/10.51537/chaos.1204681

A Lorenz-like Chaotic OTA-C Circuit and Memristive Synchronization

Şule Zeynep Aydın *,[1], **Gökçe Nur Beken** β,[2] **and Zehra Gülru Çam Taşkıran** §,[3]

*Department Electrical Electronics Engineering, Marmara University, Istanbul, Türkiye, βDepartment Electrical Electronics Engineering, İstanbul Yeni Yüzyıl University, Istanbul, Türkiye, §Department Electronics and Communications Engineering, Yıldız Technical University, Istanbul, Türkiye.

ABSTRACT In this paper, a new set of lorenz-like hyper-chaotic equation set is obtained using the anti-control procedure. The chaoticity of the system is verified by MATLAB simulations using mathematical analysis methods. A new OTA-C circuit is designed for the new equation set. In the difference term addition technique, synchronizing the OTA-C circuit with a memristor rather than a resistor is proposed. Circuit design and synchronization are performed in PSpice simulation. The fact that the transconductance of the OTA element can be easily adjusted with a bias current provides the parameters that will make the proposed dynamic circuit a chaotic oscillator. The advantage of the proposed synchronization method is that the memristor automatically reaches the value that will provide the required weight of the differential term required for synchronization, rather than the computational methods used to determine the weight.

KEYWORDS
New chaotic system
Control parameter
Operational transconductance amplifier
Synchronization
Memristor

INTRODUCTION

Chaotic systems are nonlinear systems highly sensitive to initial conditions. It is important to create new chaotic systems due to their widespread use in secure communication, cryptography, chemical reactions, etc. In 1963, the first chaotic attractor was found by Lorenz (1963). Following that, Rössler (1976), Rabinovich and Fabrikant (1979), and Chua *et al.* (1993b) generated new chaotic equations. Many different methods have been used while producing new chaotic systems. Generating a new chaotic equation set with the control parameter method is a widely used method Deng *et al.* (2014); Zhou *et al.* (2008); Lü *et al.* (2002).

Chua's chaotic circuit design with memristor pioneered the work of chaotic circuit design. Later, in most studies, chaotic circuit design was made using the operational amplifier (OPAMP) component Fan *et al.* (2019); Sundarapandian and Pehlivan (2012); Pappu *et al.* (2017); Pehlivan and Uyaroğlu (2010); Lai *et al.* (2017); Akgul *et al.* (2016); Cao and Zhao (2021). Only a few studies on circuit implementation of the chaotic system are based on OTA Karawanich and Prommee (2022); Yildirim (2022). The advantage of OTA over OPAMP component is its high output impedance, wide band gap, and transconductance gain which can be changed with bias current. This provides an important advantage in chaotic circuits. The chaotic circuit design with OTA presented in Karawanich and Prommee (2022); Yildirim (2022) has been designed, but there is no study on its synchronization. In this study, a simpler structure is proposed by using only OTA, capacitor, and analog multiplier.

According to Carroll and Pecora (1995), Pecora and Carrol proposed the concept of first chaos synchronization, which is the foundation of chaotic secure communication. Following that, passive components such as resistors, inductors, and capacitors were used Chua *et al.* (1993a); Yao *et al.* (2020); Zhang *et al.* (2020a); Xu *et al.* (2019a); Yao *et al.* (2019). Synchronization studies are available by using active components such as Deniz *et al.* (2018); Uyaroğlu and Pehlivan (2010). Considering the important effect of the memristor in chaotic circuits, synchronization studies with memristor have become widespread in recent years. The memristor has less power consumption than other components because it is a passive component. In addition, although the memristor is nonlinear, it provides linear behavior in a certain frequency range. In this study, because of the memristor's properties, the OTA-C chaotic circuit is synchronized with the memristor.

In the literature, there is a method of synchronizing memristors by connecting them in anti-parallel. With this method, it is possible to change the receiver and transmitter, but since the structure draws current from both the receiver and transmitter sub-circuits, the original ordinary differential equation set could not be preserved on the transmitter side Gambuzza *et al.* (2015). Whereas,

Manuscript received: 15 November 2022,
Revised: 14 March 2023,
Accepted: 21 March 2023.

[1] sule.aydin@marmara.edu.tr
[2] gokcenur.beken@yeniyuzyil.edu.tr
[3] zgcam@yildiz.edu.tr (**Corresponding Author**)

in most other methods, the original equations are preserved on the transmitting side, while only different terms are involved on the receiving side. There are articles that synchronize with different connection types besides anti-parallel connection, but the same mathematical deformation is also present in them Zhang *et al.* (2020b); Escudero *et al.* (2020); Wang *et al.* (2021); Xu *et al.* (2019b).

The method proposed in this study is based on the method of adding the difference term Cuomo *et al.* (1993) which is already found in the literature, to obtain this term over the memristor rather than the resistor. Instead of finding this coefficient with an optimization algorithm and producing this term with a suitable resistor, the memristor element connected instead of the resistor, both creates this coefficient and changes its value as long as there is a synchronization error due to the error expression passing over it, and reaches the value where error-free synchronization is provided by itself. In this way, the coefficient is self-adjusted by the value change of the memristor. The researcher eliminates the time cost with this self-adaptation, and this coefficient, which can change over time due to effects such as environmental noises and aging, constantly brings itself to the required value.

OTA-C circuit is designed by using fewer components of the proposed new chaotic equation. A new contribution has been made to the literature by synchronizing the designed chaotic OTA-C circuit with the memristor. In this study, the derivation and analysis of the new set of chaotic equations are explained. Designing the OTA-C circuit of the new chaotic equation is given. The synchronization of the designed circuit with the memristor is given. Finally, the results of the study are evaluated.

A NEW SET OF CHAOTIC EQUATIONS AND ANALYSIS

A new chaotic equation is derived by applying the anti-control procedure to the Lorenz equation. The Lorenz equation is shown in the Equation 1. In the equation, $\dot{x}, \dot{y}, \dot{z}$ are state variables, σ, p, β are parameters.

$$\begin{aligned} \dot{x} &= \sigma(y-x) \\ \dot{y} &= x(p-z)-y \\ \dot{z} &= xy-\beta z \end{aligned} \tag{1}$$

The anti-control method is applied to the Lorenz equation.

$$\begin{aligned} \dot{x} &= \sigma(y-x)+u = \sigma(y-x)+l_1x+l_2y+l_3z \\ \dot{y} &= x(p-z)-y \\ \dot{z} &= xy-\beta z \end{aligned} \tag{2}$$

Here, $u = 1_1x + 1_2y + 1_3z$ is the linear feedback controller.

The Jacobian matrix of the Equation 2 evaluated at a random point is given in 3.

$$J = \begin{bmatrix} -\sigma+l_1 & \sigma+l_2 & l_3 \\ p & -1 & -x \\ y & x & -\beta \end{bmatrix} \tag{3}$$

l_2, l_3 do not contribute to the Lyapunov exponents of the system, since they do not contribute to the eigenvalues.

Thus, parameters are chosen as $l_2 = 1_3 = 0$. In this case, the control parameter is $u = 1_1x$. The new Lorenz-like chaotic equation is obtained in the Equation 4.

$$\begin{aligned} \dot{x} &= \sigma(y-x)+l_1x \\ \dot{y} &= x(p-z)-y \\ \dot{z} &= xy-\beta z \end{aligned} \tag{4}$$

The new system is chaotic when parameter values $\sigma = 10, p = 28, \beta = 8/3, l_1 = 1$. At initial conditions $x(0) = 0.9, y(0) = 0.5, z(0) = 0.1$, the attractors of the system are in Figure 1. As time passes, the orbits around this created attractor scan the entire space, never passing a point they passed. The chaotic state of the new system is investigated by time series, frequency analysis, Jacobian matrix, Lyapunov exponents, and bifurcation diagram analysis.

State variables are observed over time; state variables that exhibit irrational behavior are referred to as chaotic. The time series results of the system are given in Figure 2. Depending on its sensitivity to different initial conditions and parameter values, it can exhibit various behaviors such as equilibrium and periodicity.

The frequency spectrum of chaotic signals is continuous in a wide range. The frequency spectrum of each state variable obtained for the new chaotic system is given in Figure 3.

The jacobian matrix Equation 5 obtained from each equation in the differential equation set is given.

$$J = \begin{bmatrix} -\sigma+l_1 & \sigma+l_2 & l_3 \\ p & -1 & -x \\ y & x & -\beta \end{bmatrix} \tag{5}$$

The divergence value is obtained from the jacobian matrix $\nabla V = -\sigma + l_1 - 1 - \beta = -38/3$. Since it is $\nabla V < 0$, the behavior of the system is chaotic at the right initial conditions. Lyapunov exponents are expressions of interactions and differences between trajectories of phase space characteristics formed under close initial conditions. If the largest exponent is negative, the system converges to a value over time and becomes independent of initial conditions Özer and Akın (2005). If the largest exponent is positive, the distance between the orbits increases and the system is sensitive to initial conditions, that is, chaotic. If there are multiple positive Lyapunov exponents, the system is hyperchaotic Wolf *et al.* (1985). The new system's Lyapunov exponents are shown in Figure 4. The Lyapunov exponents obtained with the parameters of the system selected as $\sigma = 10, p = 28, \beta = 8/3, l_1 = 1$ are $L_1 = 8.38652, L_2 = 0.632274, L_3 = -21.6813$. Since there are two positive Lyapunov exponents, the new set of equations is hyperchaotic.

By using Lyapunov Exponents, the Lyapunov dimension or Kaplan-Yorke dimension can be calculated as in Equation 6, Grassberger and Procaccia (1983).

$$D_{ky} = j + \frac{1}{|L_{j+1}|}\Sigma_{i=1}^{j} L_i \tag{6}$$

j is the largest integer for witch $0 \leq L_1 + ... + L_n$. For the proposed circuit $j = 2$ and the Kaplan-Yorke dimension D_{ky} can be calculated as 7.

$$D_{ky} = 2 + \frac{L_1 + L_2}{|L_3|} = 2,41597 \tag{7}$$

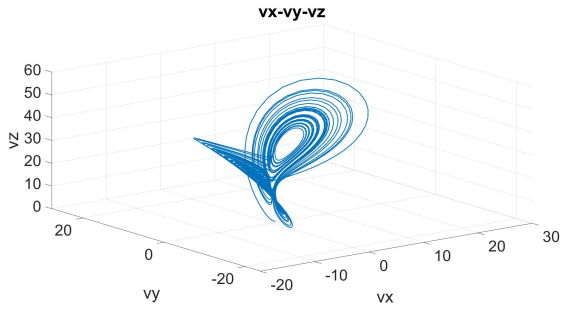

(a) $V_x - V_y - V_z$ chaotic attractor.

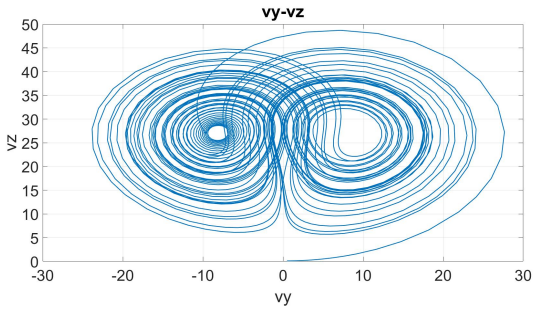

(b) $V_y - V_z$ chaotic attractor.

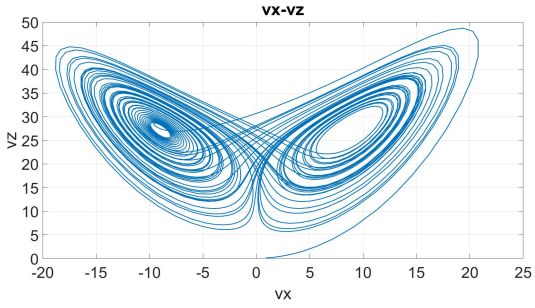

(c) $V_x - V_z$ chaotic attractor.

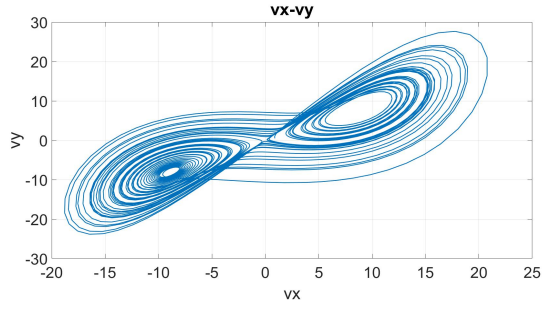

(d) $V_x - V_y$ chaotic attractor.

Figure 1 Phase portraits of the system

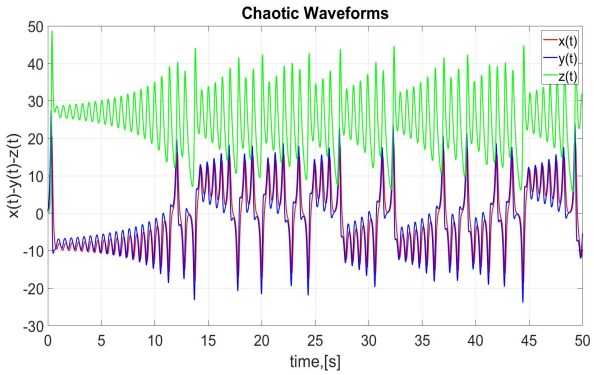

Figure 2 Time series of the system.

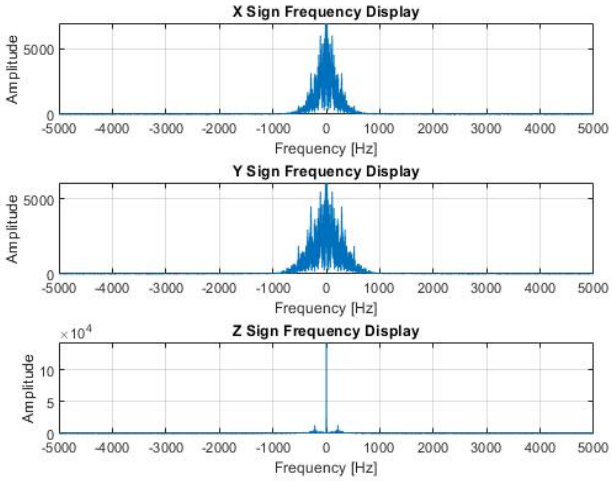

Figure 3 Frequency spectrum of the system.

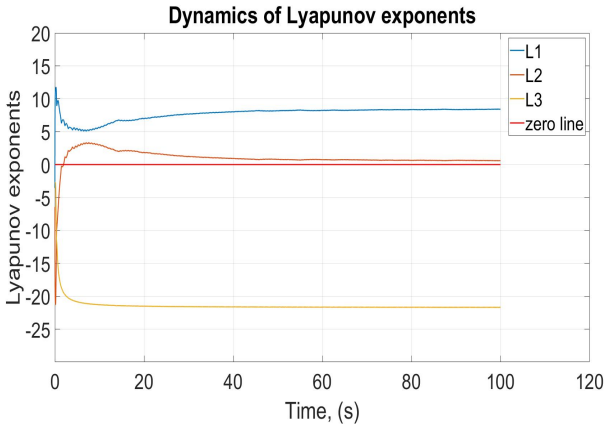

Figure 4 Lyapunov exponents of the system.

For original Lorenz system with the well-known coefficients $\sigma = 10, p = 28, \beta = 8/3$, and $L_1 = 0.054129, L_2 = 0.727225, L_3 = -14.448021$, j is also equal to 2 and the Kaplan-Yorke dimension,

$$D_{ky} = 2 + \frac{L_1 + L_2}{|L_3|} = 2,05408 \tag{8}$$

Thus, the new chaotic system has a larger Kaplan-Yorke dimension than the original Lorenz system.

The bifurcation diagram is the points at which the variables x and y intersect the equation's solution curve on the plane formed by the two variables for each value of the parameter p.The bifurcation diagram obtained for $1 < p < 350$ and initial conditions (0.9,0.5,0.1) in the new set of equations is shown in Figure 5.

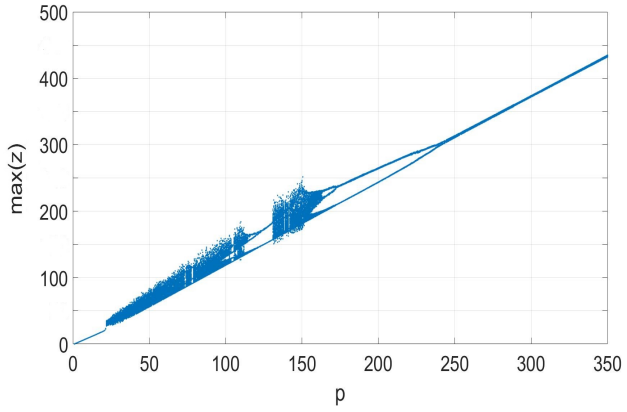

Figure 5 Bifurcation diagram of the system.

OTA-C CHAOTIC CIRCUIT DESIGN

The new chaotic equation set circuit design is created using OTA, analog multiplier (AM), and capacitor components. While generating the OTA-C circuit, each chaotic state variable is represented by voltage state variables corresponding to a capacitor voltage. The expressions of the derivatives of these state variables are tried to be formed as the sum of the terms of the current magnitudes divided by the capacitor values, according to $\frac{dv_C(t)}{dt} = \frac{1}{C} i_C(t)$ and the defining equation of the OTA $I_o = g_m(V_+ - V_-)$. A circuit as in Figure 6 is obtained electrically by collecting the currents at the nodes to which the grounded capacitors are connected. The equation set with the circuit parameters is obtained in the Equation 9.

$$\begin{aligned}
\frac{dV_x}{dt} &= \frac{g_{m_1}}{C_x}(V_y - V_x) + \frac{g_{m_2}}{C_x} V_x \\
\frac{dV_y}{dt} &= \frac{g_{m_3}}{C_y} V_x - \frac{k g_{m_4}}{C_y} V_x V_z - \frac{g_{m_5}}{C_y} V_y \\
\frac{dV_z}{dt} &= \frac{k g_{m_6}}{C_z} V_x V_y - \frac{g_{m_7}}{C_z} V_z
\end{aligned} \tag{9}$$

Taken as $C_x = C_y = C_z = 10nF, g_{m_1} = 100\mu S, g_{m_2} = 27\mu S, g_{m_3} = 1mS, g_{m_4} = 280\mu S, g_{m_5} = g_{m_7} = 10\mu S, g_{m_6} = 1nS$.

While performing PSpice simulations of the circuit in Figure 6, the ideal OTA model realized with discrete elements and the AD633 integrated circuit macro model as analog multiplier were used. The multiplier constant of the AD633 IC is $k = 0.1$ V^{-1}. The simulation results of the voltage values of the state variables of the

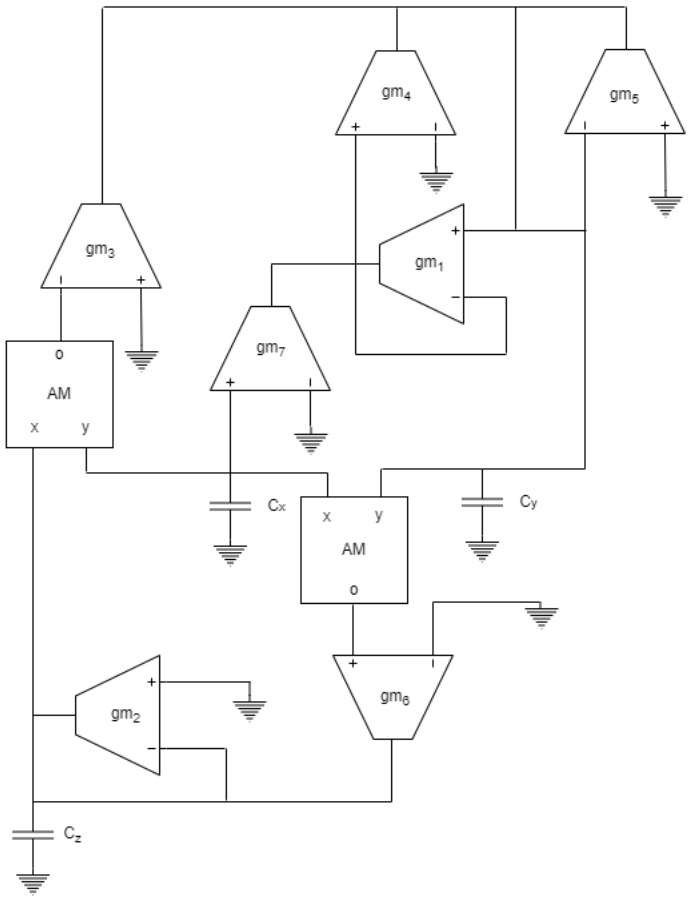

Figure 6 OTA-C chaotic circuit of the system.

circuit according to time are given in Figure 7. Chaotic attractors are also shown in Figure 8.

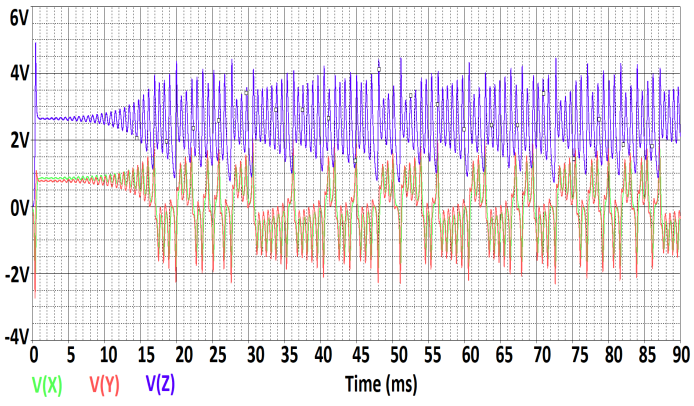

Figure 7 Time series of the simulated system.

SYNCHRONIZATION OF OTA-C CIRCUIT WITH MEMRISTOR

The synchronization of two chaotic circuits with different initial conditions is provided by a memristor and a circuit with OTA by adding the difference term attached to it (Sambas *et al.* 2013).

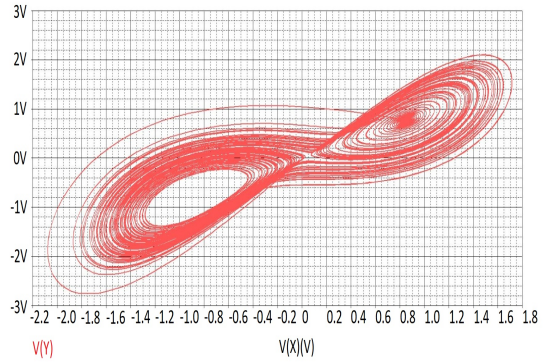

(a) $V_x - V_y$ chaotic attractor.

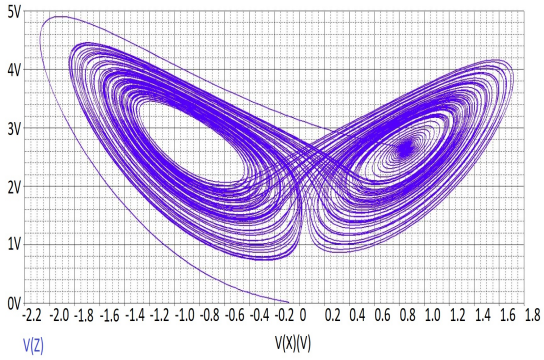

(b) $V_x - V_z$ chaotic attractor.

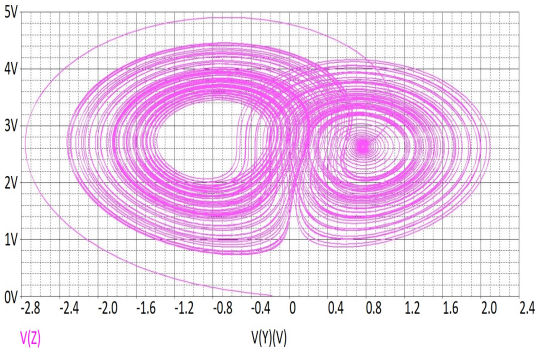

(c) $V_y - V_z$ chaotic attractor.

Figure 8 Phase portraits of the simulated system.

According to this method, the equation of the receiver is as in Equation 10.

$$\begin{aligned} V_{x_r}^{\circ} &= \sigma(V_{y_r} - V_{x_r}) + V_{x_r} \\ V_{y_r}^{\circ} &= V_{x_r}(p - V_{z_r}) - V_{y_r} \\ V_{z_r}^{\circ} &= V_{x_r} V_{y_r} - \beta V_{z_r} - \xi(V_{z_t} - V_{z_r}) \end{aligned} \tag{10}$$

To ensure that the circuits are both chaotic and synchronized, the value of ξ should be either optimized or observed by drawing a bifurcation diagram of the error as shown below. According to the bifurcation diagram in the Figure 9, synchronization is provided in the proposed circuit for ξ>1.8.

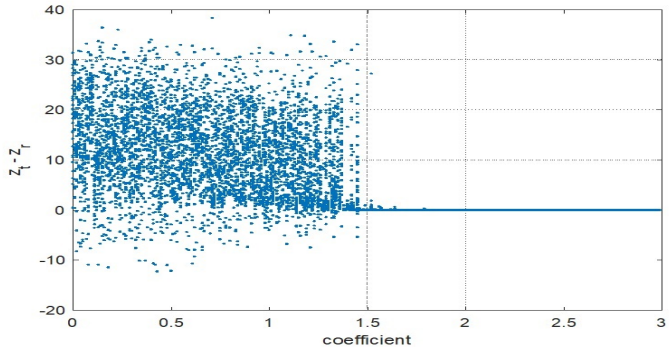

Figure 9 Bifurcation diagram of the error.

In this study, it is suggested that the necessity of optimizing the resistance value is eliminated by replacing the fixed resistor with the memristor element. The proposed method is to start from any state of the memristor and wait for the desired coefficient to occur spontaneously due to the nature of the memristor. In this way, when the coefficient needs to be updated due to a change in the circuit due to time or environmental factors, it will automatically reach the needed value and be synchronized again.

The weight of the difference term addition circuit is self-adjusted by the value change of the memristor. The synchronization circuit is given in Figure 10. Accordingly, for Equation 10, it will be $\xi = \frac{1}{C_z(M||R)}$. Due to the nature of the memristor, as long as there is an error, the memristance value will change in the direction of reducing the error, since $V_{z_t} - V_{z_r} = 0$ after synchronization is achieved, no current will flow from this part of the circuit and the circuits will operate synchronously.

The parameter values of the receiver and transmitter circuits are the same. The initial conditions of the receiver circuit are $v_x(0) = 0.05V, v_y(0) = 0.01V, v_z(0) = 0.05V$, the initial conditions of the transmitter circuit are $v_x(0) = 0.09V, v_y(0) = 0.05V, v_z(0) = 0.01V$. The value of the resistor connected in parallel with the memristor is $R = 30k\Omega$. Synchronization is realized over the z state variable of the receiver and transmitter circuit. The simulation results are shown in Figure 11. Circuits synchronized at $75ms$. It is shown that this is the contribution of the OTA-C design of the chaotic circuit and the memristor circuit model used in synchronization.

In the memristor simulations, the PSpice code of the memristor model proposed by Joglekar was used (Haron *et al.* 2014). This model has been proposed for titanium dioxide memristor nanostructures (Joglekar and Wolf 2009). The window function associated with the p exponent is used to provide the necessary nonlinearity. The p parameter is usually between 1 and 100. It is defined by Equations 11 and 12, where the memristor model represents the Joglekar window (Joglekar and Wolf 2009):

$$f_j(x) = 1 - (2x - 1)^{2p} \tag{11}$$

$$\begin{aligned} \frac{dx}{dt} &= kif(x) \\ v &= i[R_{ON}x + R_{OFF}(1-x)] \\ k &= \frac{\mu R_{ON}}{D^2} \end{aligned} \tag{12}$$

where x is the memristor state variable, $f(x)$ is the window function, $p = 10$ is a parameter of the Window Function, $k = 1000$ is a constant dependent on memristor physical parameters, $\mu = 10^{-14} m^2/(Vs)$ is the ionic drift mobility, $D = 10nm$ is the memristor length, i is the memristor current, v is the applied voltage, $R_{ON} = 100\Omega$ and $R_{OFF} = 16k\Omega$ are the ON and OFF resistances of the memristor.

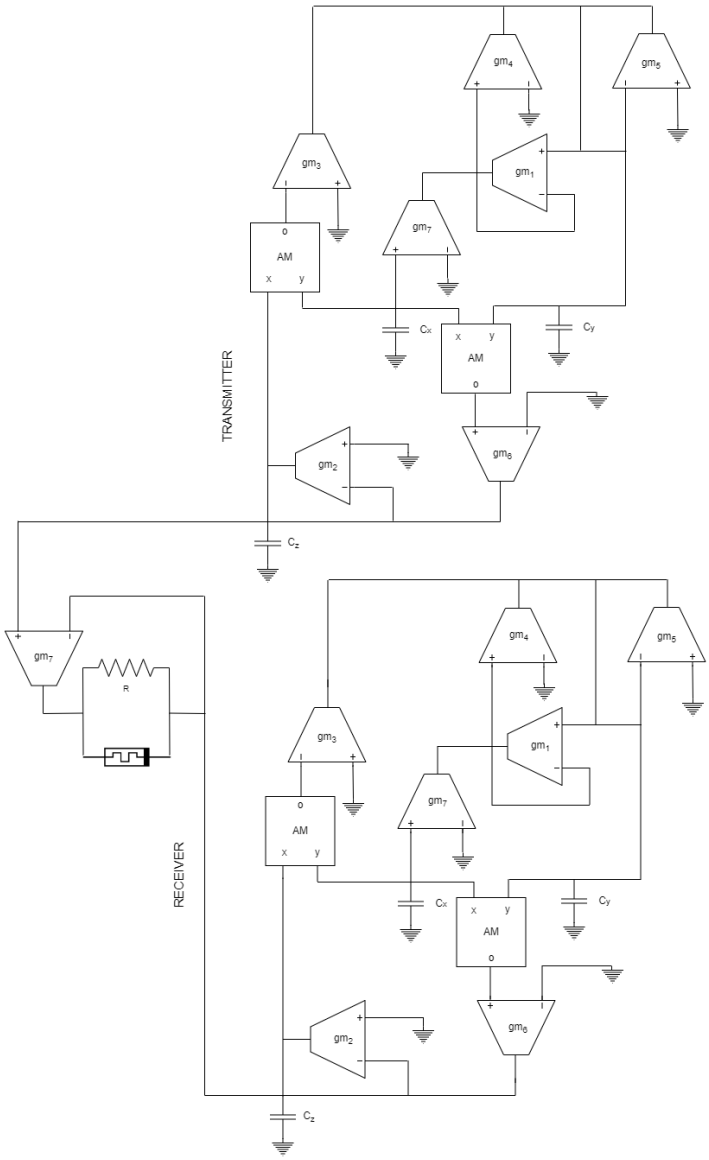

Figure 10 Synchronization of chaotic OTA-C circuits.

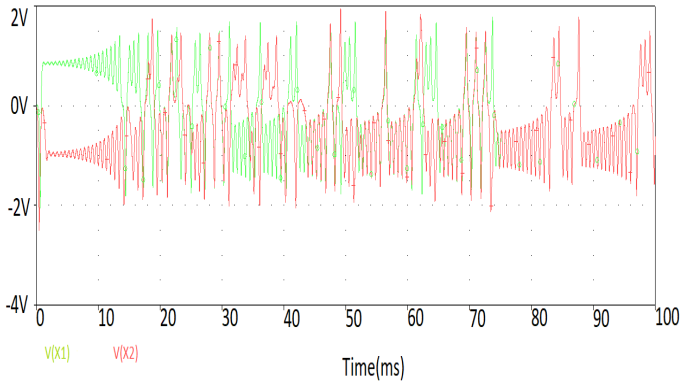

(a) Synchronization of transmitter and receiver signals v_{xt} and v_{xr} according to Figure 10.

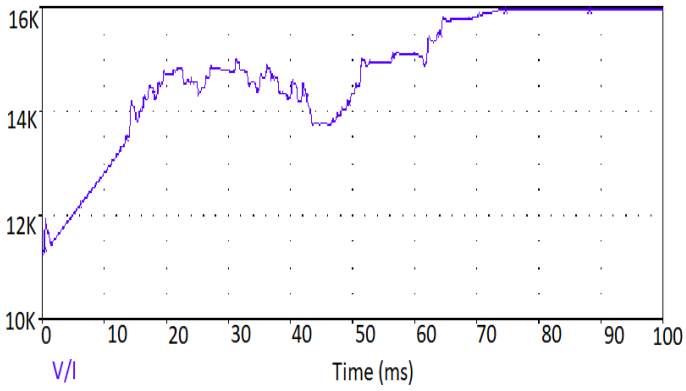

(b) Memristance value change.

Figure 11 OTA-C chaotic synchronization charts.

CONCLUSION

In this study, a new chaotic equation set is obtained from the Lorenz equation using the anti-control procedure. Then, the circuit of this equation set is designed. Ideal OTA, capacitor, and analog multiplier are used in the designed circuit. This provides it less costly in case of physical implementation. The synchronization of the circuit was realized in a short time of $75ms$ using the memristor and differential receiver circuit with OTA. At the same time, the use of a memristor component provided low power consumption and time-saving.

Conflicts of interest

The authors declare that there is no conflict of interest regarding the publication of this paper.

Availability of data and material

Not applicable.

LITERATURE CITED

Akgul, A., I. Moroz, I. Pehlivan, and S. Vaidyanathan, 2016 A new four-scroll chaotic attractor and its engineering applications. Optik **127**: 5491–5499.

Cao, H.-Y. and L. Zhao, 2021 A new chaotic system with different equilibria and attractors. The European Physical Journal Special Topics **230**: 1905–1914.

Carroll, T. L. and L. M. Pecora, 1995 Synchronizing chaotic circuits. In *Nonlinear Dynamics in Circuits*, pp. 215–248, World Scientific.

Chua, L. O., M. Itoh, L. Kocarev, and K. Eckert, 1993a Chaos synchronization in chua's circuit. Journal of Circuits, Systems, and Computers **3**: 93–108.

Chua, L. O., C. W. Wu, A. Huang, and G.-Q. Zhong, 1993b A universal circuit for studying and generating chaos. i. routes to chaos. IEEE Transactions on Circuits and Systems I: Fundamental Theory and Applications **40**: 732–744.

Cuomo, K. M., A. V. Oppenheim, and S. H. Strogatz, 1993 Synchronization of lorenz-based chaotic circuits with applications to communications. IEEE Transactions on circuits and systems II: Analog and digital signal processing **40**: 626–633.

Deng, K., J. Li, and S. Yu, 2014 Dynamics analysis and synchronization of a new chaotic attractor. Optik **125**: 3071–3075.

Deniz, H. I., Z. G. C. Taskiran, and H. Sedef, 2018 Chaotic lorenz synchronization circuit design for secure communication. In *2018 6th International conference on control engineering & information technology (CEIT)*, pp. 1–6, IEEE.

Escudero, M., I. Vourkas, and A. Rubio, 2020 Alternative memristor-based interconnect topologies for fast adaptive synchronization of chaotic circuits. Chaos, Solitons & Fractals **138**: 109974.

Fan, T., X. Tuo, H. Li, and P. He, 2019 Chaos control and circuit implementation of a class of double-wing chaotic system. International Journal of Numerical Modelling: Electronic Networks, Devices and Fields **32**: e2611.

Gambuzza, L. V., A. Buscarino, L. Fortuna, and M. Frasca, 2015 Memristor-based adaptive coupling for consensus and synchronization. IEEE Transactions on Circuits and Systems I: Regular Papers **62**: 1175–1184.

Grassberger, P. and I. Procaccia, 1983 Measuring the strangeness of strange attractors. Physica D: nonlinear phenomena **9**: 189–208.

Haron, N. Z., N. Arshad, and F. Salehuddin, 2014 Performance analysis of memristor models for rram cell array design using silvaco eda. Jurnal Teknologi **68**.

Joglekar, Y. N. and S. J. Wolf, 2009 The elusive memristor: properties of basic electrical circuits. European Journal of physics **30**: 661.

Karawanich, K. and P. Prommee, 2022 High-complex chaotic system based on new nonlinear function and ota-based circuit realization. Chaos, Solitons & Fractals **162**: 112536.

Lai, Q., A. Akgul, C. Li, G. Xu, and Ü. Çavuşoğlu, 2017 A new chaotic system with multiple attractors: Dynamic analysis, circuit realization and s-box design. Entropy **20**: 12.

Lorenz, E. N., 1963 Deterministic nonperiodic flow. Journal of atmospheric sciences **20**: 130–141.

Lü, J., G. Chen, and S. Zhang, 2002 Dynamical analysis of a new chaotic attractor. International Journal of Bifurcation and chaos **12**: 1001–1015.

Özer, A. and E. Akın, 2005 Tools for detecting chaos. Sakarya Üniversitesi Fen Bilimleri Enstitüsü Dergisi **9**: 60–66.

Pappu, C. S., B. C. Flores, P. S. Debroux, and J. E. Boehm, 2017 An electronic implementation of lorenz chaotic oscillator synchronization for bistatic radar applications. IEEE Transactions on Aerospace and Electronic Systems **53**: 2001–2013.

Pehlivan, I. and Y. Uyaroğlu, 2010 A new chaotic attractor from general lorenz system family and its electronic experimental implementation. Turkish Journal of Electrical Engineering and Computer Sciences **18**: 171–184.

Rabinovich, M. I. and A. L. Fabrikant, 1979 Stochastic self-modulation of waves in nonequilibrium media. J. Exp. Theor. Phys **77**: 617–629.

Rössler, O. E., 1976 An equation for continuous chaos. Physics Letters A **57**: 397–398.

Sambas, A., W. Mada Sanjaya, M. Mamat, and O. Tacha, 2013 Design and numerical simulation of unidirectional chaotic synchronization and its application in secure communication system. Journal of Engineering Science and Technology Review **6**: 66–73.

Sundarapandian, V. and I. Pehlivan, 2012 Analysis, control, synchronization, and circuit design of a novel chaotic system. Mathematical and Computer Modelling **55**: 1904–1915.

Uyaroğlu, Y. and İ. Pehlivan, 2010 Nonlinear sprott94 case a chaotic equation: synchronization and masking communication applications. Computers & Electrical Engineering **36**: 1093–1100.

Wang, Y., F. Min, Y. Cheng, and Y. Dou, 2021 Dynamical analysis in dual-memristor-based fitzhugh–nagumo circuit and its coupling finite-time synchronization. The European Physical Journal Special Topics **230**: 1751–1762.

Wolf, A., J. B. Swift, H. L. Swinney, and J. A. Vastano, 1985 Determining lyapunov exponents from a time series. Physica D: nonlinear phenomena **16**: 285–317.

Xu, Y.-m., Z. Yao, A. Hobiny, and J. Ma, 2019a Differential coupling contributes to synchronization via a capacitor connection between chaotic circuits. Frontiers of Information Technology & Electronic Engineering **20**: 571–583.

Xu, Y.-m., Z. Yao, A. Hobiny, and J. Ma, 2019b Differential coupling contributes to synchronization via a capacitor connection between chaotic circuits. Frontiers of Information Technology & Electronic Engineering **20**: 571–583.

Yao, Z., J. Ma, Y. Yao, and C. Wang, 2019 Synchronization realization between two nonlinear circuits via an induction coil coupling. Nonlinear Dynamics **96**: 205–217.

Yao, Z., P. Zhou, A. Alsaedi, and J. Ma, 2020 Energy flow-guided synchronization between chaotic circuits. Applied Mathematics and Computation **374**: 124998.

Yildirim, M., 2022 Optical color image encryption scheme with a novel dna encoding algorithm based on a chaotic circuit. Chaos, Solitons & Fractals **155**: 111631.

Zhang, X., C. Wang, J. Ma, and G. Ren, 2020a Control and synchronization in nonlinear circuits by using a thermistor. Modern Physics Letters B **34**: 2050267.

Zhang, X., F. Wu, J. Ma, A. Hobiny, F. Alzahrani, *et al.*, 2020b Field coupling synchronization between chaotic circuits via a memristor. AEU-International Journal of Electronics and Communications **115**: 153050.

Zhou, W., Y. Xu, H. Lu, and L. Pan, 2008 On dynamics analysis of a new chaotic attractor. Physics Letters A **372**: 5773–5777.

How to cite this article: Aydın, S. Z., Beken, G. N., and Taskiran, Z. G. C. A Lorenz-like Chaotic OTA-C Circuit and Memristive Synchronization. *Chaos Theory and Applications*, 5(1), 52-58, 2023.